STUDIES OF WHEAT FLOW IN AN EXPERIMENTAL HOPPER

A Dissertation submitted to the

University of Manchester Institute of Science and Technology

For the Degree of

Master of Science

In the

Satake Centre for Grain Process Engineering
Department of Chemical Engineering

By

QAIS ABDULLATIF BUALI

Under the Supervision of

Professor Colin Webb

This thesis is submitted in partial fulfilment of the requirements for the Degree of Master of Science of the University of Manchester Institute of Science and Technology.

September, 1999

DECLARATION

No portion of the work referred to in this dissertation has been submitted in support of an application for another degree or qualification of this or any other university or other institution of learning.

ACKNOWLEDGEMENTS

I would like to express my deepest appreciation to:

- Professor Colin Webb for his supervision, discussion, advice and confidence in my work.
- Dr. David Harris for lending his time and patience in the discussions on the modelling part of the literature survey.
- Dr. Grant Campbell for his help and advice during the photographic study.
- Mr. Andrew Evans who enthusiastically and effectively prepared the experimental rig.
- All postgraduate students of the Satake Centre for Grain Process Engineering for their support especially to Philip for his friendly help.
- The University of Bahrain for their financial support.
- My family and friends in Bahrain who have never stopped their support and prayers.

STUDIES OF WHEAT FLOW IN AN EXPERIMENTAL HOPPER

ABSTRACT

The main purpose of this work was to design an experimental hopper and use it to study how hopper geometry and particle characteristics affect granular flow.

The investigation was performed using both qualitative and quantitative observations. The qualitative study was conducted by taking and analysing photos representing different observations of the flow. The quantitative part was concentrated on the effect of the hopper geometry i.e. height, width, hopper half angle and discharge size on the discharge rate. The effect of two of the particle characteristics, size and moisture content, on the discharge rate was also investigated.

The photographic study revealed that particles located on the centreline above the hopper discharge move faster than other particles elsewhere in the hopper. Moreover, stagnant zones with different shapes were obvious adjacent to the walls for different hopper geometries. The shape of the free surface was observed to mainly decline at the centre since the particles in this place are moving with a higher speed than those at the sides. Another effect of the different velocities and stagnant zone, initiated in the hopper, was to notice much more deformation in the flow lines at the centre than those at the sides and near the walls.

In the quantitative study, the flow rate was found to be independent of the material head and the width of the hopper. A small effect of the particle size on the discharge rate was noticed, with the lower rate corresponding to the smaller particles. The increase in the hopper half angle was found to affect the discharge rate negatively with lower flowrates obtained for larger hopper half angles. A critical angle was found after which the flowrate would be constant. A decrease in the discharge rate was noticed as the moisture content of the particles increased. A linear relationship was obtained after some critical point (13.90% moisture content) below which no effect of moisture content on the flowrate was observed.

The angle of repose was found to increase linearly as the moisture content of wheat particles increases. On the other hand, particles with larger sizes were found to have smaller angles of repose. In all the cases, the angle of repose was a good measure of the material flowability with higher discharge rates were obtained for samples with lower angles of repose.

Further work would require studying the effect of different agricultural seeds and different ranges of moisture contents on the angle of repose and the flowrate. Moreover, using a camera with several seconds exposure time is recommended for studying different shapes of the stagnant zones.

Qais Abdullatif Buali MSc Dissertation September, 1999

TABLE OF CONTENTS

DECLARATION ..... **I**

ACKNOWLEDGEMENTS ..... **II**

ABSTRACT ..... **III**

TABLE OF CONTENTS ..... **IV**

LIST OF TABLES ..... **IX**

LIST OF FIGURES ..... **X**

LIST OF ABBREVIATIONS ..... **XIII**

NOMENCLATURE ..... **XIV**

CHAPTER 1: INTRODUCTION **1**

CHAPTER 2: GRANULAR FLOW IN SILOS AND HOPPERS **4**

2.1 EQUIPMENT USED TO HANDLE GRANULAR MATERIALS 5

2.2 STATISTICS SHOWING THE DIFFICULTY IN HANDLING GRANULAR MATERIALS 5

2.3 PROBLEMS WITH HANDLING GRANULAR SOLIDS IN HOPPERS AND SILOS 6

2.3.1 NO FLOW 6

2.3.2 ERRATIC FLOW 7

2.3.3 FLUSHING OR FLOODING 9

2.3.4 LIMITED CAPACITY 10

2.3.5 SEGREGATION 10

2.3.6 DEGRADATION 11

2.3.7 OTHER PROBLEMS 11

2.4 FLOW PATTERNS IN BINS AND HOPPERS 12

2.4.1 MASS FLOW 12

2.4.2 FUNNEL FLOW 13

2.4.3 EXPANDED FLOW 15

2.5 DESIGN METHODS FOR HOPPERS 16

2.5.1 WALL ANGLE 17

2.5.2 OUTLET SIZE DETERMINATION 17

2.5.3 FLOWRATE MEASUREMENT 19

2.6 PREDICTION OF DISCHARGE RATES FROM HOPPERS 20

2.6.1 EXPERIMENTAL CORRELATIONS 20

2.6.2 THEORETICAL PREDICTION OF THE MASS FLOWRATE 23

2.6.3 EFFECT OF INTERSTITIAL PRESSURE GRADIENTS 24

2.7 MODELLING OF GRANULAR FLOW IN HOPPERS 26

2.7.1 UNIVERSAL EQUATIONS GOVERNING FLUID AND BULK SOLIDS FLOW 27

2.7.2 CONSTITUTIVE EQUATIONS FOR FLUID FLOW 30

2.7.3 MAIN DIFFERENCES BETWEEN FLUID FLOW AND BULK SOLIDS FLOW 31

2.7.4 CONSTITUTIVE EQUATIONS FOR BULK SOLIDS FLOW 33

2.8 SOME NUMERICAL METHODS TO PREDICT GRANULAR FLOW IN HOPPERS 37

2.8.1 THE FINITE ELEMENT METHOD (FEM) 38

2.8.2 THE DISCRETE ELEMENT METHOD (DEM) 39

2.8.3 LIMITATIONS OF FEM AND DEM 43

2.8.4 A HYBRID NUMERICAL MODEL BASED ON FEM AND DEM 44

CHAPTER 3: REVIEW OF PAST EXPERIMENTAL WORK **46**

CHAPTER 4: DESIGN OF THE EXPERIMENTAL HOPPER **66**

4.1 DESIGN OF THE FRONT AND BACK WALLS 68

4.2 DESIGN OF THE INCLINED SIDE WALLS 69

4.3 DESIGN OF THE VERTICAL SIDE WALLS 71

4.4 GEOMETRY OF THE EXPERIMENTAL HOPPER 71

4.5 OTHER DESIGN CONSIDERATIONS 74

CHAPTER 5: MATERIALS AND METHODS **75**

5.1 WHEAT USED IN THE EXPERIMENTS 76

5.2 PREPARATION OF DIFFERENT SIZE SAMPLES 76

5.2.1 OPERATION OF THE SATAKE TEST PURIFIER 76

5.3 ANALYSIS OF THE DIFFERENT SIZE SAMPLES 77

5.4 MEASURING AND ALTERING THE MOISTURE CONTENT OF THE WHEAT 79

5.5 MEASURING THE ANGLE OF REPOSE 81

5.6 GENERAL PROCEDURE FOR MEASURING THE FLOWRATE FROM THE HOPPER 83

5.6.1 EXAMINING THE EFFECT OF MATERIAL HEAD ON THE FLOWRATE 84

5.6.2 EXAMINING THE EFFECT OF HOPPER WIDTH ON THE FLOWRATE 84

5.6.3 EXAMINING THE EFFECT OF PARTICLE SIZE ON THE FLOWRATE 85

5.6.4 EXAMINING THE EFFECT OF HOPPER HALF ANGLE ON THE FLOWRATE 85

5.6.5 EXAMINING THE EFFECT OF DISCHARGE SIZE ON THE FLOWRATE 86

5.6.6 EXAMINING THE EFFECT OF MOISTURE CONTENT ON THE FLOWRATE 87

5.7 PHOTOGRAPHIC STUDY OF FLOW IN THE HOPPER 87

CHAPTER 6: RESULTS AND DISCUSSIONS **89**

6.1 SAMPLES OBTAINED FROM THE SATAKE PURIFIER 90

6.2 GRAIN DIMENSIONS 90

6.3 MOISTURE CONTENTS OBTAINED 91

6.4 GENERAL OBSERVATIONS ON THE PERFORMANCE OF THE EXPERIMENTAL HOPPER 92

6.5 QUALITATIVE OBSERVATION OF THE FLOW IN THE HOPPER 93

6.5.1 REPEATABILITY OF THE FLOWS 93

6.5.2 DEFORMATION OF THE LAYERS OF COLOURED PARTICLES 93

6.5.3 STAGNANT ZONE 99

6.5.4 ALIGNMENT OF THE WHEAT 100

6.5.5 BLOCKAGES 101

6.5.6 SHAPES OF THE FREE SURFACE 102

6.6 ANGLE OF REPOSE 106

6.6.1 EFFECT OF THE PARTICLE SIZE 106

6.6.2 EFFECT OF MOISTURE CONTENT 108

6.7 DISCHARGE RATE FROM THE HOPPER 110

6.7.1 EFFECT OF MATERIAL HEAD 111

6.7.2 EFFECT OF HOPPER WIDTH 112

6.7.3 EFFECT OF PARTICLE SIZE 114

6.7.4 EFFECT OF HOPPER HALF ANGLE 116

6.7.5 EFFECT OF DISCHARGE SIZE 118

6.7.6 EFFECT OF MOISTURE CONTENT 121

CHAPTER 7: CONCLUSIONS AND SUGGESTIONS FOR FURTHER WORK **125**

7.1 CONCLUSIONS 126

7.2 SUGGESTIONS FOR FURTHER WORK 128

REFERENCES **130**

APPENDICES **136**

APPENDIX A: MOISTURE – AIR OVEN METHOSD 137

APPENDIX B: RESULTS OF THE SIZE ANALYSIS FROM THE GRAIN IMAGE ANALYSER 140

APPENDIX C: MOISTURE CONTENT CALCULATIONS 146

APPENDIX D: EXAMINING THE EFFECT OF PARTICLE SIZE ON THE ANGLE OF REPOSE 147

APPENDIX E: EXAMINING THE EFFECT OF MOISTURE CONTENT ON THE ANGLE OF REPOSE 149

APPENDIX F: EXAMINING THE EFFECT OF MATERIAL HEAD IN THE HOPPER ON THE FLOWRATE ... 151

APPENDIX G: EXAMINING THE EFFECT OF HOPPER WIDTH ON THE FLOWRATE 153

APPENDIX H: EXAMINING THE EFFECT OF PARTICLE SIZE ON THE FLOWRATE 155

APPENDIX I: EXAMINING THE EFFECT OF HOPPER HALF ANGLE ON THE FLOWRATE 157

APPENDIX J: EXAMINING THE EFFECT OF DISCHARGE SIZE ON THE FLOWRATE 159

APPENDIX K: EXAMINING THE EFFECT OF MOISTURE CONTENT ON THE FLOWRATE 162

LIST OF TABLES

Table 2.1 : Hopper discharge problems and reasons **12**

Table 2.2 : Advantages and disadvantages of mass and funnel flow hoppers **15**

Table 6.1 : Size analysis for the six wheat samples **90**

Table 6.2 : Results obtained for the initial moisture content **91**

Table 6.3 : Quantities of water added and the moisture contents achieved **91**

LIST OF FIGURES

Figure 2.1: Mechanical and cohesive arches will stop flow from the hopper 7

Figure 2.2 : Vibration method to control erratic discharge 8

Figure 2.3 : Fugitive dust generation and entrained air result when the product falls from the outlet of a hopper 9

Figure 2.4 : Sifting segregation in a storage bin 11

Figure 2.5 : The mass flow pattern 13

Figure 2.6 : The funnel flow pattern 14

Figure 2.7 : The expanded flow pattern 16

Figure 2.8 : Basic design for hoppers 16

Figure 2.9 : Common designs for mass flow and funnel flow hoppers 18

Figure 2.10 : Geometry and discretization of a hopper 38

Figure 2.11 : A flowchart of the soft particle method 40

Figure 2.12 : A typical contact force model used in the soft particle technique 41

Figure 2.13 : Simplified flowchart for the contact model 43

Figure 2.14 : FEM and DEM domains in the FEM and DEM hybrid model 44

Figure 3.1 : Experimental bin-hopper system used by Gardner 48

Figure 3.2 : Different photographs of the flow in hoppers 50

Figure 3.3 : Photographs of gravel discharging from hoppers 51

Figure 3.4 : Arrangement of the experimental hopper and x-ray source and film used by Lee *et al.* 52

Figure 3.5 : Flow through hoppers obtained from radiographic study 53

Figure 3.6 : Hopper Geometry and radiograph picture obtained 54

Figure 3.7 : Different zones and surfaces for course rounded sand observed by Dresher *et al.* experiments 55

Figure 3.8 : Schematic indicating the different flow regimes observed by Nguyen *et al.* 55

Figure 3.9 : Photographic examples of the flow regimes for sand 57

Figure 3.10 : Experimental hopper used by Tüzün and Nedderman .. 58

Figure 3.11 : Photographs of flow field for 1.5 mm ballotini with varying half angles 59

Figure 3.12 : Schematic of the apparatus used by Baxter and his group 60

Figure 3.13 : Flow of sand images 61

Figure 3.14 : Photographs of grass seeds flowing from a hopper with a wedge angle of 60° 62

Figure 3.15 : Arrangement of an experimental hopper used to measure wall pressures 63

Figure 3.16 : Comparison between experimental and numerical results for wall pressures 63

Figure 3.17 : Comparison between stagnant zones 64

Figure 4.1 : Schematic of experimental hopper used in the project ... 67

Figure 4.2 : Design and dimensions of pieces 1 and 2 69

Figure 4.3 : Shape and dimensions of the hopper inclined walls 70

Figure 4.4 : Shape and dimensions of piece number 5 72

Figure 4.5 : Geometry of the experimental hopper 73

Figure 4.6 : A picture of the hopper used in the experiments 74

Figure 5.1 : Satake Grain Image Analyser 78

Figure 5.2 : Various measurements of the angle of repose 81

Figure 5.3 : Method used to measure the angle of repose 82

Figure 6.1 : Development of the flow lines in the hopper 94

Figure 6.2 : Drawings of flow lines in an experimental hopper 95

Figure 6.3 : Flow lines for sand and glass beads 96

Figure 6.4 : Continuation of the flow showing the circular structure and the tongue **98**

Figure 6.5 : Initial alignment of the wheat grains inside the hopper .. **100**

Figure 6.6 : Alignment near the outlet **101**

Figure 6.7 : Front and bottom views of the blockage **102**

Figure 6.8 : Shapes of the free surface during the discharge **103**

Figure 6.9 : Different stages of the discharge and the free surface shapes **104**

Figure 6.10 : Angle of repose as a function of particle thickness **106**

Figure 6.11 : Angle of repose as a function of moisture content **108**

Figure 6.12 : Effect of material head in the hopper on the flowrate **111**

Figure 6.13 : Effect of the hopper width on the flowrate **113**

Figure 6.14 : Effect of the particle size on the flowrate **115**

Figure 6.15 : Effect of the hopper half angle on the flowrate **117**

Figure 6.16 : Effect of the discharge opening on the flowrate **119**

Figure 6.17 : The linear relation obtained between $W^{2/5}$ and D_h **120**

Figure 6.18 : Effect of moisture content on the flowrate **122**

Figure 6.19 : Effect of the angle of repose obtained for different moisture contents on the flowrate **123**

LIST OF ABBREVIATIONS

FEM	Finite Element Method
DEM	Discrete Element Method
PVC	Poly Vinyl Chloride
LED	Light Emitting Display
AACC	American Association of Cereal Chemists
w.b.	Wet basis
S. D.	Standard Deviation
Avg.	Average

NOMENCLATURE

a_1	magnitude of shear rate in equation (2.45)	
a_2	magnitude of shear rate in equation (2.46)	
A	orifice area	cm^2
A^*	effective cross-sectional area of the orifice	cm^2
b_c	orifice width in chisel shaped hopper	cm
b_h	hopper breadth	cm
b_s	breadth of slot orifice	cm
c	cohesion	
C	Beverloo coefficient	
C'	modified Beverloo coefficient	
C^*	predicted value of the Beverloo parameter	
C_D	drag coefficient	
d	particle diameter	mm
D	hopper diameter, width of the experimental hopper	cm
D_o	orifice diameter, orifice width for the two dimensional experimental hopper	cm
D_h	hydraulic mean diameter of the orifice	cm
D_h^*	effective hydraulic mean diameter	cm
D_w	diameter of circular outlet or width of rectangular outlet in equation (2.1)	cm
g	acceleration due to gravity	$g\ cm^{-2}$
$F(\alpha,\chi)$	Rose and Tanaka function	
H	height of the hopper, material head	cm
$\boldsymbol{I}$	identity tensor	

k	parameter in Beverloo correlation	
K	ratio of the principal stesses	
K_1	empirical function of material properties	
K^*	parameter in equation (2.13)	
l	slot length	cm
l_c	thickness of chisel shaped hopper	cm
m	constant in equation (2.1)	
M	parameter in equation (2.13)	
MC	moisture content	
M_f	desired moisture content of the sample	
M_i	initial moisture content of the sample	
M_l	moisture loss	g
M_{la}	percent moisture loss in air drying	
M_{lo}	percent moisture loss by oven-drying	
n	direction normal to the plane	
p	pressure	$N\ m^{-2}$
P	hydrostatic pressure	$N\ m^{-2}$
Q	maximum rate of discharge	$g\ sec^{-1}$
Q_m	mass of water added	kg
r	radial co-ordinate	
r_o	radial distance to orifice plane from virtual apex	cm
t_p	particle thickness	mm
W	mass discharge rate	$g\ sec^{-1}$
W_s	original weight of the sample	g

CHAPTER 1

INTRODUCTION

A granular material is a large group of discrete solid particles enclosed by a fluid, usually air (Gao, 1997; Wassgren, 1998; Hunt, 1998). We deal with these particles in our daily lives, and they are abundant in both nature and industry. Examples of granular materials are food products such as rice, corn and sugar, building materials such as sand and gravel, chemicals like coal, plastic and pharmaceuticals (Jaeger and Nagel, 1992; Wassgren, 1998; CMIS, 1999).

The study of how these particles move or flow is becoming more important as the time is passing. This is due to the vast industries dealing with them and the curiosity of human beings to know more about the environment they are living in. Industrial applications of granular flow are the handling and conveying of powders and foods, particle segregation, mixing, drying, heating and the applications of fluidised beds (Hsiau, 1997; Hunt, 1998; Wassgren, 1998). Approximately three fifths of the products in the chemical industry are in solid form (Bridgwater, 1995).

In nature we see granular flows, for example, in the motion of ice sheets, dune formation and river sedimentation (Hsiau, 1997; Hunt, 1998). Dealing with granular flow is a difficult subject for which there is still not a good understanding of the behaviour that particles tend to follow when they move (Behringer, 1995; Clift, 1996; Gao, 1997; Wassgren, 1998; CMIS, 1999).

Granular particulate handling is an extremely important area to be concerned with. Bins, hoppers, chutes, bunkers and conveyor belts are well known terms in dealing with storing and transporting granular matter. Knowlton *et al.* (1994) reported that over 1,000 silos, bins and hoppers fail in North America each year. In order to avoid

solids handling problems, a proper design of handling and storage equipment joined with a good understanding of how granular particles act can greatly reduce these problems.

The aim of this project was to design an experimental hopper and use it to study the effect of hopper geometry and material characteristics on the discharge rate. The factors related to the hopper geometry are the height of the hopper, the width, the hopper half angle and the discharge area. The two factors studied which are related to the particle characteristics are particle size and moisture content. Another aim was to investigate the effect of the particle characteristics on the angle of internal friction (angle of repose) and show the connection of this effect to the discharge rate. During these studies, photographs representing general observations of the flow characteristics were taken and analysed to get a better understanding of the flow mechanism of granular media in the hopper.

CHAPTER 2

GRANULAR FLOW IN SILOS AND HOPPERS

- Knowlton *et al.* (1994) reported the findings of a six-year study of 40 solids processing plants in the U.S. and Canada. The study found that 80% of these plants are suffering from solids handling problems.
- Estimates revealed that nearly 60% of the capacity of industrial plants handling granular materials is lost when transporting these materials from one part of the factory to another (Jaeger *et al.*, 1996).

2.3 PROBLEMS WITH HANDLING GRANULAR SOLIDS IN HOPPERS AND SILOS

From the mentioned statistics, one should concentrate more on studying the properties of these particles and the equipment used in dealing with them. Silos and hoppers are the most commonly used equipment to store and handle granular materials. To avoid handling problems in hoppers, a combination of a good hopper design and a comprehensive knowledge of the characteristics and behaviour of the granular materials is needed.

In storing granular materials, the most common method is to put it in a silo made of a cylindrical or rectangular part with a hopper at the bottom. The bulk is withdrawn under the force of gravity via an opening at the bottom of the hopper. It seems very simple to remove the solids from the hopper, however, here is where the most problems arise (Kooi, 1999). These problems are discussed in the following sections.

2.3.1 NO FLOW

This problem is the worst in dealing with the flow of the materials. This can result from the formation of a stable arch, bridge or dome at the outlet (figure 2.1) or by the

formation of a stable vertical cavity above the outlet that extends to the top of the bin (ratholing or piping) (Berkovitch, 1983; Johanson, 1985; Knowlton *et al.*, 1994; Das *et al.*, 1997).



Fig. 2.1 Mechanical and cohesive arches will stop flow from the hopper (Das *et al.*, 1997) .

The mechanical arch shown in figure 2.1 usually occurs when dealing with large particle materials. This is the result of the hopper outlet being small compared to the size of the particles (Berkovitch, 1983; Das *et al.*, 1997).

2.3.2 ERRATIC FLOW

This problem occurs when hammers or vibrators are used to break down a rathole or arch (Knowlton *et al.*, 1994). If the vibration is strong enough to break the rathole or arch, then some of the material will fall and discharge. Unfortunately, this is an unstable situation and the material will soon form another arch or rathole, stopping the flow once more (Johanson, 1985).

The usual method to restart material flow is to use a hammer to stroke the hopper. However, discharge aids, air or mechanical vibrators can also be used to either promote or control flow from the hopper (Berkovitch, 1983; Thomson, 1985; Bates, 1996). All of these methods agitate the solids to break-up the particle cohesion and encourage flow through the outlet. Berkovitch (1983) proposed the following automatic methods to break-up arches and control flowrates through the discharge:

2.3.2.1 Aeration methods

In this technique, different approaches can be used. These include using porous aeration pads when discharging or rushing a high-pressure air to expand the mass. Another way is to use elastic pads that are enlarged with air as needed to breakdown arches or pipes.

2.3.2.2 Vibration methods

Here the hopper walls are shaken or vibrated. Another way is to apply some devices within the product such as a steel dish across the outlet, angled blades near the discharge or vibratory cages at the bottom part of the hopper. Figure 2.2 shows the vibration method when applied as a discharge aid.

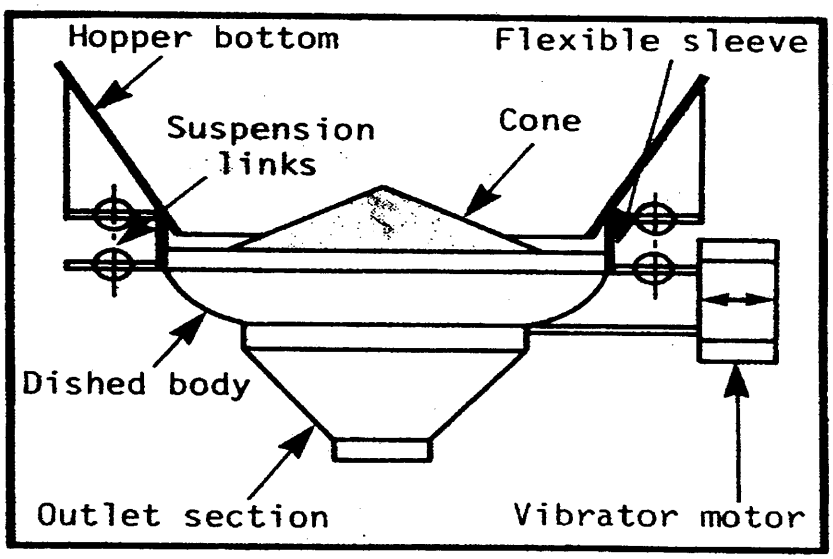


Fig. 2.2 Vibration method to control erratic discharge (Berkovitch, 1983).

2.3.2.3 Mechanical methods

In this approach, moving chains or paddles, screw feeders or rotating arms arranged to work at any part of the hopper are applied to break the arch.

2.3.3 FLUSHING OR FLOODING

This happens if powder is present with the stored material. If the rathole still exists, and by some means it is broken, then the flow of solids will exhibit fluid like characteristics (Johanson, 1985; Knowlton *et al.*, 1994). As a result, clouds of dust, unmanageable flow of particles and loss of the product will occur (Knowlton *et al.*, 1994). Moreover, the discharged solids will form a pile with air engaged inside it. When the bubbles of air escape from the solid media, more clouds of dust and loss of product will result (Johanson, 1985; StanleyWood, 1996). Figure 2.3 shows the loss of dusty product from the hopper outlet.

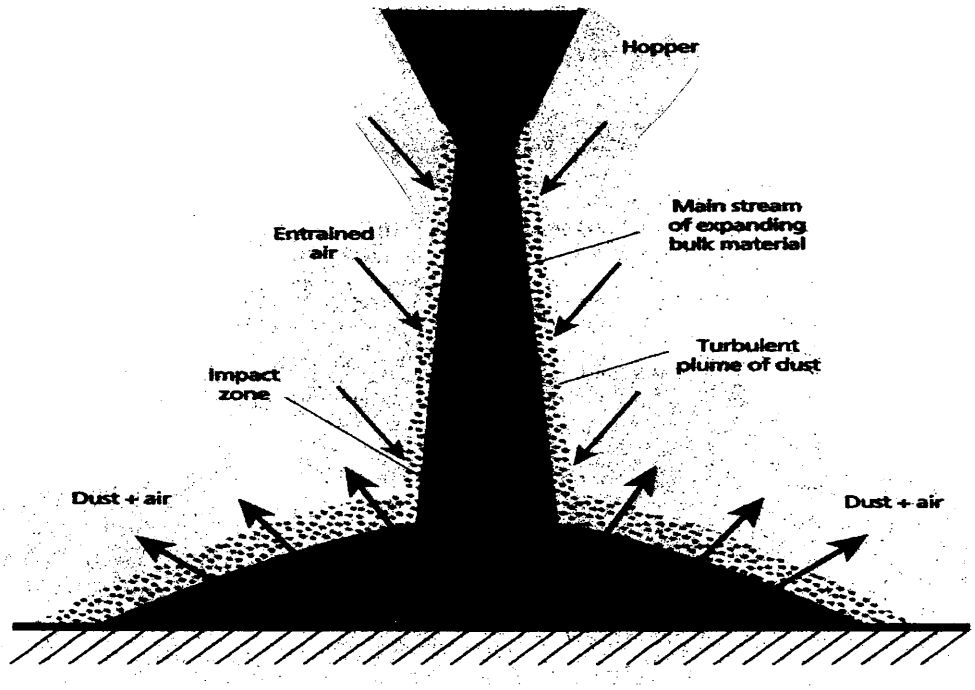


Fig. 2.3 Fugitive dust generation and entrained air result when the product falls from the outlet of a hopper (StanleyWood, 1996).

2.3.4 LIMITED CAPACITY

This problem is connected again to the rathole. When a rathole is established, 80 to 90 percent of the storage capacity of the silo will be occupied by the stable particles. The real storage capacity of the silo will therefore become effectively equal to the volume of the rathole (Johanson, 1985).

2.3.5 SEGREGATION

When the material stored contains large and small particles, i.e. a granular material with variable sized grains, the finer or the smaller particles will accumulate near the discharge (Johanson, 1985; Thomson, 1985; Knowlton *et al.*, 1994; Jenike & Johanson, 1999). Conversely, the coarse or large particles will remain at the top of the bin. The main problem here is that the product discharged at the beginning is mostly a fine powder. This product may not satisfy the product quality, in addition, a rathole or an arch may be formed by the particles (Johanson, 1985; Knowlton *et al.*, 1994).

If the operation of filling and discharging continues with the same problem unresolved, multi-layers of fine and coarse materials will be formed and the problem will become more severe (Knowlton *et al.*, 1994). Figure 2.4 shows the multi-layers resulting from the segregation problem.

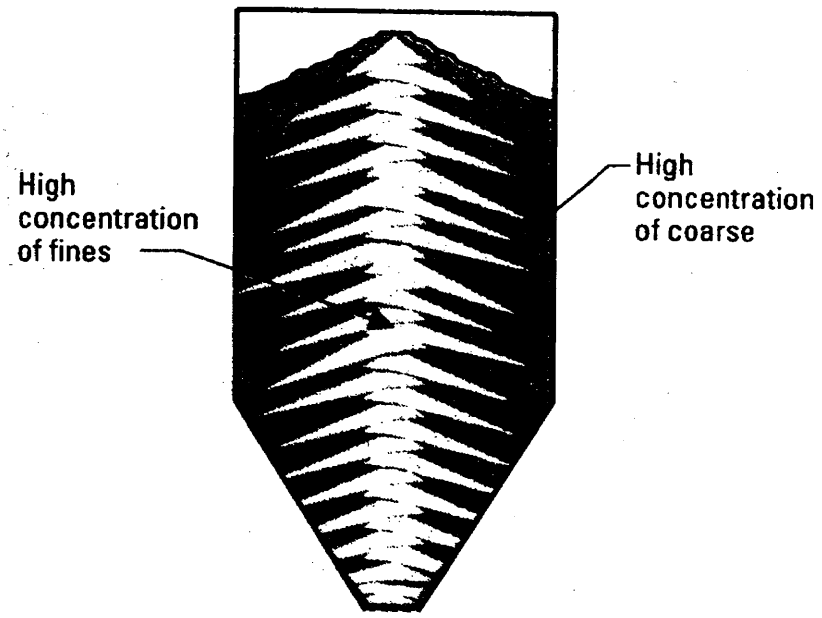


Fig. 2.4 Sifting segregation in a storage bin (Knowlton *et al.*, 1994).

2.3.6 DEGRADATION

Degradation is a result of bad storing and discharging techniques. Examples are spoilage of food products and agglomeration of fine powders after a long stay in the bin. Degradation can be a result of fracturing the particles by falling into the silo or by large pressure combined with friction with other particles or walls while moving down the silo or the hopper (Johanson, 1985).

2.3.7 OTHER PROBLEMS

In addition to the previously mentioned problems, structural failure and non-uniform flow can also cause real trouble as well. The former problem results from bad judgement or underestimating of loads exerted on the hopper. The latter is caused by the breakage of the arches of particles and will decrease the efficiency and cost effectiveness of the process (Berkovitch, 1983; Knowlton *et al.*, 1994).

Berkovitch presented a useful summary of the different problems and the expected cause of each of them. Table 2.1 lists these problems with the most obvious reason for each.

Table 2.1 Hopper discharge problems and reasons.

Problem	*Reason*
• No flow	❖ Outlet too small
• Flow does not occur after other than a short storage time	❖ No allowance made during design for the time consolidation during storage
• Incomplete emptying	❖ Outlet of core flow hopper too small or walls not steep enough
• Flooding and starving alternately	❖ Intermittent unstable arching occurring some distance above outlet
• Irregular flow	❖ Lumps of material breaking off an arch which is slightly unstable
• Segregation during discharge	❖ Rolling segregation occurring as material flows into the discharging core of a core flow hopper
• Low flowrate	❖ Outlet too small
• Fracture of hopper wall	❖ Wall strength too low for the stresses occurring on discharge

2.4 FLOW PATTERNS IN BINS AND HOPPERS

The problems mentioned previously are direct results of the different flow patterns which occur in a hopper. The flow pattern is mainly concerned with the flow of particles from the hopper discharge and how this is connected with the flow of the whole material in the bin or the silo (Johanson, 1985; Kooi, 1999). Three flow patterns can be identified; these are mass flow, funnel flow and expanded flow.

2.4.1 MASS FLOW

In mass flow, all the material inside the hopper will move when some of the product is taken away from the outlet (Thomson, 1985; Gao, 1997; Das *et al.*, 1997; Jenike & Johanson, 1999; Kooi, 1999). Mass flow hoppers are most appropriate for fine

powders, cohesive bulk material, particles that degrade if exposed to long periods of time without movement and for cases where segregation is involved (Johanson, 1985; Marinelli and Carson, 1992). The mass flow pattern is shown in figure 2.5.

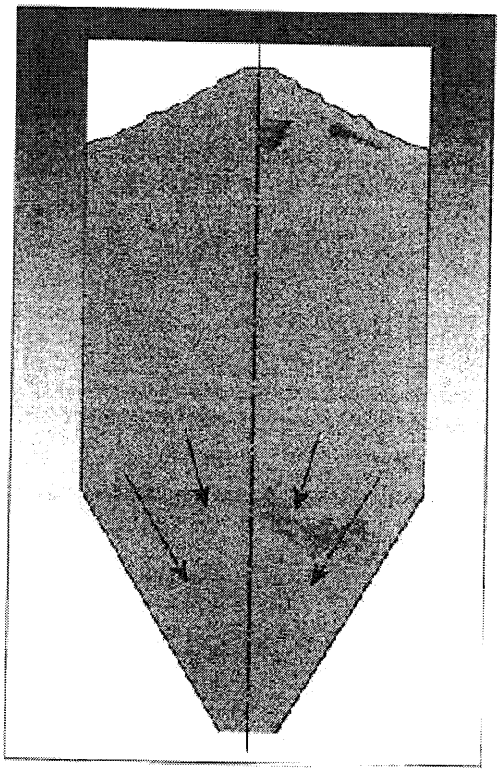


Fig. 2.5 The mass flow pattern (Marinelli and Carson, 1992).

2.4.2 FUNNEL FLOW

This type of flow is also called core flow. In funnel flow, some of the material moves out of the hopper while the rest stays stationary (Das *et al.*, 1997; Jenike & Johanson, 1999; Kooi, 1999). Funnel flow bins are characterised by shallow hopper walls and large storage capacity with no need for tall installations (Johanson, 1985). The particles that will accumulate in the stagnant zones when funnel flow occurs will cause the following problems:

- Ageing and decay of the stored material that forms the stagnant zones.
- Contamination and mixing between different products (if more than one product is stored in the bin) (Kooi, 1999).
- Growth of the stagnant zone to form a rathole.
- Uncontrollable flow when stagnant zones collapse.

Funnel flow bins will be the economical choice when dealing with coarse, non-degrading, free-flowing solids and if segregation is unimportant (Johanson, 1985; Knowlton *et al.*, 1994; Kooi, 1999). A representation of funnel flow pattern is shown below in figure 2.6.

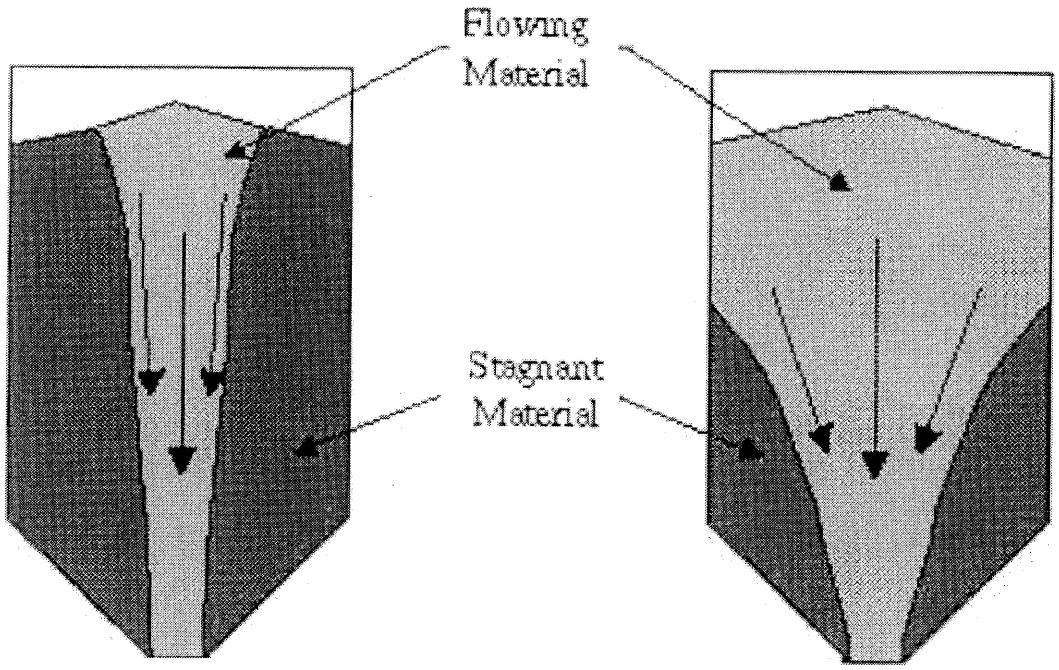


Fig. 2.6 The funnel flow pattern (Jenike & Johanson, 1999).

Mass and funnel flow patterns each have some advantages and disadvantages. Table 2.2 summarises the main merits and demerits of both mass flow and funnel flow hoppers.

Table 2.2 Advantages and disadvantages of mass and funnel flow hoppers.

	Advantages	*Disadvantages*
Mass flow	❖ First in first out ❖ No formation of stagnant areas ❖ Smaller outlet size is needed ❖ No formation of rathole or arching ❖ Steady flow with controllable discharge	❑ Tall structure ❑ Wear effects at the wall ❑ More expensive
Funnel flow	❖ less expensive ❖ Minimum headroom is required	❑ First in- last out ❑ Formation of rathole ❑ Segregation ❑ Decreasing silo capacity ❑ Uncontrollable flow when the arch or the rathole collapse ❑ Collapsing as a result of unbalanced loads due to the formation and breakdown of stagnant zones

2.4.3 EXPANDED FLOW

Expanded flow is a combination of both mass flow and funnel flow (Jenike & Johanson, 1999). It is developed when the hopper is designed to operate with a mass flow pattern at the lower part and a funnel flow pattern located above the mass flow section (Roberts and Scott, 1991; Jenike & Johanson, 1999).

Storage bins with expanded flow arrangements are used for large storage capacities, at the same time, tall constructions are not needed (Roberts and Scott, 1991). Figure 2.7 demonstrates the shape and the flow patterns formed in an expanded flow hopper.

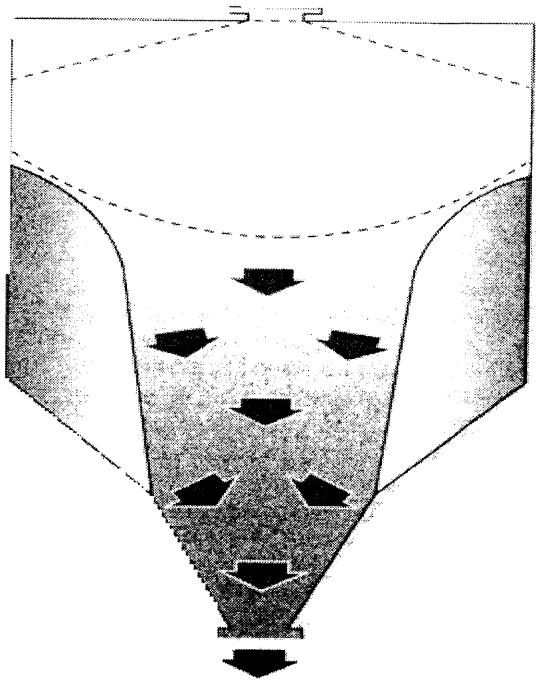


Fig.2.7 The expanded flow pattern (Bates, 1996).

2.5 DESIGN METHODS FOR HOPPERS

In order to achieve a mass flow pattern, that is a flow with least potential problems, three main parameters need to be determined. These three parameters are the wall angle to achieve mass flow; the outlet size and the discharge rate required (Marinelli and Carson, 1992). Figure 2.8, demonstrates the basic design parameters, that is, the wall angle and the outlet size.

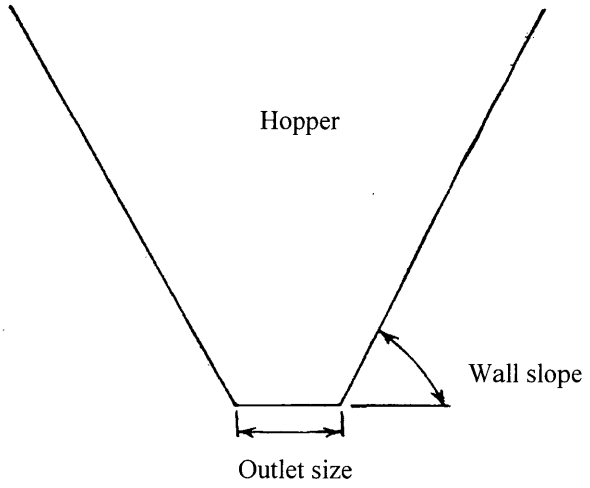


Fig. 2.8 Basic design for hoppers (Das *et al.*, 1997).

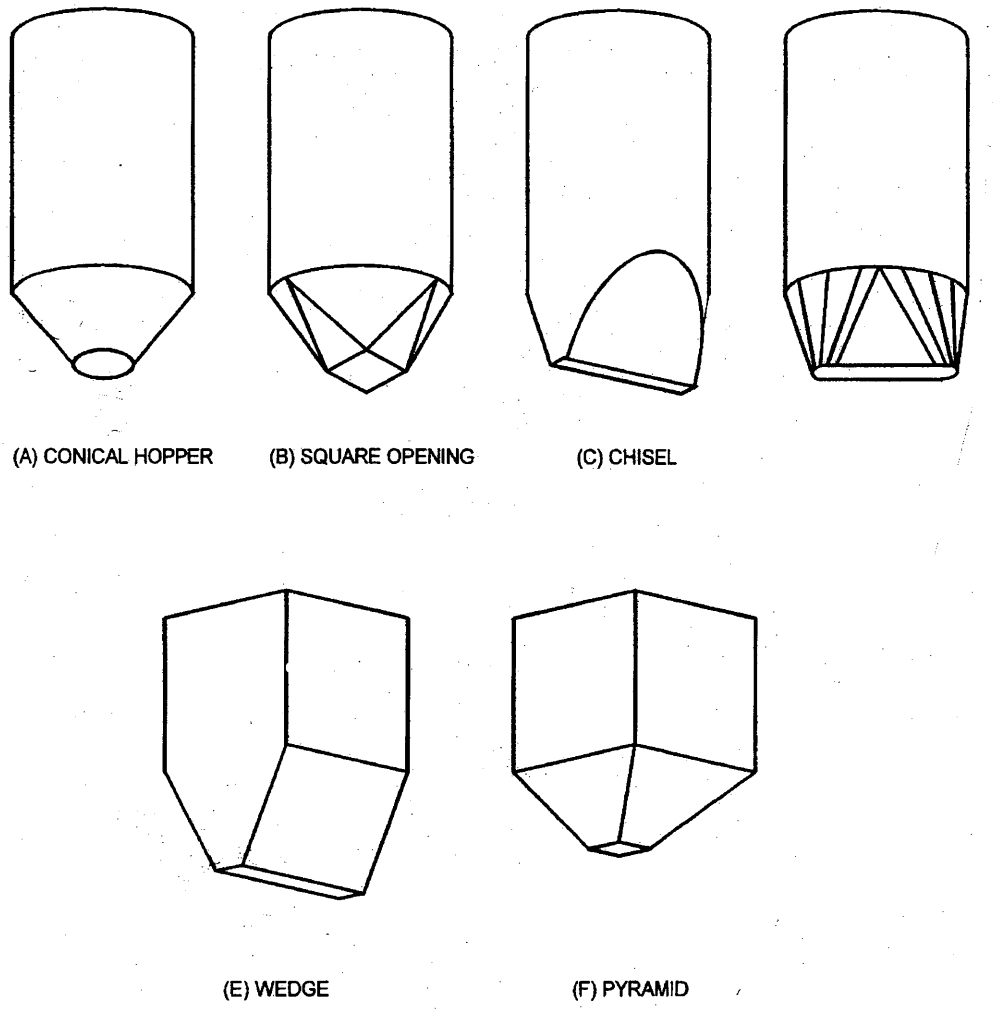
2.5.1 WALL ANGLE

Two main factors are used to determine the wall angle of a hopper. These are the frictional resistance of the material sliding against the wall and the hopper geometry (Johanson, 1985; Marinelli and Carson, 1992). Wall material, temperature, moisture, corrosion, abrasion wear and time at rest all affect the wall friction (Marinelli and Carson, 1992). A steeper wall angle is required for higher wall frictions in order to achieve mass flow. The required design charts that relate the angle of wall friction and the required hopper wall can be found in Johanson (1985) and Thomson (1985).

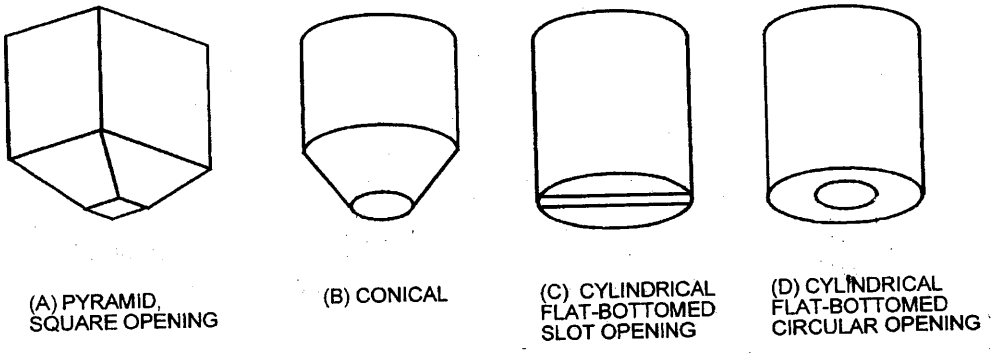
Many shapes of hoppers are available, among these are conical, wedge, pyramid, chisel, etc. The shape of the hopper also affects the choice of the wall angle and different design charts are available for each shape. Different shapes and configurations of mass flow and funnel flow designs are given in figure 2.9.

2.5.2 OUTLET SIZE DETERMINATION

This is a very important parameter in designing a hopper. Choosing the right size will prevent arching in mass flow or ratholing in funnel flow hoppers (Johanson, 1985). The minimum outlet size in order to avoid the two problems mentioned above is related to the size of the particles. If the particles have a size of 4 inches (100 mm) or larger, then a circular outlet should be 6 to 8 times the largest particle size. For wedge hoppers, the opening width should be at least 3 to 4 times the size of the largest particle (Marinelli and Carson, 1992). For particles less than 4 inches in size the flow function and the flow factor should be determined. The flow function is a measure of the relationship between cohesive strength of a bulk solid and consolidating pressure



Mass flow hoppers



Funnel flow hoppers

Fig. 2.9 Common designs for mass flow and funnel flow hoppers (Chase, 1999).

(Johanson, 1985; Marinelli and Carson, 1992). The flow factor is defined as the ratio of the major consolidating pressure at a point in the hopper to the minimum stress in the abutment of an arch at this point (Johanson, 1985).

Equations to calculate the flow function and the flow factors in addition to design charts relating these two parameters with the required outlet size are given in Johanson (1985) and Thomson (1985).

2.5.3 FLOWRATE MEASUREMENT

The flow rate measurement is concerned with calculating the maximum rate of discharge of the bulk material given the particle size and the outlet dimensions. For coarse particles, this is far in excess of the required rate, however, fine powders possess lower maximum discharge rates at the hopper outlet (Marinelli and Carson, 1992).

For coarse and free flowing material, the following equation, given by Johanson (1985) can be used:

$$Q = \rho_b A \sqrt{\frac{D_w g}{2(1+m)\tan\alpha}} \tag{2.1}$$

Where

Q : maximum rate of discharge,

ρ_b : bulk density of solid,

A : cross sectional area of the outlet,

D_w : diameter of circular outlet or width of rectangular outlet,

g : acceleration due to gravity,

α: hopper half angle measured from vertical,

m =1 for conical hoppers, 0 for wedge hopper

Factors that affect flow rates of fine powders are particle size and shape, the level of material in the bin, the residence time and outlet size and shape.

2.6 PREDICTION OF DISCHARGE RATES FROM HOPPERS

Different attempts to predict the discharge rates from hoppers have been reviewed by Nedderman *et al.* (1982). In their paper, they covered the work done on this topic since 1895 to the year the paper was published. Since then, Nedderman and many researchers have continued their work both experimentally and theoretically to improve equations and models representing the flow rates. The main correlations developed to predict the discharge rate, both experimentally and theoretically, are highlighted below. Most of the equations represented here are taken from Nedderman *et al.* (1982) except more recent equations developed since 1982.

2.6.1 EXPERIMENTAL CORRELATIONS

Most of the initial work done to predict the mass flow rate (W) was concerned with the effect of the height (H), that is the quantity of the material in the hopper, on the discharge rate. Researchers attempted to get a correlation between W and H and to specify a critical height above which W is independent of H. The outcome of these attempts was that W is independent of H except for small values of H when the hopper is nearly empty. However, there is no agreement on the critical height below which an effect will be noticed on the discharge rate.

Using dimensional analysis, W was correlated with the hopper outlet diameter D_o by $W \propto \rho\, g^{1/2}\, D_o^{5/2}$ by ignoring the effect of the particle diameter (d), where ρ is the initial bulk density achieved during the filling process and g is the acceleration due to gravity.

In 1961, Beverloo did more work on the previous relation between W and D_o and proposed this relation:

$$W = C\rho\sqrt{g}\left(D_o - k\,d\right)^{5/2} \tag{2.2}$$

Where k is a constant that depends on the particle shape with a value of about 1.5 for spherical particles and C was found to be in the range 0.55 – 0.65.

Huntington and Rooney in 1971 used the same expression but with a different value for the density and the constant C

$$W = C'\rho_f\sqrt{g}\left(D_o - k\,d\right)^{5/2} \tag{2.3}$$

Where C' is in the range 0.575-0.595 and ρ_f is the flowing density defined as the ratio of the mass flow rate to the volumetric flow rate calculated from the observed rate of descent of the top surface. All the previous correlations are inapplicable when d is less than 500 μm, that is for fine materials (Nedderman *et al.*, 1982).

In 1959, Fowler and Glastonbury studied the effect of the orifice shape on the discharge rate and they reported the following equation

$$W \propto A\sqrt{D_h}\left(D_h / d\right)^{0.185} \tag{2.4}$$

Where A is the area of the orifice and D_h is the orifice hydraulic mean diameter. Following the Beverloo's approach the above correlation could be written as:

$$W = \frac{4C}{\pi}\rho A^*\left(g\, D_h^*\right)^{0.5} \tag{2.5}$$

In the above equation, $4C/\pi > 0.75$ and A^* is the area, and D_h^* is the hydraulic mean diameter of the space remaining after a zone of width $0.5\ k\ d$ has been removed from the perimeter of the orifice.

In 1977 Myers and Sellers worked on rectangular orifices of size b_s x l where b_s is the breadth of a slot orifice and l is the slot length and $b_s << l$, and here $D_h = 2b_s$. Their results are given in the following equation:

$$W = 1.03\,\rho\sqrt{g}\,(l - k\,d)\left(b_s - k\,d\right)^{3/2} = 0.73\,\rho\,A^*\sqrt{g\,D_h^*} \tag{2.6}$$

Rose and Tanaka (1959) studied the effect of wall friction on the flow rate and they suggested using a multiplicative factor F(α, χ) given by

$$F(\alpha, \chi) = (\tan\alpha \tan\chi)^{-0.35} \quad \alpha < 90 - \chi \tag{2.7}$$

$$F(\alpha, \chi) = 1 \quad \alpha \geq 90 - \chi \tag{2.8}$$

Here, χ is the inclination to the horizontal of the stagnant boundary when core flow occurs and α is the hopper half angle, which is the angle between the wall and the centreline of the discharge orifice for axi-symmetric hoppers. It is important to stress again that all the mentioned equations were reported in Nedderman *et al.* (1982).

2.6.2 THEORETICAL PREDICTION OF THE MASS FLOWRATE

Davidson and Nedderman in 1973 predicted the mass flow rate for a conical hopper by

$$W = \frac{\pi}{4}\frac{\rho\sqrt{g}D_o^{5/2}}{\sqrt{\sin\alpha}}\left(\frac{1+K}{2(2K-3)}\right)^{0.5} \tag{2.9}$$

Where

$$K = \frac{1+\sin\phi}{1-\sin\phi} \tag{2.10}$$

And ϕ is the angle of internal friction.

Equation 2.9 can be used only for narrow angled, smooth-walled hoppers and it over-predicts the mass flow rate (Verghese and Nedderman, 1993).

For an orifice of width b_c in a chisel shaped hopper of thickness l_c, the following equation is reported

$$W = \frac{\rho\sqrt{g}\,l_c\,b_c^{3/2}}{\sqrt{sin\alpha}}\left(\frac{1+K}{2(K-2)}\right)^{1/2} \tag{2.11}$$

K in the above equation is similar to K in equation 2.9 and can be calculated using equation (2.10)

Verghese and Nedderman (1993) reported another theoretical based equation which can be used for wider angles

$$W = C^{*} \rho \sqrt{g}\ D_o^{5/2} \tag{2.12}$$

In the above equation, C^{*} can be represented by

$$C^{*} = \frac{2\pi(1-\cos\alpha)}{M(2\sin\alpha)^{2.5}} \sqrt{\frac{1+K^{*}}{2K^{*}-3}} \tag{2.13}$$

And the method to calculate K^{*} and M is given in detail in Verghese and Nedderman, 1993.

2.6.3 EFFECT OF INTERSTITIAL PRESSURE GRADIENTS

In addition to the previous work, the effect of interstitial pressure on the flow rate was also reviewed by Nedderman *et al.* (1982). Different equations to correlate the flowrate with the pressure gradients were presented, some of these are given below:

Bulsara, Zenz and Eckert in 1964 reported the following equation

$$W = C_D (\rho_b \Delta P)^{1/2} (D_o - k\,d)^2 \tag{2.14}$$

Where C_D is the drag coefficient, ρ_b is the bulk density and ΔP is the pressure difference.

Equation (2.14) incorrectly suggests that W tends to zero as $\Delta P \rightarrow 0$. This was corrected by McDoughall and Knowles in 1969 in their equation

$$W = K_1 \left(\Delta P_o + \Delta P\right)^{1/2} D_O^{5/2} \tag{2.15}$$

K_1 is an empirical function of the material properties.

In other work, researchers argued that both the weight of the particles in addition to the interstitial pressure would influence the flow rate.

Crewdson, Ormond and Nedderman in 1977 suggested to use the following equation

$$W = C\,\rho_b \left(g + \frac{1}{\rho_b} \frac{\mathrm{d}p}{\mathrm{d}r}\Big|_{r_o} \right)^{1/2} \left(D_o - k\,d\right)^{5/2} \tag{2.16}$$

In the above equation, C is the Beverloo coefficient and $(\mathrm{d}p/\mathrm{d}r)|\mathrm{r_o}$ is the pressure gradient at the orifice.

Harrison and Mushin in 1979 suggested that there should be an extra constant in the previous equation

$$W = C\,\rho_b \left(g + \frac{C'}{\rho_b} \frac{\mathrm{d}p}{\mathrm{d}r}\Big|_{r_o} \right)^{1/2} \left(D_o - k\,d\right)^{5/2} \tag{2.17}$$

Where they predicted that

$$C' = \frac{2K - 3}{2K - 1} \tag{2.18}$$

For most granular materials K has a large value and C' is very close to unity (Nedderman *et al.*, 1982).

Ducker *et al.* (1985) and Gu *et al.* (1992) have given more equations to calculate the discharge rate by considering that the flow is driven by both the weight of the particles and the interstitial pressure.

2.7 MODELLING OF GRANULAR FLOW IN HOPPERS

The flow of particulate solids is a complicated process which requires further investigation and study. Most of the work done to model granular flow in hoppers is based on two approaches. The first approach models the grains as discrete particles. It predicts the forces acting on individual grains and the velocity of each grain comprising the system. The second approach considers the granular material as a continuum and deals with average values of velocities and stresses. In this method, the granular material is either treated as a fluid (Haff, 1983; Hogue and Newland, 1994) or as a plastic material (Spencer, 1964; Brennen and Pearce, 1978; Mehrabadi and Cowin, 1978).

The discrete particle approach solves the equations resulting for each of the individual particles, and this makes the simulation very lengthy. In addition, it requires a large computational ability and it is therefore limited to either two dimensional or small three-dimensional problems. On the other hand, the continuum approach needs less simulation time and computational ability since it requires fewer equations.

This section aims to introduce the main requirements needed to model granular flows as a continuum. The fundamental physical quantities required to model granular flows

are the velocity, the stress and the bulk density. These physical quantities, which are also called field variables, are defined everywhere in the material and in which the forces are represented as stresses. To solve the problem of hopper flow, the following ingredients are required:

1) Governing equations,

2) Hopper geometry,

3) Boundary conditions.

All of these items are essential to find the values of the field variables in the granular material flow.

The equations governing the continuum theory are the momentum equations, the continuity equation and the constitutive equations. Examples of constitutive equations are those for a Newtonian fluid and those for plastic deformation of granular materials.

To give an idea about the models available to represent granular flow, some examples of the models available are presented. Details concerning these models may be found in the original references.

2.7.1 UNIVERSAL EQUATIONS GOVERNING FLUID AND BULK SOLIDS FLOW

The flow and deformation of matter may be represented by universal equations regardless of its state as solid or fluid. These equations are valid for all continua (solids, liquids and gases) and are of two types, the equations of motion and the

continuity equation. Equations (2.19-2.21) are the equations of motion written in terms of rectangular Cartesian co-ordinates (Deen, 1998).

X component:

$$\rho\left[\frac{\partial \upsilon_x}{\partial t}+\upsilon_x\frac{\partial \upsilon_x}{\partial x}+\upsilon_y\frac{\partial \upsilon_x}{\partial y}+\upsilon_z\frac{\partial \upsilon_x}{\partial z}\right]=\rho g_x+\frac{\partial \sigma_{xx}}{\partial x}+\frac{\partial \sigma_{xy}}{\partial y}+\frac{\partial \sigma_{xz}}{\partial z} \qquad (2.19)$$

Y component:

$$\rho\left[\frac{\partial \upsilon_y}{\partial t}+\upsilon_x\frac{\partial \upsilon_y}{\partial x}+\upsilon_y\frac{\partial \upsilon_y}{\partial y}+\upsilon_z\frac{\partial \upsilon_y}{\partial z}\right]=\rho g_y+\frac{\partial \sigma_{xz}}{\partial x}+\frac{\partial \sigma_{yz}}{\partial y}+\frac{\partial \sigma_{zz}}{\partial z} \qquad (2.20)$$

Z component:

$$\rho\left[\frac{\partial \upsilon_z}{\partial t}+\upsilon_x\frac{\partial \upsilon_z}{\partial x}+\upsilon_y\frac{\partial \upsilon_z}{\partial y}+\upsilon_z\frac{\partial \upsilon_z}{\partial z}\right]=\rho g_z+\frac{\partial \sigma_{xz}}{\partial x}+\frac{\partial \sigma_{yz}}{\partial y}+\frac{\partial \sigma_{zz}}{\partial z} \qquad (2.21)$$

In the above equations:

ρ is the density,

υ_x, υ_y, and υ_z are the velocity components in the x, y and z directions respectively,

g_x, g_y, and g_z are the gravitational forces in the x, y and z directions respectively,

σ_{xx}, σ_{yy} and σ_{zz} are the normal stresses in the x, y and z directions respectively,

σ_{xy}, σ_{xz} and σ_{yz} are the shear stresses.

For fluids i.e. liquids and gases, where the hydrostatic pressure P plays a special role then it is usual to write

$$\boldsymbol{\sigma} = \boldsymbol{\tau} - P\boldsymbol{I} \qquad (2.22)$$

Where

$\boldsymbol{\sigma}$ is the total stress tensor,

τ is the viscous stress tensor,

and I denotes the identity tensor.

So the equations of motion for liquids and gases can be written as:

X component:

$$\rho\left[\frac{\partial \upsilon_x}{\partial t}+\upsilon_x\frac{\partial \upsilon_x}{\partial x}+\upsilon_y\frac{\partial \upsilon_x}{\partial y}+\upsilon_z\frac{\partial \upsilon_x}{\partial z}\right]=\rho g_x+\frac{\partial \tau_{xx}}{\partial x}+\frac{\partial \tau_{xy}}{\partial y}+\frac{\partial \tau_{xz}}{\partial z}-\frac{\partial P}{\partial x} \quad (2.23)$$

Y component:

$$\rho\left[\frac{\partial \upsilon_y}{\partial t}+\upsilon_x\frac{\partial \upsilon_y}{\partial x}+\upsilon_y\frac{\partial \upsilon_y}{\partial y}+\upsilon_z\frac{\partial \upsilon_y}{\partial z}\right]=\rho g_y+\frac{\partial \tau_{xy}}{\partial x}+\frac{\partial \tau_{yy}}{\partial y}+\frac{\partial \tau_{yz}}{\partial z}-\frac{\partial P}{\partial y} \quad (2.24)$$

Z component:

$$\rho\left[\frac{\partial \upsilon_z}{\partial t}+\upsilon_x\frac{\partial \upsilon_z}{\partial x}+\upsilon_y\frac{\partial \upsilon_z}{\partial y}+\upsilon_z\frac{\partial \upsilon_z}{\partial z}\right]=\rho g_z+\frac{\partial \tau_{xz}}{\partial x}+\frac{\partial \tau_{yz}}{\partial y}+\frac{\partial \tau_{zz}}{\partial z}-\frac{\partial P}{\partial z} \quad (2.25)$$

Where

τ_{xx}, τ_{yy} and τ_{zz} are the normal viscous stresses in the x, y and z directions respectively,

τ_{xy}, τ_{xz} and τ_{yz} are the viscous shear stresses.

The other equation which is required is the continuity equation, which expresses the conservation of mass of the material,

$$\frac{\partial \rho}{\partial t}+\upsilon_x\frac{\partial \rho}{\partial x}+\upsilon_y\frac{\partial \rho}{\partial y}+\upsilon_z\frac{\partial \rho}{\partial z}=-\rho\left(\frac{\partial \upsilon_x}{\partial x}+\frac{\partial \upsilon_y}{\partial y}+\frac{\partial \upsilon_z}{\partial z}\right) \quad (2.26)$$

2.7.2 CONSTITUTIVE EQUATIONS FOR FLUID FLOW

The constitutive equations are necessary to relate the stresses to the rate of strain and to material properties. For fluids, the constitutive equations which express the viscous stresses in terms of velocity gradients and the fluid viscosity μ for Newtonian fluids in rectangular co-ordinates are given below:

$$\tau_{xx} = 2\mu\frac{\partial \upsilon_x}{\partial x} - \frac{2}{3}\mu\left(\frac{\partial \upsilon_x}{\partial x} + \frac{\partial \upsilon_y}{\partial y} + \frac{\partial \upsilon_z}{\partial z}\right) \tag{2.27}$$

$$\tau_{yy} = 2\mu\frac{\partial \upsilon_y}{\partial y} - \frac{2}{3}\mu\left(\frac{\partial \upsilon_x}{\partial x} + \frac{\partial \upsilon_y}{\partial y} + \frac{\partial \upsilon_z}{\partial z}\right) \tag{2.28}$$

$$\tau_{zz} = 2\mu\frac{\partial \upsilon_z}{\partial z} - \frac{2}{3}\mu\left(\frac{\partial \upsilon_x}{\partial x} + \frac{\partial \upsilon_y}{\partial y} + \frac{\partial \upsilon_z}{\partial z}\right) \tag{2.29}$$

$$\tau_{xy} = \mu\left(\frac{\partial \upsilon_x}{\partial y} + \frac{\partial \upsilon_y}{\partial x}\right) \tag{2.30}$$

$$\tau_{yz} = \mu\left(\frac{\partial \upsilon_y}{\partial z} + \frac{\partial \upsilon_z}{\partial x}\right) \tag{2.31}$$

$$\tau_{xz} = \mu\left(\frac{\partial \upsilon_z}{\partial x} + \frac{\partial \upsilon_x}{\partial z}\right) \tag{2.32}$$

Substituting equations (2.27-2.32) in equations (2.23-2.25) and assuming that a fluid has a constant viscosity and density we can obtain the equations of motion for Newtonian fluids in the x, y and z co-ordinates respectively:

$$\rho\left[\frac{\partial \upsilon_x}{\partial t}+\upsilon_x\frac{\partial \upsilon_x}{\partial x}+\upsilon_y\frac{\partial \upsilon_x}{\partial y}+\upsilon_z\frac{\partial \upsilon_x}{\partial z}\right]=\mu\left[\frac{\partial^2 \upsilon_x}{\partial x^2}+\frac{\partial^2 \upsilon_x}{\partial y^2}+\frac{\partial^2 \upsilon_x}{\partial z^2}\right]-\frac{\partial P}{\partial x}+\rho g_x \quad (2.33)$$

$$\rho\left[\frac{\partial \upsilon_y}{\partial t}+\upsilon_x\frac{\partial \upsilon_y}{\partial x}+\upsilon_y\frac{\partial \upsilon_y}{\partial y}+\upsilon_z\frac{\partial \upsilon_y}{\partial z}\right]=\mu\left[\frac{\partial^2 \upsilon_y}{\partial x^2}+\frac{\partial^2 \upsilon_y}{\partial y^2}+\frac{\partial^2 \upsilon_y}{\partial z^2}\right]-\frac{\partial P}{\partial y}+\rho g_y \quad (2.34)$$

$$\rho\left[\frac{\partial \upsilon_z}{\partial t}+\upsilon_x\frac{\partial \upsilon_z}{\partial x}+\upsilon_y\frac{\partial \upsilon_z}{\partial y}+\upsilon_z\frac{\partial \upsilon_z}{\partial z}\right]=\mu\left[\frac{\partial^2 \upsilon_z}{\partial x^2}+\frac{\partial^2 \upsilon_z}{\partial y^2}+\frac{\partial^2 \upsilon_z}{\partial z^2}\right]-\frac{\partial P}{\partial z}+\rho g_z \quad (2.35)$$

2.7.3 MAIN DIFFERENCES BETWEEN FLUID FLOW AND BULK SOLIDS FLOW

Haff (1983) explained in detail how granular material can be considered as a fluid. He mentioned 7 ways in which granular material and fluids differ, below are some of these:

- Grain size vs. Molecule size

The main difference here is that grains have larger sizes (or masses) than molecules in a fluid. The grain size has a crucial effect on the application of the continuum hypothesis, however, as far as the microscopic description of particle motion is concerned, laws of classical mechanics can be applied to both grains and molecules.

- Grains are not identical particles

Molecules in a fluid are identical, however, this is not the case in a granular system. Grains tend to have different shapes and no two of them are precisely the same. So in order to apply the continuum approach, all the grains are assumed to have approximately the same size.

- Noncentral grain- grain interaction

Grains are not spherical and they usually have rough surfaces. Consequently, when they collide, frictional forces are present which will lead to the rotation of the grains as they move. In a simple fluid system, the macroscopic friction force does not exist.

Jenike (1964) reported that particulate solids and liquids exhibit different behaviour as they flow due to the differences between the properties of solid particles and fluids. In addition, he discussed the fundamental differences between particulate solids and liquids which make the mechanisms of flow for these two states of matter quite different.

The first difference is that solids have a static angle of friction greater than zero so they can support shearing stresses under static conditions. On the other hand, liquids can not support shearing stresses under static conditions and this is why liquids form level surfaces while solids form piles.

Another difference appears when particulate solids are consolidated or subjected to pressure. After applying pressure on solid particles, they possess strength and may retain a shape if the load is maintained. A stable dome or well could be formed under pressure whereas in a liquid this can not happen.

Lastly, the shearing stresses generated when granular materials flow is independent of the rate of shear and mainly dependent on the mean pressure within the solid. The situation is totally different in liquids where the shearing stresses are dependent on the rate of shear and independent of the mean pressure.

In addition to these differences reported by Jenike(1964), Haff (1997) gave a further reason for the major differences between solids and fluids. There is no approximation involved in the assumption that all fluid molecules have identical properties. However, for granular materials, e.g. sand grains, every grain in the sample is physically different from each other. So in the case of granular materials, no two diameters, masses, shapes or friction coefficients are the same. As a result, he concluded that constitutive equations which are able to predict the flow of fluids very well are not suitable to be used to represent the flow of granular materials.

These differences give an idea why the flow criteria of particulate solids is different from fluid flow and this leads us to consider the granular particles as a plastic material rather than a viscous fluid. In the following section, a short account of plasticity models is given.

2.7.4 CONSTITUTIVE EQUATIONS FOR BULK SOLIDS FLOW

For granular flow, many models are available in the literature. The first constitutive equation is the yield condition. One form of the yield criterion is the Mohr-Coulomb condition:

Where

$$|\tau_n| = c + \sigma_n \tan\phi \tag{2.36}$$

$|\tau_n|$ is the magnitude of the shear stress on a plane,

σ_n is the effective normal stress on the plane,

n denotes the normal direction to the plane,

c is the cohesion,

and ϕ is the angle of internal friction.

Many models which represent the other constitutive equations needed to solve the problem of granular flow are available in the literature. The equations given in the models are used in addition to the equations of motion (2.19-2.21) and the continuity equation (2.26) presented before. All the models are two dimensional in the x and y co-ordinates and all the derivatives with respect to z co-ordinate are equal to zero. Here are four of the models which have been proposed:

2.7.4.1 Jenike Model:

$$\frac{\partial \upsilon_x}{\partial x} + \frac{\partial \upsilon_y}{\partial y} = 0 \tag{2.37}$$

$$\left(\frac{\partial \upsilon_x}{\partial x} - \frac{\partial \upsilon_y}{\partial y}\right)\sin 2\psi - \left(\frac{\partial \upsilon_x}{\partial y} + \frac{\partial \upsilon_y}{\partial x}\right)\cos 2\psi = 0 \tag{2.38}$$

Where

ψ denotes the angle of inclination of the direction of the algebraically greater principal stress to the x axis and is given by:

$$\tan 2\psi = \frac{2\sigma_{xy}}{\sigma_{xx} - \sigma_{yy}} \tag{2.39}$$

Equation (2.37) is the same as equation (2.26) written for incompressible material and equation (2.38) represents the coaxiality. For further details see Brennen and Pearce (1978).

2.7.4.2 Drucker - Prager Model:

$$\left(\frac{\partial \upsilon_x}{\partial x} - \frac{\partial \upsilon_y}{\partial y}\right)\sin 2\psi - \left(\frac{\partial \upsilon_x}{\partial y} + \frac{\partial \upsilon_y}{\partial x}\right)\cos 2\psi = 0 \qquad (2.38)$$

$$\sin\phi\left[\left(\frac{\partial \upsilon_x}{\partial x} - \frac{\partial \upsilon_y}{\partial y}\right)\cos 2\psi + \left(\frac{\partial \upsilon_x}{\partial y} + \frac{\partial \upsilon_y}{\partial x}\right)\sin 2\psi\right] - \left(\frac{\partial \upsilon_x}{\partial x} + \frac{\partial \upsilon_y}{\partial y}\right) = 0 \qquad (2.40)$$

Where

ϕ denotes the angle of internal friction. See Mehrabadi and Cowin (1978).

2.7.4.3 Spencer Model:

$$\frac{\partial \upsilon_x}{\partial x} + \frac{\partial \upsilon_y}{\partial y} = 0 \qquad (2.37)$$

$$\sin 2\psi\left(\frac{\partial \upsilon_x}{\partial x} - \frac{\partial \upsilon_y}{\partial y}\right) - \cos 2\psi\left(\frac{\partial \upsilon_y}{\partial x} + \frac{\partial \upsilon_x}{\partial y}\right) + \sin\phi\left(\frac{\partial \upsilon_y}{\partial x} - \frac{\partial \upsilon_x}{\partial y} - 2\dot{\psi}\right) = 0 \qquad (2.41)$$

Where

$\dot{\psi}$ denotes the material derivative of ψ:

$$\dot{\psi} = \frac{\partial \psi}{\partial t} + \upsilon_x \frac{\partial \psi}{\partial x} + \upsilon_y \frac{\partial \psi}{\partial y} \qquad (2.42)$$

More details about this model may be obtained from Spencer (1964).

2.7.4.4 Mehrabadi and Cowin Model:

$$\sin\phi\left[\left(\frac{\partial \upsilon_x}{\partial x}-\frac{\partial \upsilon_y}{\partial y}\right)\cos 2\psi+\left(\frac{\partial \upsilon_x}{\partial y}+\frac{\partial \upsilon_y}{\partial x}\right)\sin 2\psi\right]-\left(\frac{\partial \upsilon_x}{\partial x}+\frac{\partial \upsilon_y}{\partial y}\right)\cos(\phi-\nu)=0 \quad (2.43)$$

$$\cos\phi\left[\left(\frac{\partial \upsilon_x}{\partial x}-\frac{\partial \upsilon_y}{\partial y}\right)\sin 2\psi-\left(\frac{\partial \upsilon_x}{\partial y}+\frac{\partial \upsilon_y}{\partial x}\right)\cos 2\psi\right]-\left(\left(\frac{\partial \upsilon_x}{\partial y}-\frac{\partial \upsilon_y}{\partial x}\right)+2\dot{\psi}\right)\sin(\phi-\nu)=0 \quad (2.44)$$

Where

ν is the angle of dilatancy. For more information see Mehrabadi and Cowin (1978).

2.7.4.5 De Josselin De Jong Model:

$$\frac{\partial \upsilon_x}{\partial x}+\frac{\partial \upsilon_y}{\partial y}=0 \quad (2.37)$$

$$-\left(\frac{\partial \upsilon_x}{\partial x}+\frac{\partial \upsilon_y}{\partial y}\right)-\left(\frac{\partial \upsilon_x}{\partial x}-\frac{\partial \upsilon_y}{\partial y}\right)\sin(2\psi-\phi)+\left(\frac{\partial \upsilon_x}{\partial y}+\frac{\partial \upsilon_y}{\partial x}\right)\cos(2\psi-\phi)=a_1\sin 2\phi \quad (2.45)$$

$$-\left(\frac{\partial \upsilon_x}{\partial x}+\frac{\partial \upsilon_y}{\partial y}\right)+\left(\frac{\partial \upsilon_x}{\partial x}-\frac{\partial \upsilon_y}{\partial y}\right)\sin(2\psi+\phi)-\left(\frac{\partial \upsilon_x}{\partial y}+\frac{\partial \upsilon_y}{\partial x}\right)\cos(2\psi+\phi)=a_2\sin 2\phi \quad (2.46)$$

Where

a_1 and a_2 denote magnitudes of the two rates of shear which make up the total deformation. Further details are available in De Josselin De Jong (1971).

2.8 SOME NUMERICAL METHODS TO PREDICT GRANULAR FLOW IN HOPPERS

The use of computer simulations to study granular flows has greatly increased since the early 1980s after the development in processing speed and storage capabilities of computers. These developments allow researchers to use computers that have become more powerful to study granular material systems which consist of thousands of particles (Wassgren, 1998).

Simulations can be used to model environments that are difficult to be examined experimentally. Moreover, using simulation methods, the state of the particulate system can be predicted at any time during the simulation (Wassgren, 1998).

Two of the methods available to solve the granular flow problem numerically are the Finite Element Method (FEM) and the Discrete Element Method (DEM). The first method is used to solve the equations resulting from the continuum approach (Hogue and Newland, 1994; Flekkøy and Måløy, 1998). On the other hand, the DEM is applied to equations representing the granular material as individual particles (Babic, 1995; Lu *et al.*, 1997; Wassgren, 1998).

2.8.1 THE FINITE ELEMENT METHOD (FEM)

The Finite Element Method (FEM) is used to solve the resulting differential equations and to predict the behaviour of particulate materials in silos and hoppers (Lu *et al.*, 1997). The use of FEM enables problems with more realistic assumptions to be analysed.

Rombach and Eibl (1995) used FEM to calculate the principal stress field, velocity field and the bulk density contours during the discharge of sand from a silo. The results they obtained from the numerical simulation may be used when designing a silo or a hopper. Figure 2.10 shows how they use FEM to discretise one half of a symmetric hopper to smaller sections that can be studied at different time intervals.

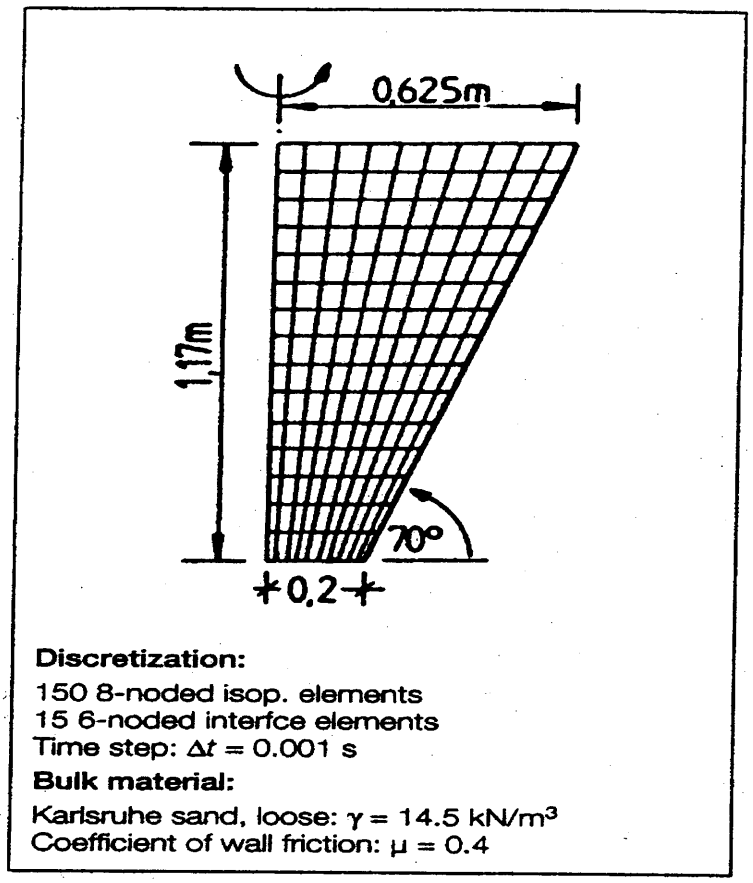


Fig. 2.10 Geometry and discretization of a hopper (Rombach and Eibl, 1995).

Another recent paper by Flekkøy and Måløy (1998) also applied the continuum approach to deal with granular flow. In their work they set a threshold density ρ_o, above this density the granular material will behave as a solid block with the container walls. On the other hand, when the density is lower than ρ_o, the granular matter behaves as a fluid governed by local drag forces. They examined the validity of their model with experiments and found an agreement between the experiments and the simulations. The agreement was on the qualitative shape of the stagnant zones as well as the exponent that governs the relation between the hopper angle and the distance from the hopper opening to the stagnant zone.

2.8.2 THE DISCRETE ELEMENT METHOD (DEM)

This approach is conceptually simpler, however, it depends mainly on the computing power available (Hogue and Newland, 1993). In this second approach, the mechanical behaviour of the granular materials is simulated by solving the equations of motion for all particles numerically (Babic, 1995). The numerical method applied here is the Discrete Element Method (DEM). Most granular flow computer simulations use the DEM method (Wassgren, 1998). This approach can be divided into three main categories of models. These are: (i) classical Newtonian dynamics model; (ii) statistical mechanics models; and (iii) hybrid models (Hogue and Newland, 1993). A brief description of the three classes is given below.

2.8.2.1 Classical Newtonian dynamics approach

In this method, Newtonian dynamical equations are applied to a system of impacting particles. By this method, all the forces and moments affecting each particle at every time step are determined. Moreover, the equations of motion are integrated to get the

new state of the granular system at each interval (Hogue and Newland, 1993). An example of this approach is the soft particle method. In this method, the forces acting on each particle are determined. Then, acceleration for each particle is calculated using Newton's second law. Finally, the resulting accelerations for each particle are integrated in time to find the new particle states and locations (Wassgren, 1998). Figure 2.11 shows a flowchart of the simulation procedure.

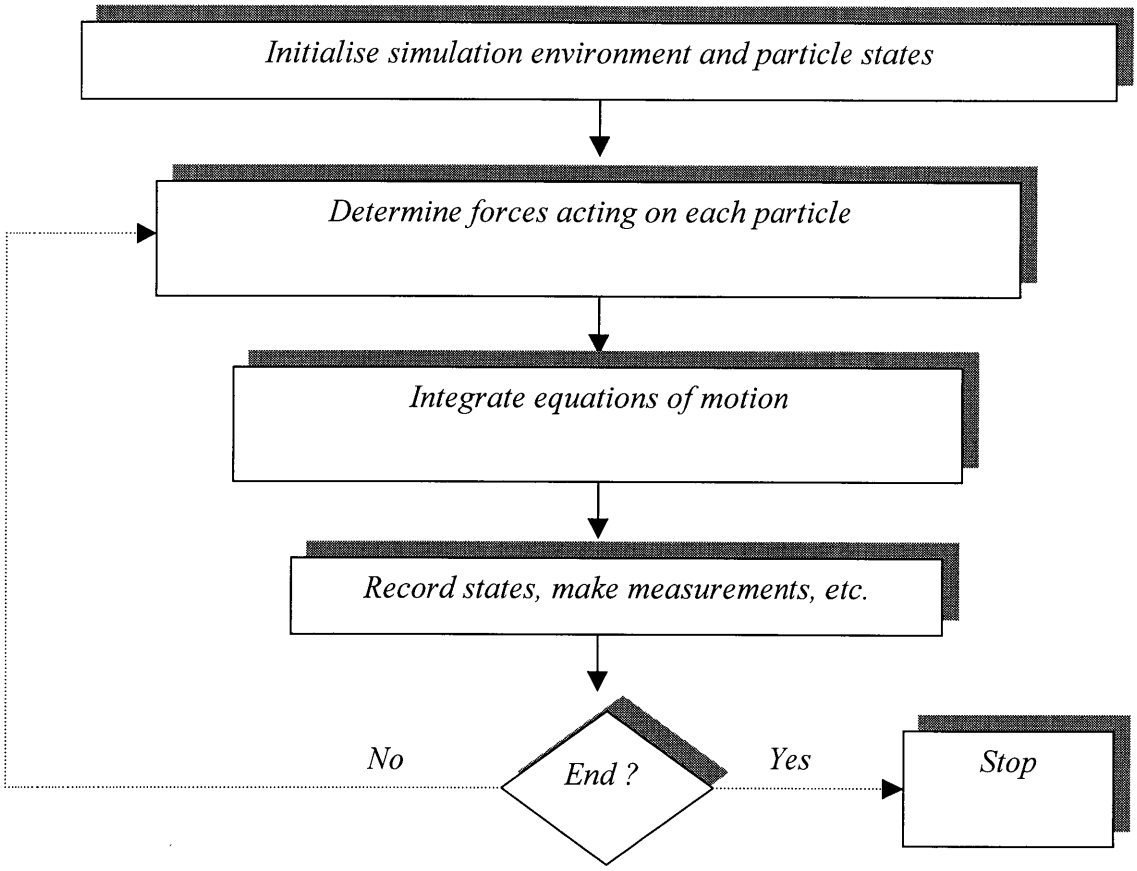


Fig. 2.11 A flowchart of the soft particle method (Wassgren, 1998).

In order to calculate the forces acting on each particle in the system, a force model should be developed. Gravity forces are considered as body forces. Furthermore,

surface forces resulting from contact between particles can be determined using a model shown in figure 2.12.

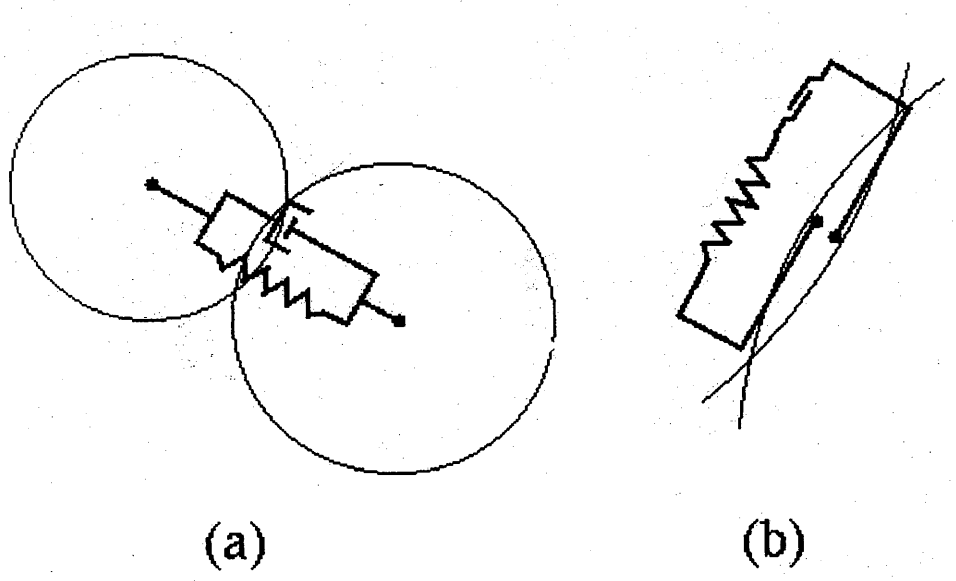


Fig. 2.12 A typical contact force model used in the soft particle technique. Figure (a) shows the contact model in the normal direction and figure (B) shows the contact model in the tangential direction (Wassgren, 1998).

The above model which was originally proposed by Cundall and Strack in 1979, consists of a linear damped spring in the normal direction between two particles and a linear spring in series with a sliding friction element in the tangential direction. The springs provide an elastic restoration force while the dashpot and sliding friction element dissipate energy in the contact (Wassgren, 1998).

The large computational power required to apply this method prevents it from being used efficiently as a design tool or in industrial applications. Another disadvantage is the difficulty of handling more than one shape of grain at the same time e.g. spherical and polygonal shapes. This results from the different representation of particles and the contact detection algorithms used for both spherical and polygonal particles (Newland and Hogue, 1994).

2.8.2.2 Statistical mechanics approach

In this approach, it is not required to calculate the forces or integrate the equations of motion, instead a statistical approach is used. The state of the particles is determined according to an assumed statistical distribution (Newland and Hogue, 1994). The resulting models are simple and efficient, however, they are inflexible. The particles can be modelled as hard spheres and the vibrations must be harmonic. Moreover, these models can be used for specific applications only (Newland and Hogue, 1994).

2.8.2.3 Hybrid approach

This is a combination of the Classical Newtonian dynamics and the statistical mechanics approaches. An example of this approach is the Hawkins model which simulated the granular flow of 2-D rigid disks by using stochastic boundaries and binary collisions. Another example is the Goldreich-Tremaine model for the study of the motion of particles in planetary rings (Newland and Hogue, 1994). In addition to the previously mentioned models, Newland and Hogue (1994) proposed another model which they called the contact model. The flowchart of this model is shown in figure 2.13.

One of the advantages of this model over the others is that it can handle particles of different shapes. The results obtained from this model show that it offers a significant computational saving. At the same time it is more realistic in its assumptions and gives satisfactory agreement with analytical solutions and existing less efficient computer simulations (Newland and Hogue, 1994).

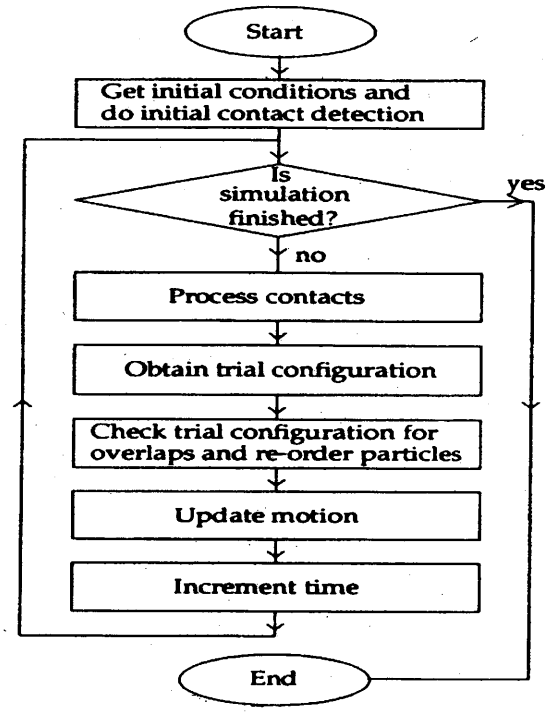


Fig. 2.13 Simplified flowchart for the contact model (Newland and Hogue, 1994).

2.8.3 LIMITATIONS OF FEM AND DEM

Both FEM and DEM are unable to represent the real case of the granular flow. The FEM will not be a correct representation of the granular flow at certain positions such as the lower part of the hopper. In that part, the continuum approach fails due to the separation of the particles near the outlet. In addition, FEM fails near the cylinder-hopper transition where large shear deformations occur (Lu *et al.*, 1997). The DEM is limited to model either two dimensional or small three-dimensional problems (Hustrulid, 1999). In addition, it can not deal with very large numbers of particles since it is extremely computationally intensive (Lu *et al.*, 1997).

2.8.4 A HYBRID NUMERICAL MODEL BASED ON FEM AND DEM

In order to overcome the deficiencies of these models, a hybrid model was developed by Lu, Negi and Jofriet in 1997. This model can be used to predict the velocity profiles and stress distributions of granular materials flowing out from a hopper. The model has these assumptions:

1.The granular material is modelled as an assembly of round particles of the same size and shape.

2.The material is non-cohesive.

3.Only the elastic deformation of individual particles is considered in DEM. Plastic deformations of individual particles are assumed to be negligible.

4.The movements of particles are restricted to two dimensions.

The basic governing equations of motion for both FEM and DEM were presented. The DEM is applied in regions where FEM fails to describe the flow such as the outlet and near the cylinder-hopper transition. On the other hand, FEM is used for the rest of the system. Figure 2.14 represents FEM and DEM domains in this model.

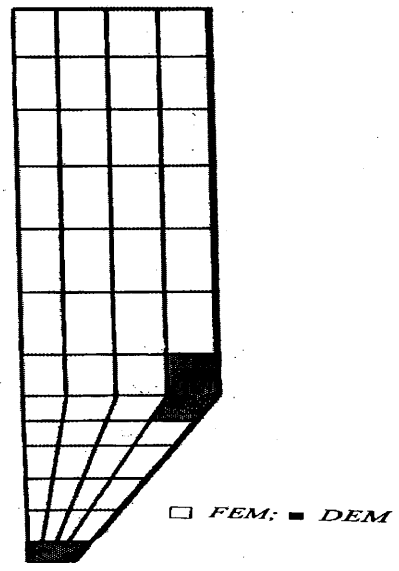


Fig. 2.14 FEM and DEM domains in the FEM and DEM hybrid model (Lu *et al.*, 1997).

Results of computer simulations using the hybrid model have been compared with laboratory experiments with good agreement being achieved (Negi, *et al.*, 1997).

Much work nowadays is directed towards developing new models to solve granular flow problems. However, limitations in the computational ability is the main obstacle to solve the more complicated models. Until computational power increases significantly beyond current capabilities, it will be necessary to develop the use of hybrid FEM/DEM methods further for all but the smallest applications.

CHAPTER 3

REVIEW OF PAST EXPERIMENTAL WORK

Granular materials discharging from bins have received a great deal of attention in the past. A lot of experiments have been done to study and analyse the behaviour which the granular materials follow when they flow inside storage bins and hoppers. Moreover, many studies have been directed towards studying the effects of the geometry of these storage devices on the flow patterns initiated inside them. Photographic methods, x-ray radiography and radioactive tracers are just examples of the different techniques used to trace the movement of the granular material inside hoppers. In this section, an overview of past experimental work done in this area is given. This chapter serves two purposes. The first is to give an idea about the geometry of previous experimental hoppers which has been of help in choosing the parameters and construction materials for the design of a hopper for lab scale experiments. The second aim of this chapter is to highlight the main findings from previous experiments that may be compared with the experimental results from this study.

In 1966, Gardner used a non-cohesive granular material with a known angle of internal friction to determine experimentally the shape of the boundary of the flow regions in a symmetrical plane system for a non-cohesive granular material. The apparatus shown in figure 3.1 was constructed to achieve this purpose. Two vertical wooden walls were used to provide the bin hopper profile; the wooden walls were bevelled at the bottom so that two shorter plane walls could be used at angles between 0° and 65° to the horizontal immediately beneath them. These two sloping walls represent the hopper section and their position could be adjusted to give a sharp edge slot discharge of any chosen width.

The material could be observed through the other two walls of the bin, which were made of Perspex, which is smooth and transparent. These two walls were not quite vertical, because the two vertical wooden walls to which they were screwed changed in width over their 122 cm height from 7.62 cm at the top to 8.23 cm at the bottom.

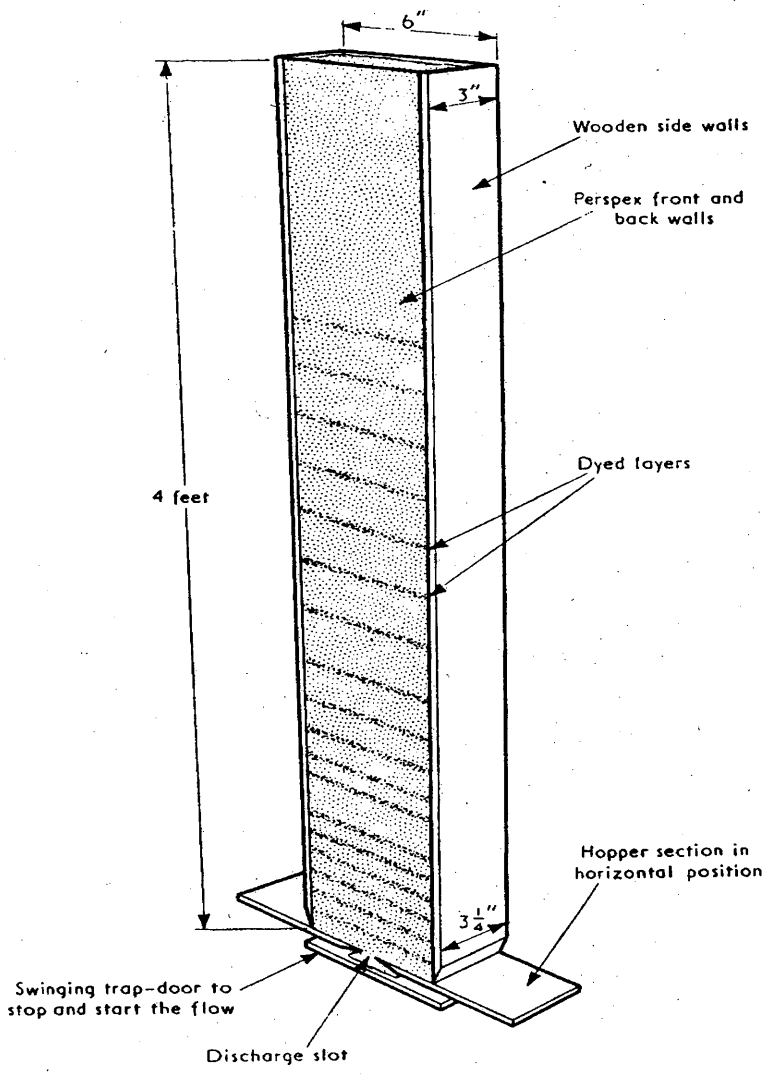


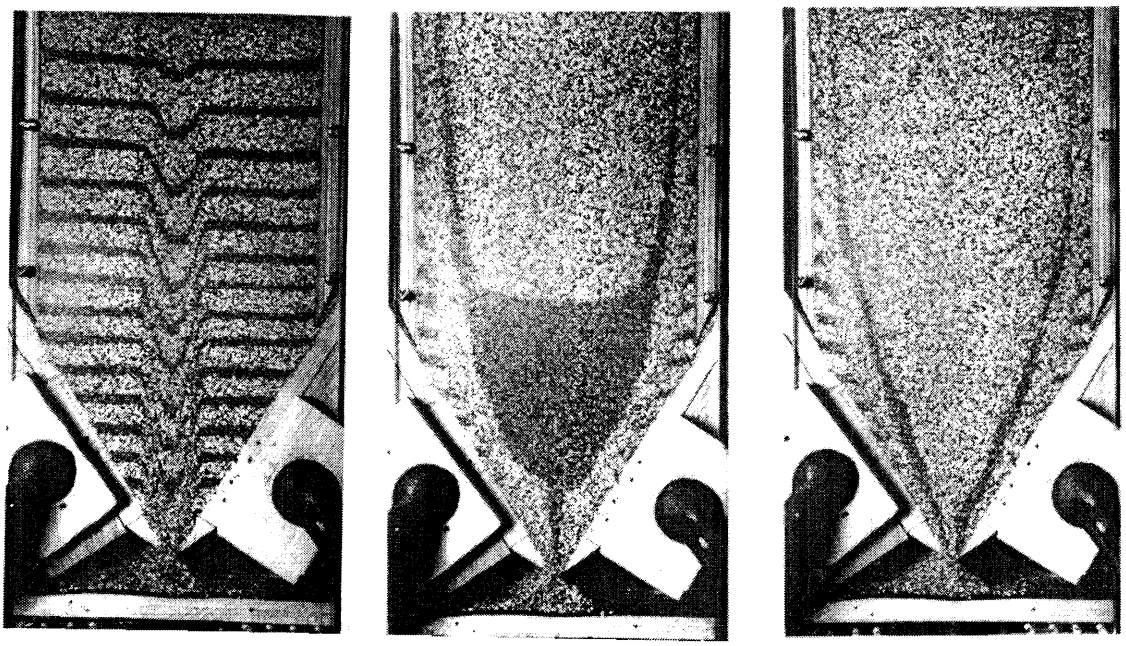
Fig. 3.1 Experimental bin-hopper system used by Gardner (Gardner, 1966).

The purpose of changing the width over the height was to avoid any tendency to convergent flow normal to the plane of observation. The wooden walls of the bin were 15.24 cm apart. The walls normal to the plane of observation were made rough by coating the internal wooden surfaces of the apparatus with adhesive followed by a

layer of experimental granular material. A hinged trap set about 1.9 cm was used to stop the discharge through the slot at the bottom of the hopper. The trap set was held in place by an easily removed pin. The experimental material was an angular calcined flint named "Durite" ranging from 0.79 mm to 1.59 mm in size. This material was non-cohesive and porous and thus easily dyed with deep blue ink.

The apparatus was filled with horizontal layers of dyed and undyed "Durite". The dyed layers were spaced more closely at the bottom of the apparatus than the top. The material was allowed to discharge from the slot until the top surface in the bin was about 76 cm above the slot. The width of the slot was about 0.65 cm and the discharge rate was about 5 cm^3 sec^{-1}. During the discharge, photographic time exposures of 1/2 sec to 1 min duration were taken of the flowing material. In addition, the position of the edge of the dyed layers nearest the axis of symmetry was measured in terms of x and y where x is the horizontal co-ordinate and y is the vertical co-ordinate.

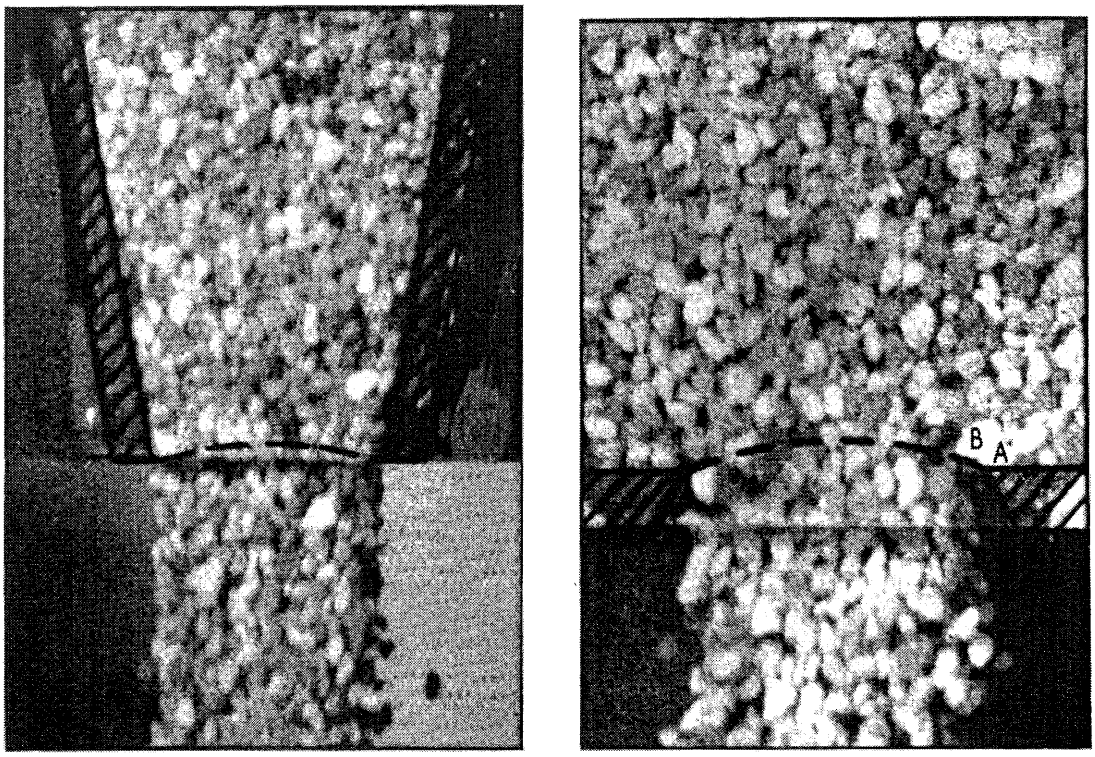
From the experiment the following observations were noticed. When the flow is stopped, and started again, the flow region continues to develop from the point at which it stopped. Another important observation was the initiation of a tongue of the flow material above the discharge slot moving much faster than the surrounding material. Finally, the last observation was that the edge of the flow region never reached the bin walls completely. The walls of the bin were sufficiently rough to ensure that the material failed within itself and not with respect to the walls. Figure 3.2 shows some of the photographs taken during the discharge operation.



(a) (b) (c)

Fig. 3.2 Different photographs of the flow in hoppers (a) development of flow (b) dyed material forming a tongue near the discharge slot (c) trail showing fast moving core (Gardner, 1966).

Bosley *et al.* (1969) used flat-bottomed hoppers and hoppers with steep slopes to study the effects of hopper shape, granule size and granule density upon the velocity profiles in hopper discharge. The experiment was based on a photographic study in which successive photographs were taken through a transparent wall. In the experiment, a two dimensional flow of four granular materials i.e. gravel, polystyrene chips, crushed gravel and sand from hoppers of five different geometries was studied. It was found that the velocity profiles depend primarily on the shape of the hopper. For hoppers with steep slopes, those which make 70° or 80° with respect to the horizontal, the flow appeared to be radial near the orifice. On the other hand, for flat-bottomed hoppers and for hoppers with 45° to the horizontal, small components of velocity perpendicular to the radial direction were found in the vicinity of the orifice. Typical photographs of the hopper during discharge are shown in figure 3.3.



(a) (b)

Fig. 3.3 Photographs of gravel discharging from hoppers (a) mass flow hopper (b) non mass flow hopper (Bosley *et al.*, 1969).

Lee *et al.* (1974) used an x-ray radiographic technique to experimentally determine simultaneous velocity and porosity fields in a granular material flowing through a model hopper. The model hopper used in the experiments was a mass flow hopper and the granular materials used were densely packed materials. The investigators preferred densely packed materials over loosely packed material for two reasons. Firstly, materials normally become densely packed due to the manner in which they are loaded into the hopper. Secondly, the observation of the velocity and porosity fields is more accentuated for densely packed materials.

Figure 3.4 shows a schematic of the model hopper and the x-ray source and film.

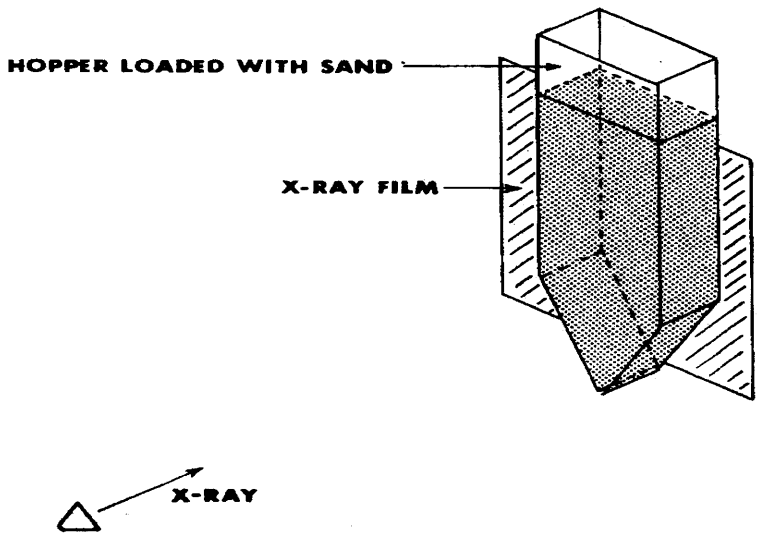
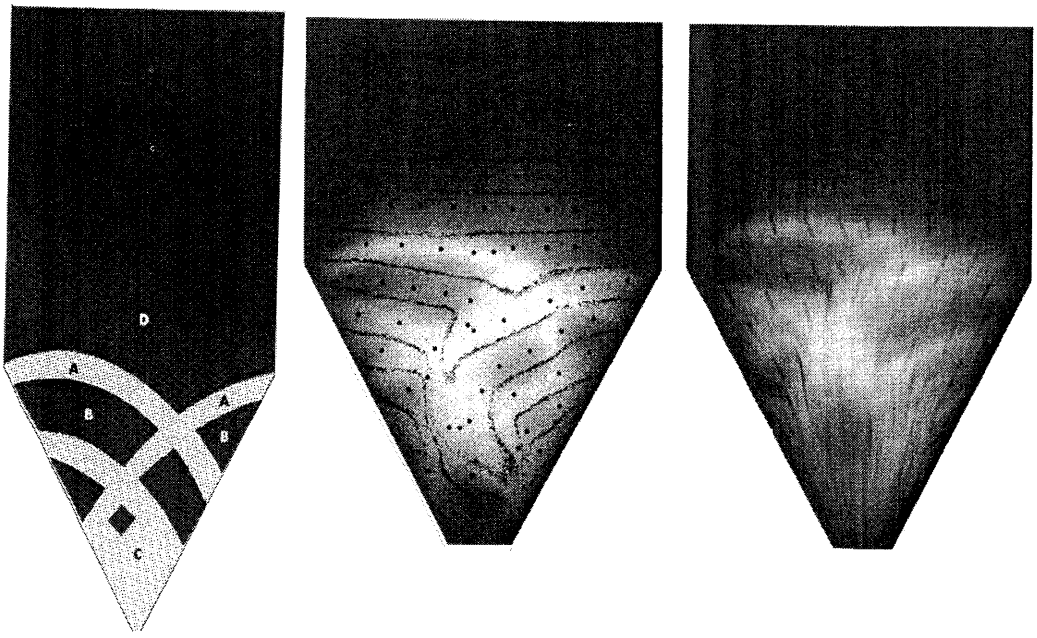


Fig. 3.4 Arrangement of experimental hopper and x-ray source and film used by Lee *et al.* (Lee *et al.*, 1974).

The hopper was 50.8 cm high overall (both the vertical and the converging section), 15.2 cm wide in the vertical section and 7.6 cm deep. The inclined sidewalls of the hopper made an angle of 60° with the horizontal. 1.3 cm thick Plexiglas was used to form the front and the rear walls. A 1.27 cm Plexiglas or 1.27 cm aluminium plates were used to construct the sidewalls, these different materials were used for different test runs. The discharge opening at the bottom of the hopper was 5 mm.

The material used was sand with 0.584 to 0.838 mm diameter and it was loaded inside the hopper by an overhead device which was representative of the way in which full-scale operating hoppers are loaded. Layers of lead powder and lead shot were placed in between the sand layers in order to track the development of the flow in the hopper. The finding of the experiments was that the flow of granular materials through hoppers is characterised by regions of rigid body motion interseparated with narrow bands of great change in void ratio and velocity. Figure 3.5 (a) shows the different zones of material behaviour. These four observed zones were the plug flow zone D,

the rupture zone A, the free flow zone C and the collection of A and B is called the core feed zone. Figure 3.5 (b) and (c) shows radiograph images taken through the discharge process.

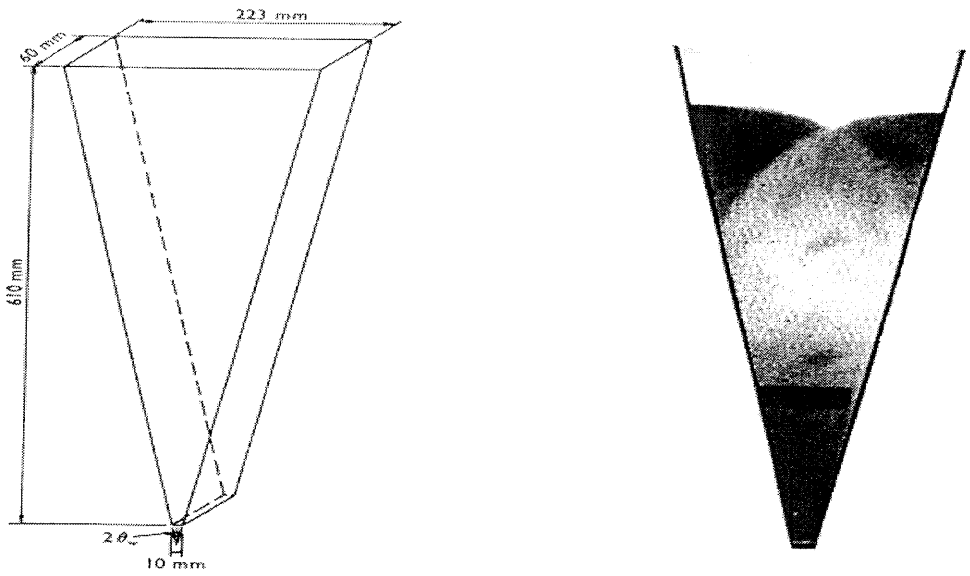


(a) (b) (c)

Fig. 3.5 Flow through hoppers obtained from radiographic study (a) schematic representation of different zones observed on radiographs (b) radiograph taken in static situation (c) radiograph taken during discharge (Exposure time: 1.2 sec) (Lee *et al.*, 1974).

Drescher *et al.* (1978) proposed a model to represent the kinematics of the mass flow of granular material through a plane hopper. The proposed solution was based on assumptions suggested by the flow pattern observed during the experiments. The experimental work was limited to the observation of displacements only and no attempt was made to measure wall stresses.

In the experiments, a small Perspex hopper was used. The hopper included angle, 2α, could be chosen to be either 20° or 30°. Figure 3.6 (a) shows the dimensions of the hopper used and the radiograph obtained.



(a) (b)

Fig. 3.6 Hopper geometry and radiograph picture obtained (a) dimensions of the hopper (b) radiograph of the hopper (Drescher *et al.*, 1978).

In the first set of experiments a dense, course rounded sand of particle size 0.6 to 1.2 mm was used. When the sand was allowed to flow, and during the discharge operation, radiographs were taken. A typical positive print is shown in figure 3.6 (b). The two darker zones represent dense unsheared sand and the lighter areas characterise sheared sand that experienced some dilatation and is therefore looser. In addition to the previous experiments, a second series of tests was performed to get more information on the displacements. Here also a dense sample of sand was used with a row of 2 mm lead markers placed to form a regular grid on the mid plane of the sample. The positions of the lead markers were measured and a computer program was used to display plots of displacement vectors of the markers between radiographs. Different flow zones were observed, and figure 3.7 shows the flow pattern obtained from the experiments.

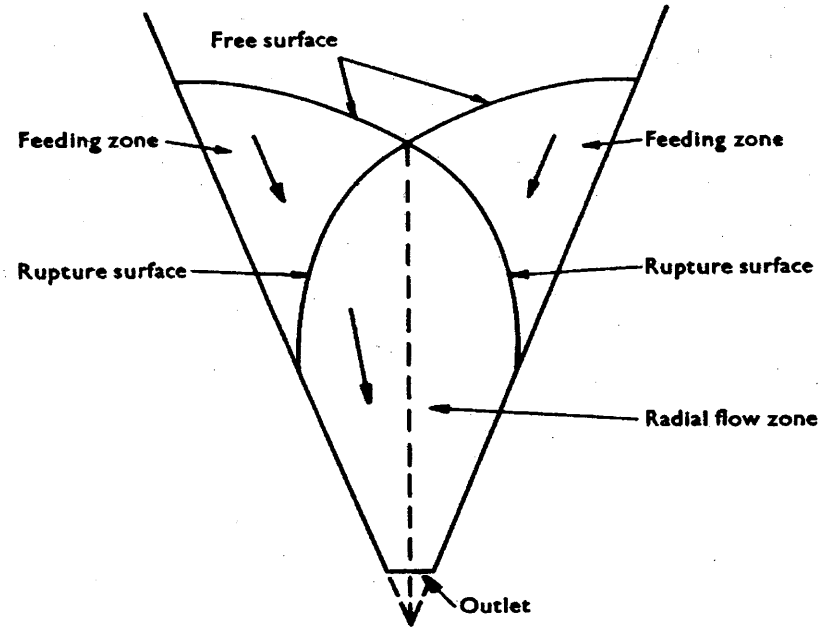


Fig. 3.7 Different zones and surfaces for course rounded sand observed by Drescher *et al.* (Drescher *et al.*, 1978).

Nguyen *et al.* (1980) performed experiments to study the variations of the flow regime with changes in the height of the material in the hopper, the width of the vertical bin, the hopper angle and the hopper opening width. Figure 3.8 represents the different types of flow obtained from the experiments.

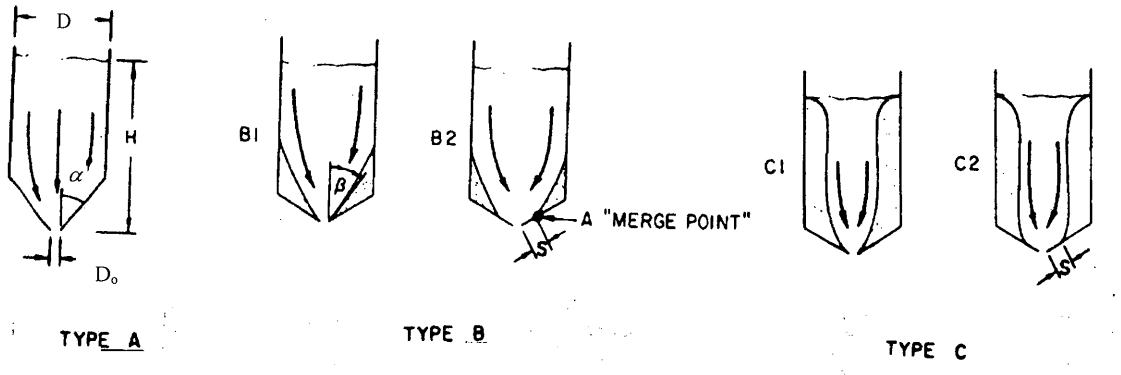


Fig. 3.8 Schematic indicating the different flow regimes observed by Nguyen *et al.* Type A is the mass flow regime. Types B and C are funnel flows, B having stagnant material at the corner and C stagnant material on the sides of the bin (Nguyen *et al.*, 1980).

In addition, the definitions of α, D_o, D, and H (the hopper half angle, the opening width, the bin width and the total height to the upper free surface, respectively) are also shown on the same figure.

The experimental apparatus used in the experiments was a plane hopper made of Lucite and surmounted by a vertical bin. The dimensions of the hopper were all adjustable. α, the hopper half angle, could be varied continuously, D_o, the exit opening, ranged from 0.5 cm to 3.8 cm and bin width, D, from 17.8 cm to 33 cm. Most of the experiments were performed using a breadth, b_h, of 15.2 cm. For sand breadths of 7.6 cm and 22.9 cm were also used. In some tests a second supply bin was used to maintain the height, H, constant, while in other tests, H was left to decrease naturally with discharge. In addition to the previous variations in the experimental conditions, a combination of rough inclined walls and smooth vertical walls was also investigated to study the effects of inclined wall roughness.

The granular materials used were sand, glass beads, polystyrene pellets and rice which varied in shapes from spherical to elongated shapes. Figure 3.9 shows some photographic examples of flow patterns for sand.

The experiments performed revealed that funnel flow will result at lower values of hopper half angles α. Moreover, it was found that the ratio of the height of the material in the bin to its width (H/D) is crucial in determining the type of flow and the transition from one type of flow to another. In addition, the flow patterns were affected by the wall roughness by causing stagnant material to appear at lower values of α.

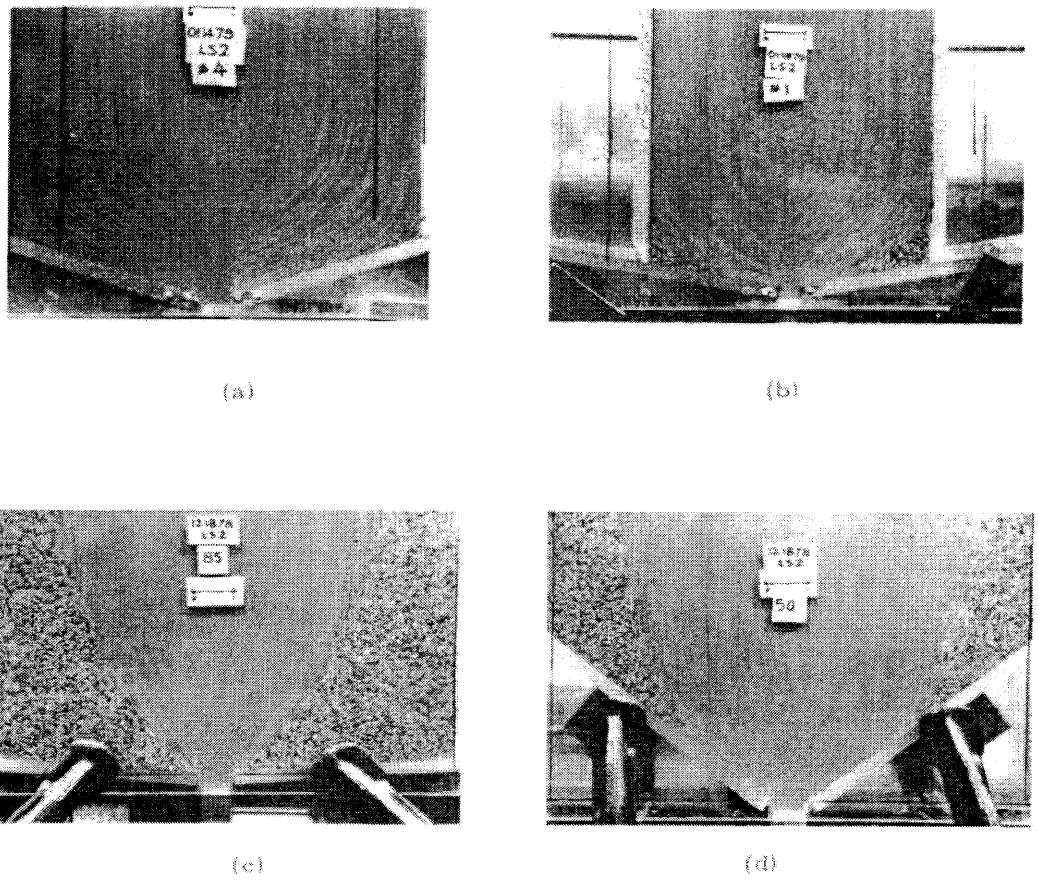


Fig. 3.9 Photographic examples of the flow regimes for sand (angle of repose=35°, grain size = 0.5 - 1 mm). The breadth is 15.2 cm in all cases. The values of α, D_o, D, H (in cm): (a) 70°, 1.91, 22.9, 36.8 (b) 80°, 1.37, 17.8, 58.4 (c) 70°, 2.54, 30.5, 35.6 (d) 50°, 2.54, 30.5, 35.6 (Nguyen *et al.*, 1980).

The experimental work of Tüzün and Nedderman (1982) was mainly to investigate the formation, position and shape of the stagnant zone boundary arising during discharge from flat-bottomed bins and shallow convergent hoppers. Closely graded glass ballotini with mean particle diameter ≥ 1.0 mm were used. Black glass ballotini were used as a tracer material with each run in 5 % concentration by volume.

The experimental apparatus was made of two parallel plates of 0.65 cm thick float glass, they were 150 cm long and 60 cm wide. The two glass sheets were separated by 2.2 cm thick planed-wood spacers. Changing the position of the wooden spacers between the glass walls could alter the width of the bin. In the experiments dealing

with flat-bottomed bins, interchangeable aluminium sheets with a single central slot of different sizes were used to get different discharge rates. In the other set of experiments, pairs of wedge shaped pieces of wood were placed on either side of the discharge slot to obtain different half angles. In addition, pieces of float glass stuck on the wooden surfaces were used to study the effect of wall roughness. Figure 3.10 shows the experimental rig used in the experiments. As seen in figure 3.10 (b), a large feed reservoir was used in some of the experiments to obtain a steady state profile of the flow under constant material head.

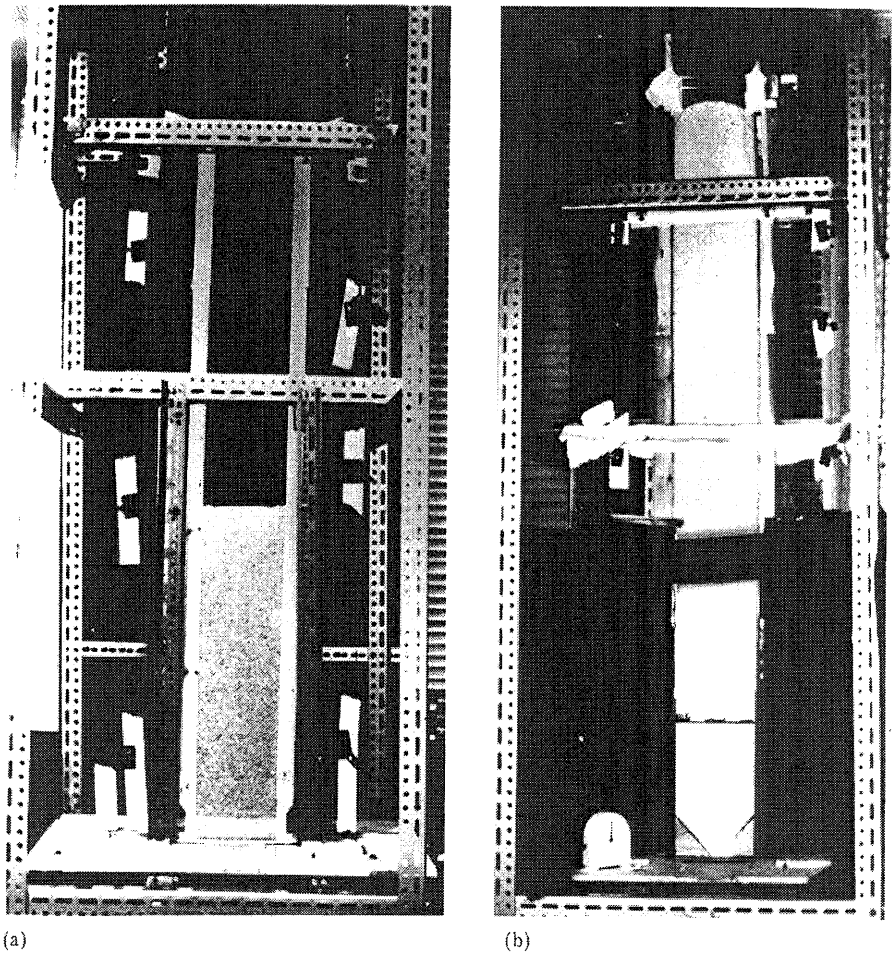


Fig. 3.10 Experimental bin-hopper system used by Tüzün and Nedderman (a) two-dimensional, flat-bottomed bin and feed reservoir (b) parallel-sided bin and convergent hopper set-up (Tüzün and Nedderman, 1982).

The principal conclusion from the experiments performed was that the discharge of solids from bunkers gives rise to a characteristic angle called the angle of discharge, ϕ_d, which is usually higher than the angle of repose of the material. Moreover, the experimental results suggest that the wall roughness becomes an effective factor on the flow field only in steep hoppers of half angles $\alpha < (\pi/2)- \phi_d$ and has little or no influence on the flow field when $\alpha > (\pi/2)- \phi_d$. Figure 3.11 shows some photographs of the flow field for different half angles.

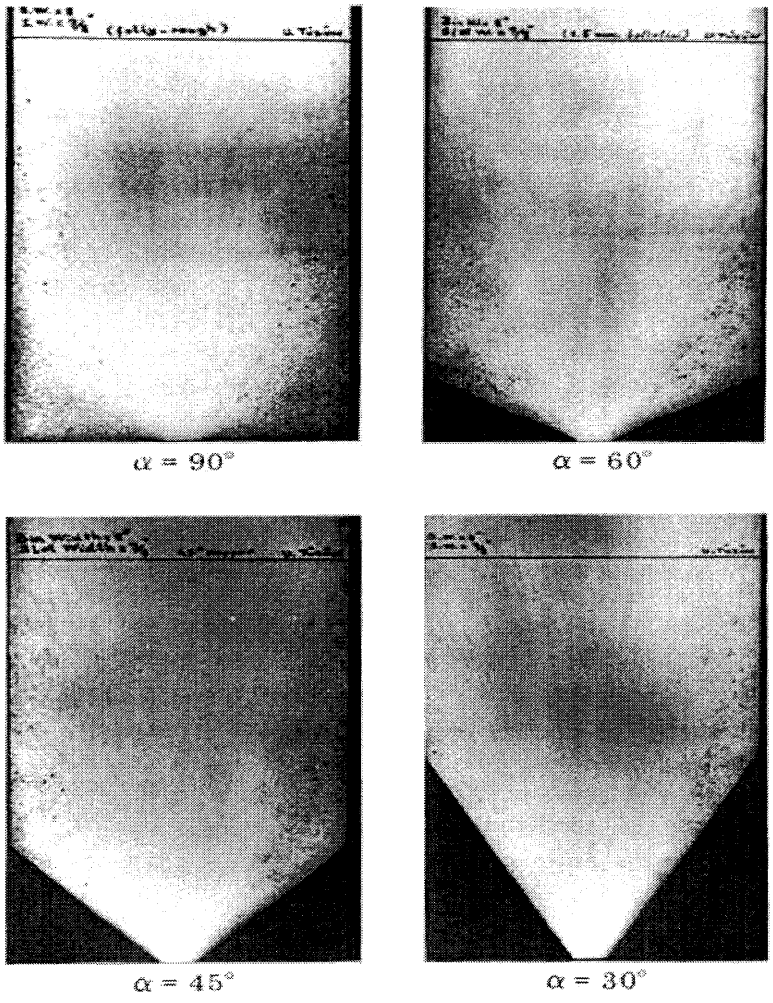


Fig. 3.11 Photographs of flow field for 1.5 mm ballotini with varying half angles. Time exposure =1 sec, width = 20.3 cm, orifice width = 2.2 cm (Tüzün and Nedderman, 1982).

Baxter *et al.* (1989) used digital subtraction radiography to study experimentally the effect of the formation and propagation of the density waves on the flow through a flat hopper.

The experiments were carried out in an apparatus made of Plexiglas which is shown in figure 3.12. The experimental hopper was 1.27 cm thick and 30 cm high. The effect of several parameters on the flow such as the angle of the wedge and the width of the bottom opening were investigated. The materials used in the experiments were two types of sand. The first was rough, faceted sand with a size range between 0.04 – 0.08 cm. The second type was smooth and nearly spherical with a mean size of about 0.07 cm. Both smooth and rough sands were used as the flow material in addition to mixtures.

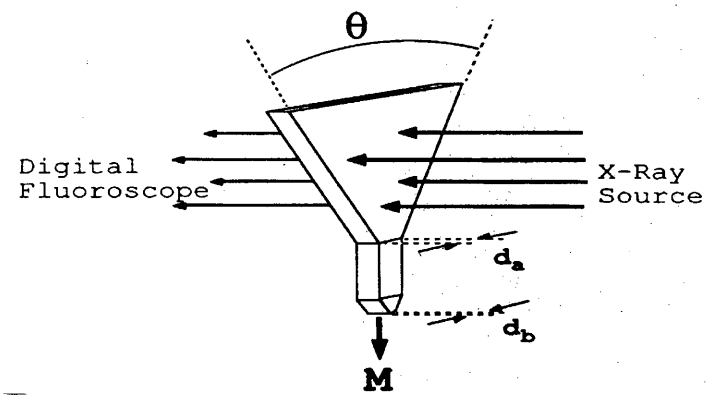


Fig. 3.12 Schematic of the apparatus used by Baxter and his group (Baxter *et al.*, 1989).

It was concluded from the experiments that for large opening angles, density waves propagate upward from above the aperture against the direction of particle flow, but downwards for opening angles less than 35°.

Figure 3.13 shows images of the flow patterns for both rough and smooth sand. In mixtures of smooth and rough sand a proportion of at least 25% rough, faceted sand was found to be necessary in order to observe the propagation patterns.

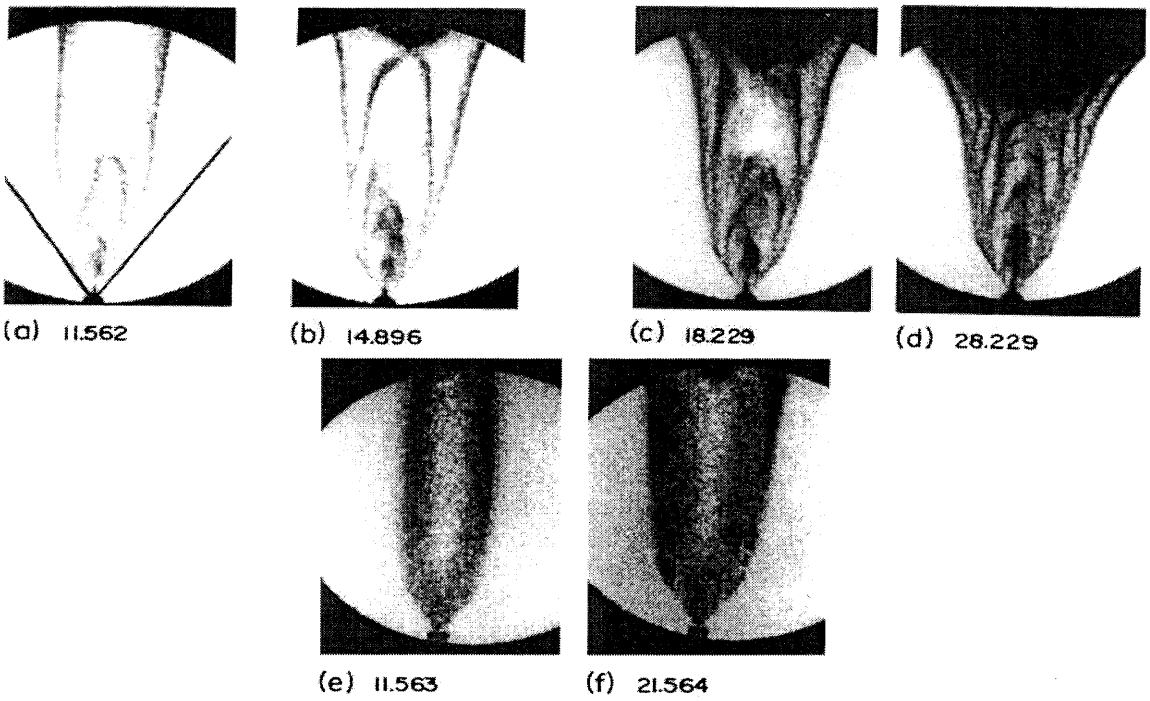


Fig. 3.13 Flow of sand images (a)-(d) images taken for rough sand. (e) and (f) images for smooth sand with no waves formed (Note: The numbers below the images represent time in seconds and black lines in (a) represent the confining walls) (Baxter *et al.*, 1989).

In 1990, Baxter and Behringer continued the work on studying granular flow. They performed experiments to demonstrate the importance of particle irregularity on the flow of granular material. In the experiments, grass seeds which have a non-spherical shape were used as the granular material. Figure 3.14 shows a series of images taken as the seeds were discharging out of a thin Plexiglas wedge. The thickness of the hopper used was 1.2 cm which is about twice the length of the seed. From the experiments, it was observed that the orientation of the grass seeds was affected by the flow and the long axis of the seeds becomes arranged to point along the direction of motion.

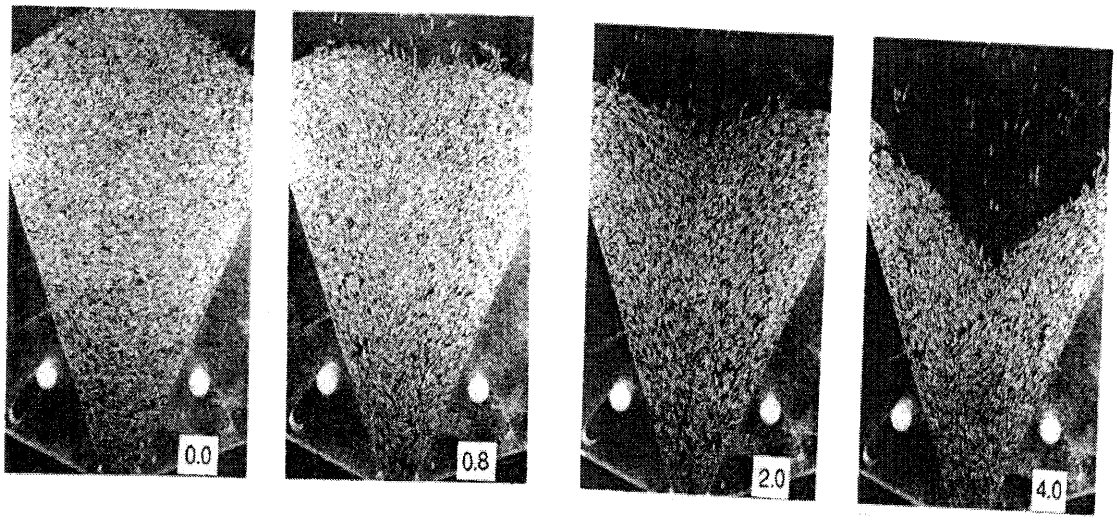


Fig. 3.14 Photographs of grass seeds flowing from a hopper with a wedge angle of 60°. The numbers under the pictures show elapsed time in seconds (Baxter and Behringer, 1990).

Negi *et al.* (1997) studied the effect of the flow of granular materials on the wall pressures in silos. They used laboratory experiments to calculate the wall pressures and compared the results with those from computer simulations.

The dimensions of the experimental arrangement used are shown in figure 3.15. The bin was of rectangular cross section with a hopper shaped outlet with an adjustable wall slope. Galvanised steel sheets with 0.5 mm thickness were used to construct the sidewalls. The other two walls were built from 5 mm clear acrylic sheets to ease observations. The depth of the bin was 1.25 m and the particulate matter used was soybean. As shown in figure 3.15, the wall pressures were measured at 0.06 m above and 0.06 m below the intersection of the rectangular bin and the hopper sections. Five outlet widths of 50, 60, 70, 80, and 90 mm were used in the tests.

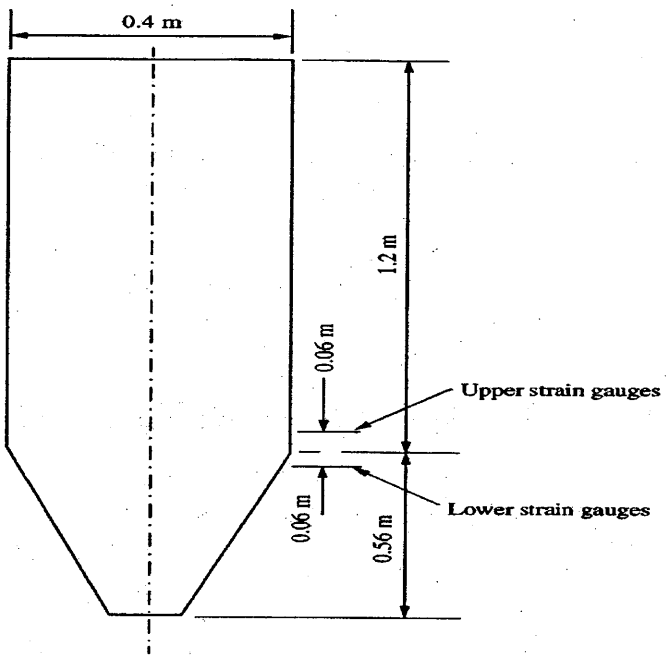


Fig. 3.15 Arrangement of an experimental hopper used to measure wall pressures (Negi *et al.*, 1997).

The results showed that the maximum wall pressures occurred near the transition region between the parallel and the convergent flow near the top of the hopper. Figure 3.16 shows the agreement between the experimental and the simulation results.

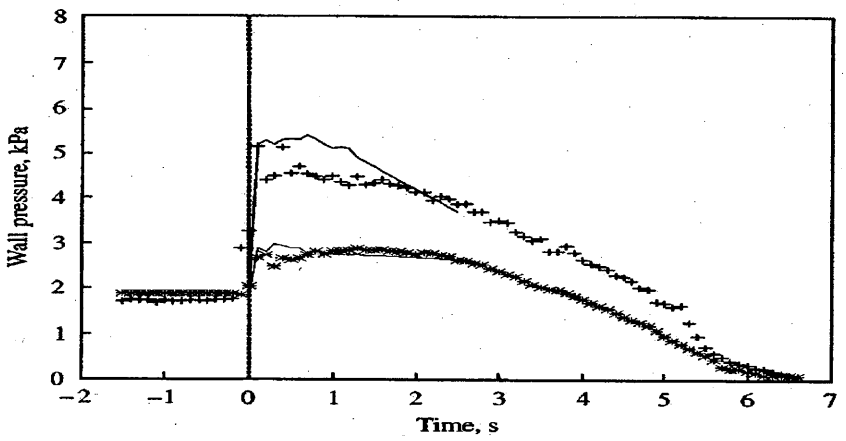


Fig. 3.16 Comparison between experimental and numerical results for wall pressures for an outlet width of 70 mm: (+) Exp. lower; (*) Exp. Upper; lines represent DEM simulations (Negi *et al.*, 1997).

Flekkϕy and Målϕy (1998) studied the stagnant zones developed in a hopper both experimentally and numerically. In the experimental part, a quasi-two-dimensional hopper consisting of two glass sheets 5 mm apart and two inclined walls was used to represent the converging section of the hopper. These walls were made rough by gluing glass beads on a double sided tape. The width of the discharge orifice was 10.1 mm and it was initially closed by a piece of tape. The hopper was filled with glass beads of diameter 1mm, and the flow was initiated by removing the tape at the orifice. Photographs were taken during the discharge process and the stagnant zones become visible by subtraction of the pictures from the picture before the flow started. Simulations and experiments were found to agree qualitatively which gave the impression that stagnant regions could be predicted by the proposed model. Figure 3.17 (a) shows a picture in which the stagnant regions are made visible as distinct dark zones with very little noise. Figure 3.17 (b) represents these regions predicted from the numerical model.

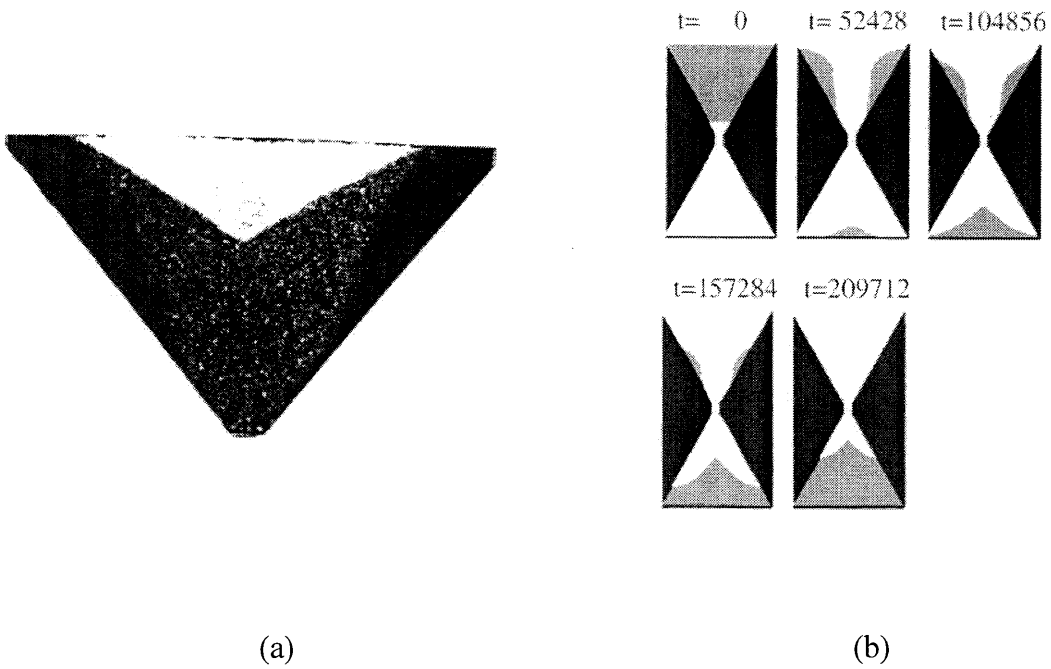


Fig. 3.17 Stagnant regions (a) photograph from experiment using glass beads (b) images from simulation with (t) showing the time in seconds (Flekkϕy and Målϕy, 1998).

From the work reviewed in this chapter, it is clear that most of the work done in the granular flow area has been directed towards non-living granular materials such as sand and glass beads. Fewer experiments have been performed using wheat or other cereals, consequently, experience in this field should be borrowed from the study of other granular materials to be applied here in studying the flow of wheat.

CHAPTER 4

DESIGN OF THE EXPERIMENTAL HOPPER

The experimental hopper used in the present study was designed in a way which allows variation of all its dimensions and geometry. The five main geometrical aspects in the experimental hopper are the width, the height, the discharge opening, the hopper angle and the depth or breadth of the hopper. The hopper consisted of six pieces (see figure 4.1).

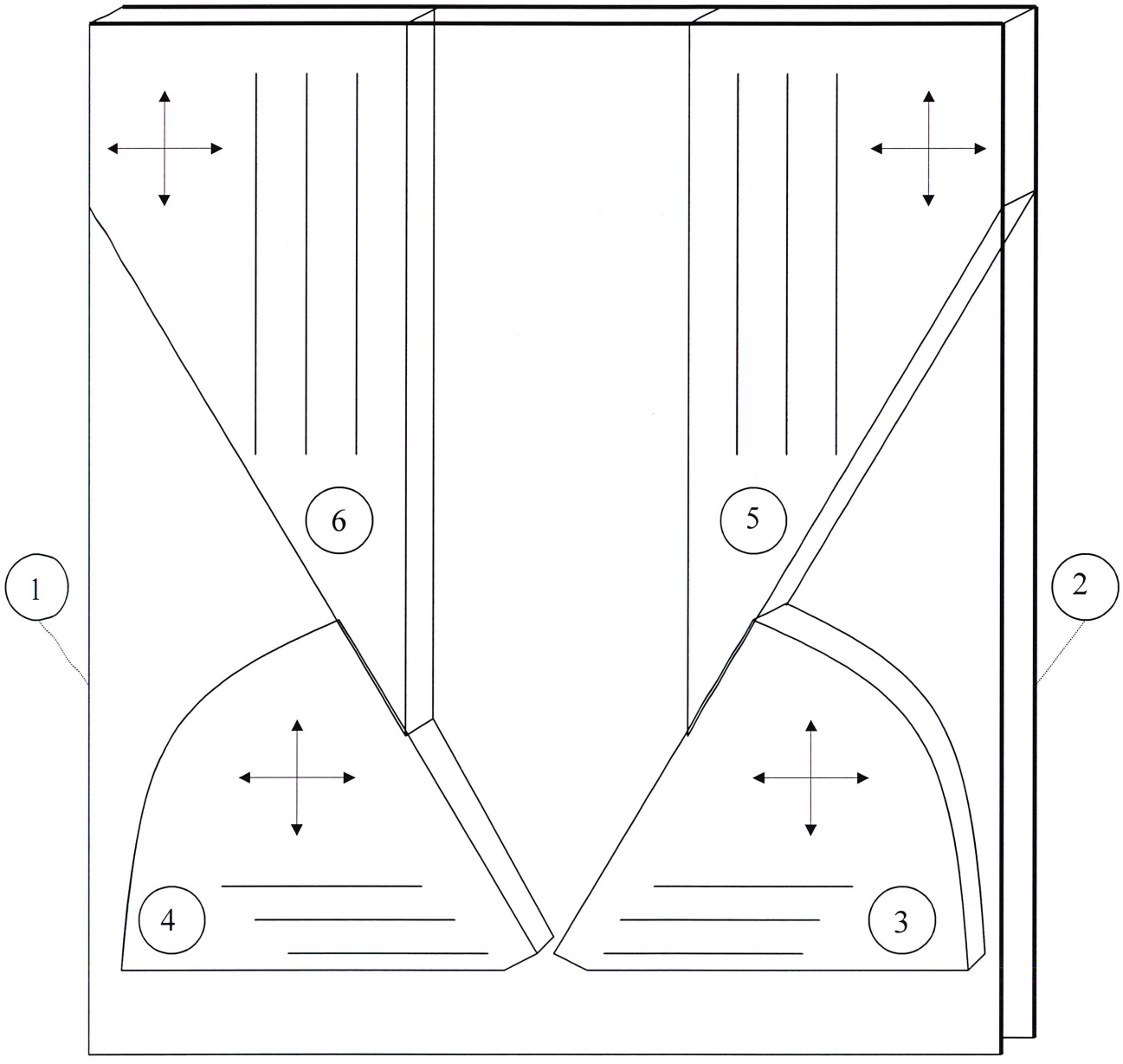


Fig. 4.1 Schematic of experimental hopper used in the project. Arrows indicate possible adjustments and numbers in the circles represent each piece number.

Two of the six pieces represent the front and the back walls which are pieces 1 and 2. The next two pieces, pieces 3 and 4, represent the inclined hopper sidewalls. The last two pieces, pieces 5 and 6, represent the vertical bin walls.

4.1 DESIGN OF THE FRONT AND BACK WALLS

These two pieces were made of Poly Vinyl Chloride (PVC) which is smooth and allows observation of the flow inside the hopper. This material is sufficiently frictionless to cause negligible boundary effects. The movement of the particles next to the PVC walls is visible and represents flow in the interior of a hopper. Eight sets of ten holes were drilled through the PVC sheets in addition to two holes at the bottom. The positions of these holes were chosen so that the other pieces of the hopper could be fixed to the walls in different positions to get the desired variation in hopper geometry. Figure 4.2 shows the dimensions and the location of the holes on the front and back walls of the hopper. The diameter of each hole was 6.5 mm and the centres of adjacent holes were 1 cm apart.

These two PVC pieces were clamped together with the lower two pieces of the hopper by metal guides in the hopper stand. The lower two holes were used to vary the discharge opening and the hopper half angle while the other eight sets were used to control the width and the height of the hopper.

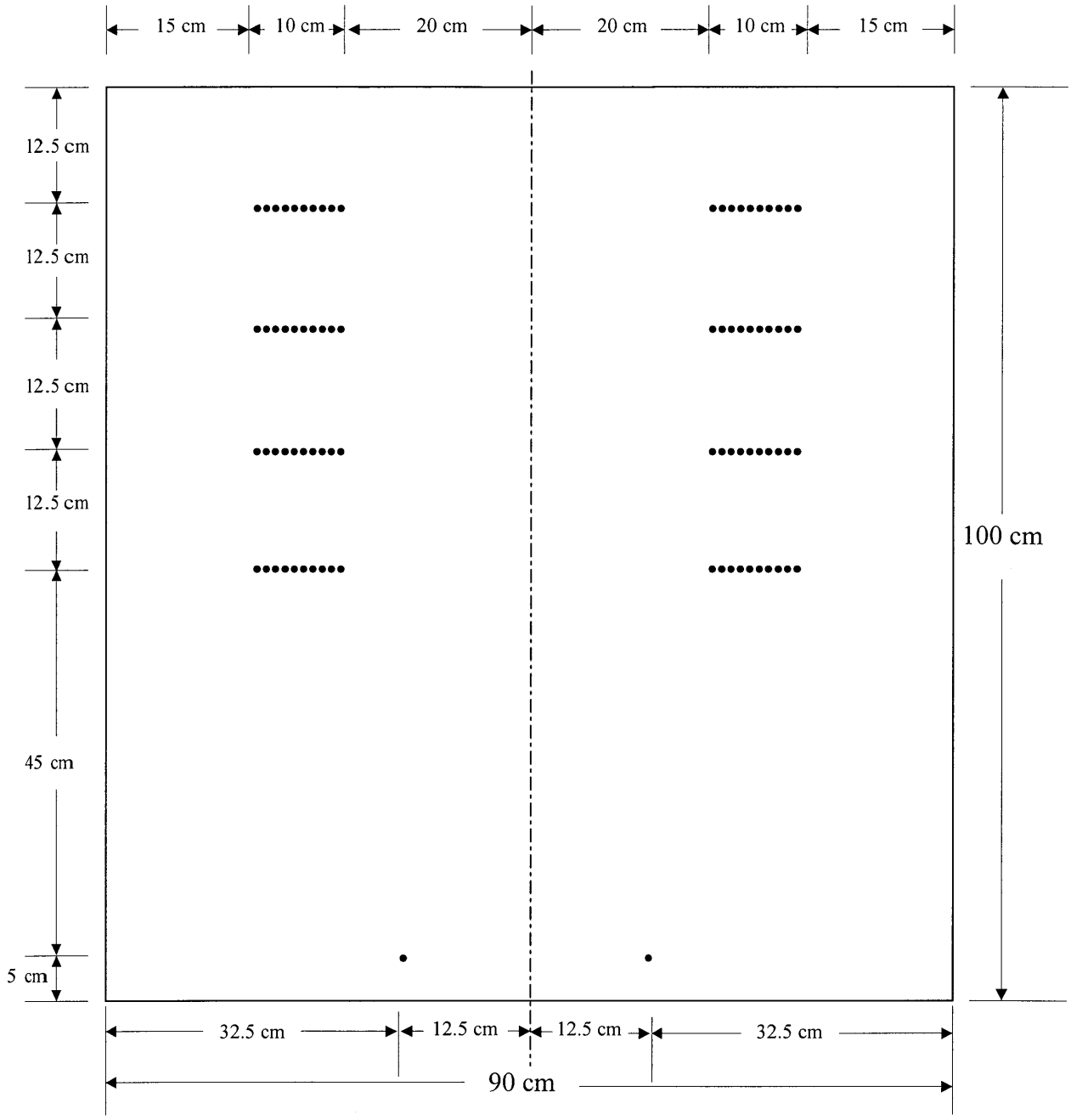
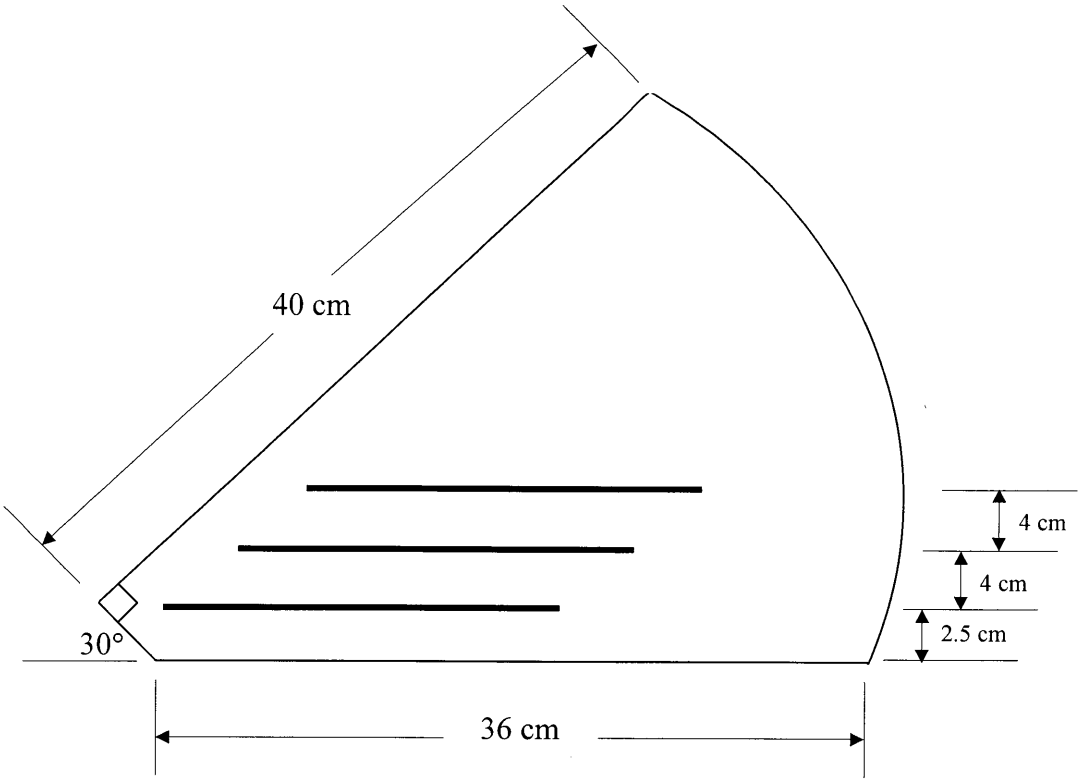


Fig. 4.2 Design of pieces 1 and 2 (The front and back walls) of the experimental hopper showing the main dimensions and the locations of the holes .

4.2 DESIGN OF THE INCLINED SIDE WALLS

The next two pieces, pieces 3 and 4, were designed in a way such that the hopper angle and the discharge opening could be changed. These two pieces construct the walls of the converging part of the hopper and were made of MDF wood. Figure 4.3 shows the shape and the dimensions of these two pieces with the positions of the slots,



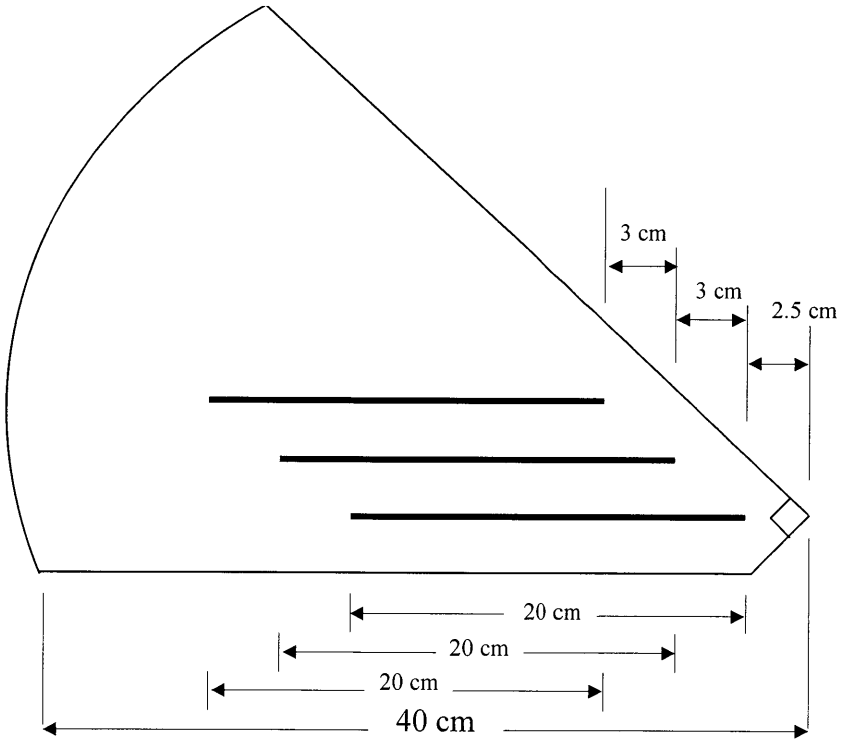


Fig.4.3 Shape and dimensions of the inclined walls (pieces 3 and 4) of the experimental hopper.

which were used to vary the angle and the discharge size of the hopper. Each slot in these pieces was 20 cm long and 6 mm thick. Pieces 3 and 4 were clamped to the front and the back walls to fix them in position by the hopper stand, in addition to a wing nut and bolt used as a support and a pivot for rotation.

4.3 DESIGN OF THE VERTICAL SIDE WALLS

The last two parts, pieces 5 and 6 were used to construct the vertical bin walls. These pieces were also made of MDF wood. Three long vertical slots were made in each of the two pieces. Each slot was 37.5 cm long and 6 mm thick. The slots were used to fix these two parts of the hopper to the front and back walls. Moreover, the positions of the slots were chosen to allow maximum flexibility in the hopper width and height. Wing nuts were used to fasten the two pieces to the back and front walls. Figure 4.4 shows the shape and the different dimensions of piece number 5 which is a mirror image of piece number 6.

4.4 GEOMETRY OF THE EXPERIMENTAL HOPPER

After putting all the pieces together, the experimental hopper is constructed. The maximum height that could be achieved by loading the grains is 95 cm. This height can be changed easily by increasing or decreasing the quantity of grains inside the hopper. The maximum width that could be achieved by moving pieces 5 and 6 was 38 cm. This width could be changed by moving the two pieces inside and outside the bin area and fixing them in position with the front and back walls. Varying the hopper angle could be achieved by rotating pieces 3 and 4 around their axes using the hinged point.

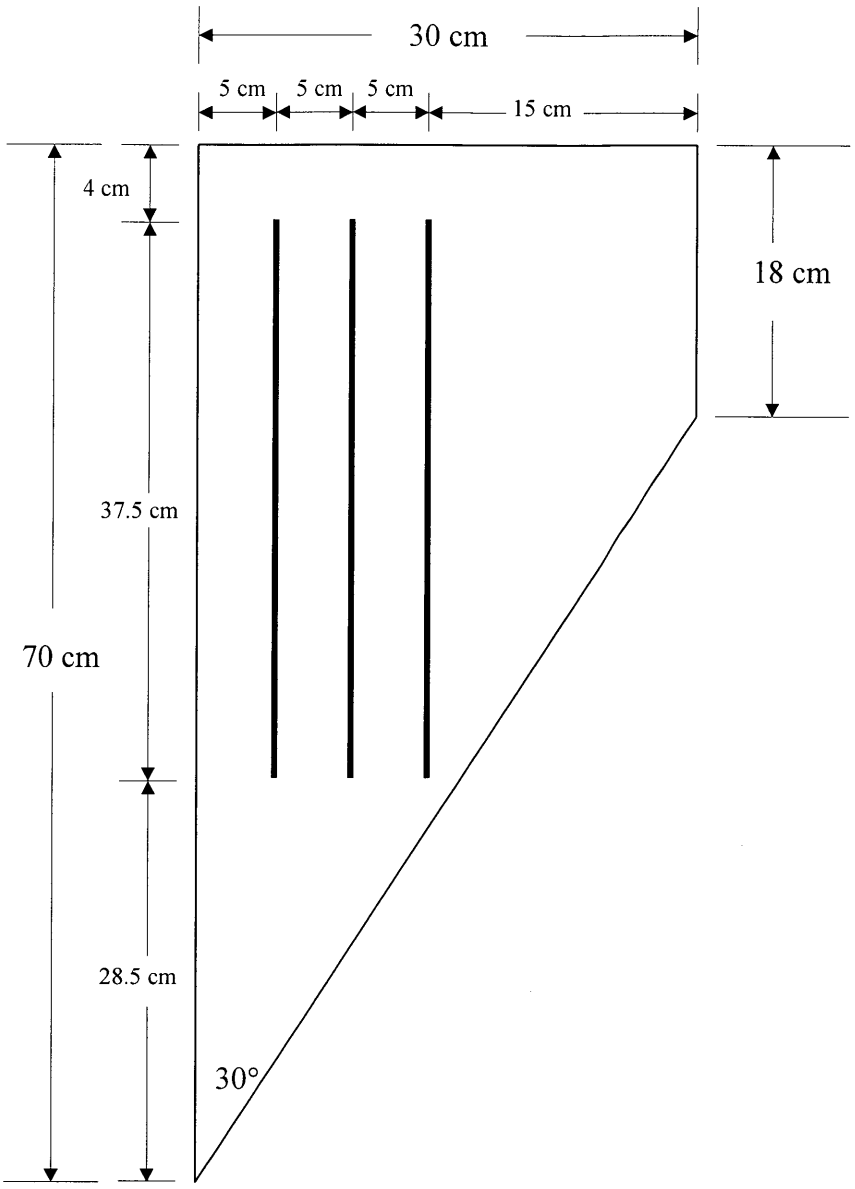


Fig. 4.4 Shape and dimensions of piece number 5 (piece 6 is a mirror image of this piece).

The minimum half angle for the hopper was 30° and this could be increased to get a flat bottomed hopper, that is 90° half angle or 90° with the vertical. In addition to varying the angle, the previously mentioned pieces were also used to vary the discharge opening area. The length of the orifice could be changed from 0, in the case of no flow, to a maximum discharge opening length of 20 cm. Clamping pieces 3 and 4 to the front and back walls using the metal guides in addition to the hinge was

essential to keep these pieces in position and fix them tightly to build the experimental hopper.

Finally the depth of the hopper could, in principle, be changed by adding more identical pieces to parts 3,4,5 and 6 and putting them together between the walls to get different thicknesses or depth of the hopper.

The dimensions of the experimental hopper i.e. the width, height, breadth, half angle and the discharge opening width are represented by the following symbols: D, H, b_h, α and D_o respectively. These are shown in figure 4.5 below.

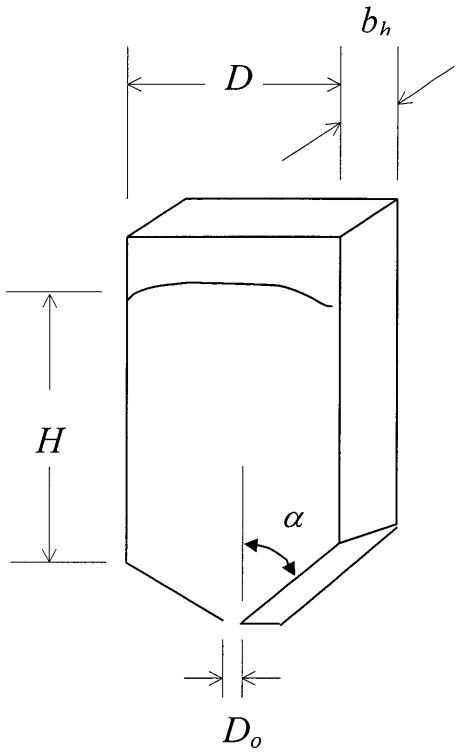


Fig. 4.5 Geometry of the experimental hopper.

4.5 OTHER DESIGN CONSIDERATIONS

One of the things that must be noticed is that for flat bottomed hopper experiments, i.e. when the hopper half angle is 90°, the majority of pieces 3 and 4 will be below the front and back walls. The maximum distance these two pieces could extend below the PVC sheets was 30 cm. As a result, the experimental hopper should include sufficient clearance from the ground to allow the flexibility of moving parts 3 and 4 and to make the collection of the discharging grains easy. For all experiments, the hopper was mounted on a rigid steel frame (100 cm above the floor) so that level and vibration-free operation could be achieved. A small wooden wedge was used to keep the wheat grains inside the hopper while filling. Figure 4.6 shows the experimental hopper after it had been constructed.

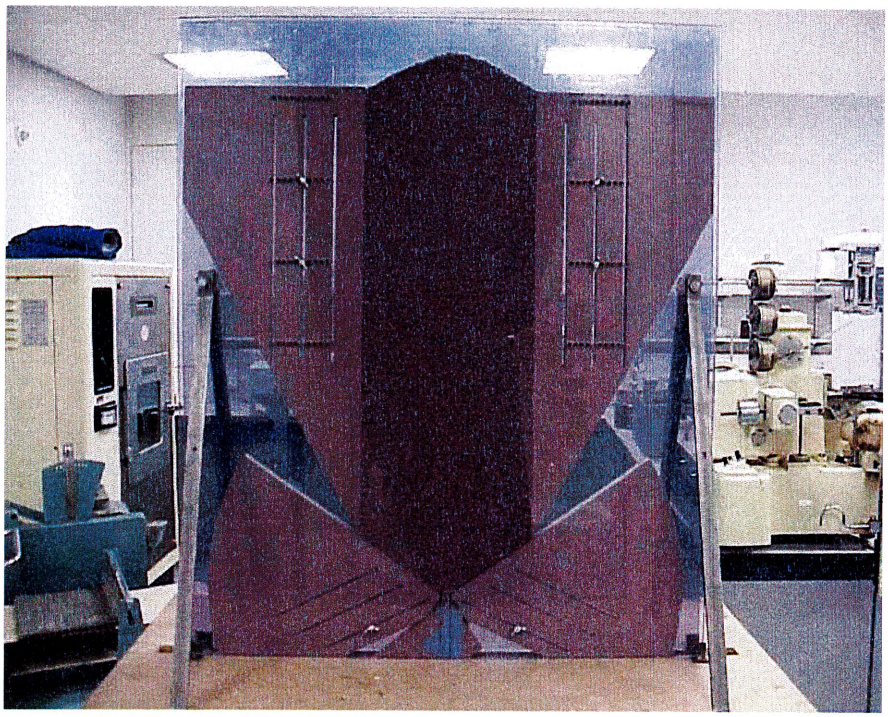


Fig. 4.6 A picture of the hopper used in the experiments, with width set at 28 cm, hopper half angle set at 52° and discharge set at 3 cm.

CHAPTER 5

MATERIALS AND METHODS

5.1 WHEAT USED IN THE EXPERIMENTS

A sample of hard wheat (Hereward) with 11.4% protein and bulk density of 0.781g cm^{-3} was used for all the experiments. While performing the experiments, all the wheat was stored in large covered cylindrical boxes. The moisture content of the sample was found to be 11.30% and 11.66% when measured on two different days. The wheat used was from the 1997 harvest in Humberside.

5.2 PREPARATION OF DIFFERENT SIZE SAMPLES

The original sample of wheat was separated into thickness fractions using the Satake SPU 125 AU Purifier, with slotted stainless steel sieves of sizes: 2.00, 2.25, 2.50, 2.75, 3.00 and 3.50 mm to produce five fractions of the wheat. The purifier, which was operated without air flow functioned effectively as a reciprocating table sifter. It is fed continuously and produces several product streams according to the sieves chosen. Smaller material is removed first, leaving larger material to pass to the next sieve(s). Operation of the Satake SPU 125 AU Purifier is described below:

5.2.1 OPERATION OF THE SATAKE TEST PURIFIER

5.2.1.1 Changing the sieve covers

1. The purifier was disconnected from the mains power supply by turning the dial on the 3-phase switch box to the off position.
2. The sieve frames were pulled out and all residues brushed off into a bin.
3. Since the sieves are glued onto the frames, a screwdriver was used to prise them off the frames. The glue deposits were removed by tapping the frames at an angle of 45° using a hard object like a metal file.
4. When the surfaces of the frames are smooth, the sieve trays were replaced by the required sizes which are 3.5, 3.0, 2.75, 2.5, 2.25, 2.0 mm in width.

5. The sieves were attached to the cleaned frames using Framefast Adhesive 280 (glue) and Framefast Activator 300 (spray).
6. When the glue has set, the sieves were inserted into the purifier for use according to the configuration required for classification.

5.2.1.2 Operating the purifier

1. The power supply was turned on by turning the dial on the 3-phase switch box to the ON position. The LED on the varispeed control box next to the switch box indicates the current setting for the frequency of the purifier.
2. The >/RESET button was used to select the figure on the LED, and the frequency was set at 50 Hz by pressing the $\wedge$ or $\vee$ buttons.
3. The purifier was started by pressing the RUN button.
4. When the purifier was running, the upper hopper was filled with wheat and the feed rate was controlled using the slide gate located above the purifier inlets.
5. When the required quantity was collected, the purifier was stopped using the stop button.
6. The product bins were removed and transferred to the storage bins used to collect the different sizes.

5.3 ANALYSIS OF THE DIFFERENT SIZE SAMPLES

The size of the grains was described by measuring the length, width and thickness. To determine the average size of the wheat samples, three hundred seeds were randomly picked from each sample and their three principal dimensions were measured using the Satake Grain Image Analyser. The Satake Grain Image Analyser (Model RIA-1A) measures the three main dimensions of the grains i.e. length, width and thickness.

In addition to these measurements, it can also be used to separate the grains into different categories based on their length, width or thickness.

Figure 5.1 shows a schematic diagram of the Satake Grain Image Analyser. Two feeders are used to pass the grains onto a tray which is located on a light source. The feeders vibrate to move the grains from the feeding area to the analysis position on the tray. When a grain reaches the analysis area on the tray, the vibration in the feeders stops and the measuring analysis starts.

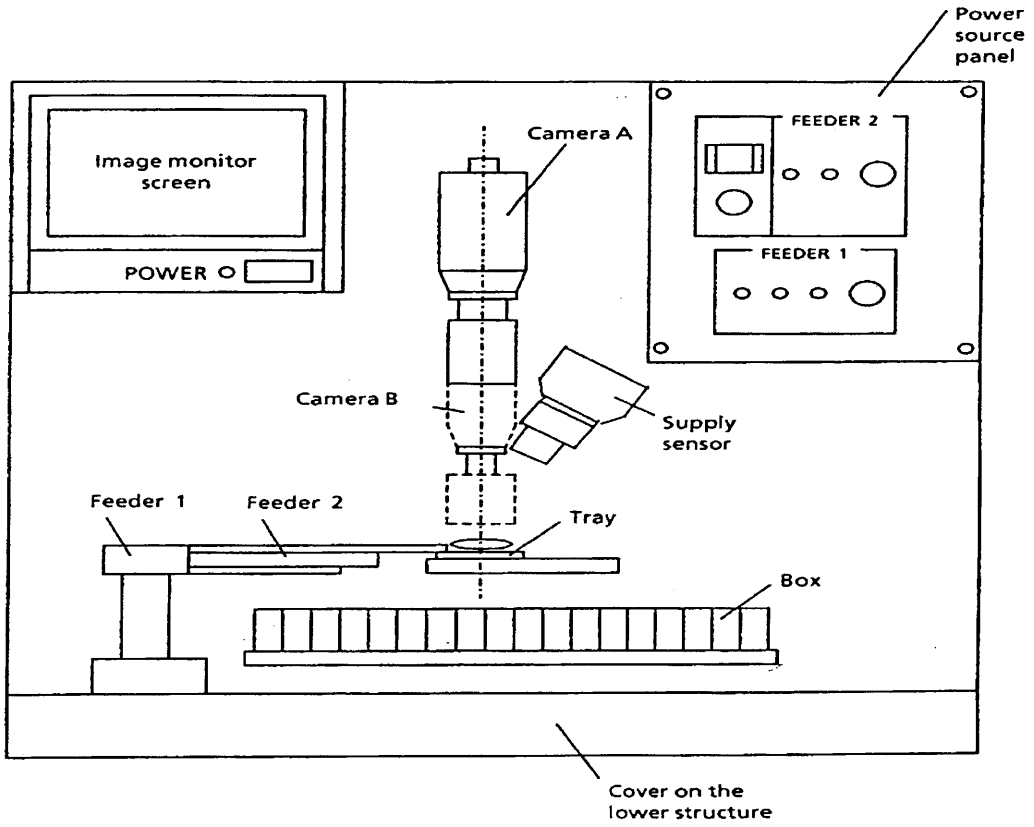


Fig. 5.1 Satake Grain Image Analyser.

In the measuring analysis, two cameras are used. The first is a top camera which measures the length and the width of the grain by taking an image of the grain from above. The second camera, which is a side camera, captures an image from the side of the grain measuring the thickness. The results from the size analysis of the samples

can be saved in data files to be used for subsequent analysis and can be printed immediately using a printer connected to the system (Baival, 1998).

5.4 MEASURING AND ALTERING THE MOISTURE CONTENT OF THE WHEAT

The initial moisture content of the wheat was determined using the air oven method explained in the Approved Methods of the American Association of Cereal Chemists, (AACC) methods. The full procedure to determine the initial moisture content is given in Appendix A. The equation used to calculate the moisture content, as it is shown in the manual is

$$\%\, Moisture = \frac{M_l}{W_s} \text{x}\, 100 \tag{5.1}$$

Where

M_l is the moisture loss in grams;

and W_s is the original weight of the sample.

To vary the moisture content, five samples of six kilograms each were taken from the original non-separated wheat (sample 6) and specific quantities of water were added to each of them in order to reach the required moisture content. The required amount of water was measured using a graduated cylinder, and then added to the wheat to increase the moisture content to the desired value. The desired moisture contents were 13%, 15%, 17%, 19%, and 21%. The equation used to calculate the required quantities of water is

$$Q_m = \frac{W_s\left(M_f - M_i\right)}{(100 - M_f)} \tag{5.2}$$

Where

Q_m: Mass of water to be added, kg;

M_i: Initial moisture content of the sample % (w.b);

and M_f is the final (desired) moisture content of the sample % (w.b) (Visvanathan *et al.*, 1996).

After that, the wheat was weighed and put in a conditioning box. This conditioning box was made of PVC with a maximum capacity of approximately 7.5 kgs. The box was sealed tightly using butterfly screws on the sides of the lid. The cap sealing the sampling point in the centre of the lid was unscrewed, the water poured from the measuring cylinder into the conditioning box, and the cap screwed back on (Odhuba, 1999). Each sample was mixed with the required quantity of water for 15 minutes. Next, all the samples were transferred to sealed bags which were kept for two weeks to enable the moisture to distribute uniformly through each sample. The bags were opened just before performing the experiments.

To ensure that the samples have reached the target moisture content, another test was done to each sample after the two weeks. A two-stage moisture content test was used which is fully explained in Appendix A. The equation used here is

$$\%\,\text{Total moisture} = M_{la} + \frac{\left(100 - M_{la}\right)M_{lo}}{100} \tag{5.3}$$

Where

M_{la}: Percent moisture loss in air drying,

and M_{lo} is the percent moisture loss as determined by oven-drying (refer to Appendix A).

5.5 MEASURING THE ANGLE OF REPOSE

The angle of repose (ϕ) is a measure of the friction between the particles. It is used interchangeably to represent the angle of internal friction for non-cohesive materials. Many methods to measure the angle of repose are reported in the literature. Figure 5.2 shows the different methods given by Thomson (1985).

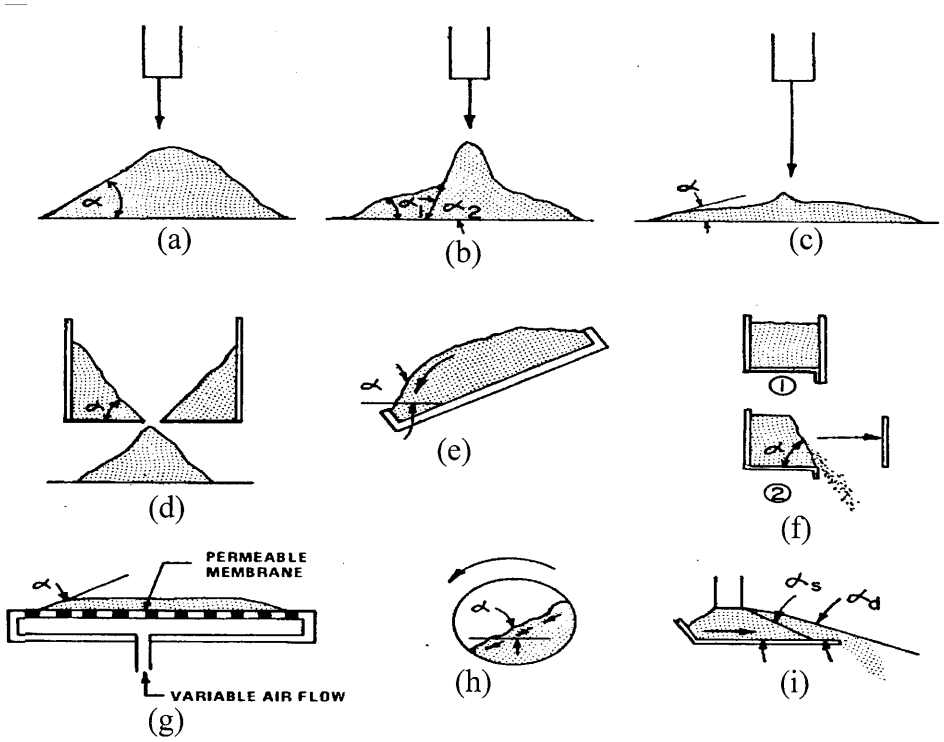
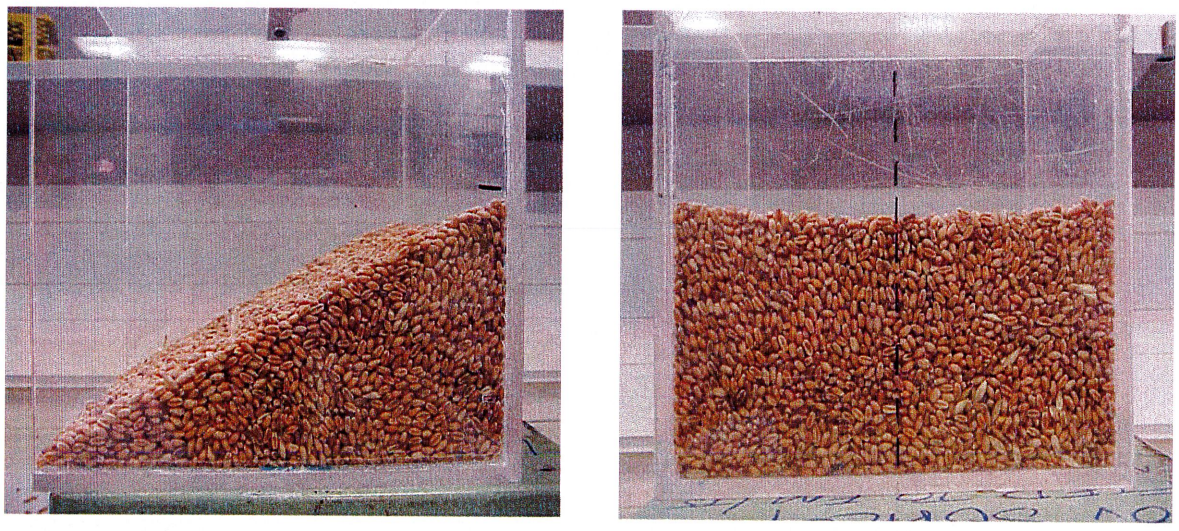


Fig. 5.2 Various measurements of the angle of repose: (a) loose, poured, heap, (b) impacted (some wet and cohesive materials), (c) impacted fluidising-type powders, (d) drained, (e) sliding, (f) compacted, (g) aerated, (h) rolling, (i) discharge from a vibrating feeder (Thomson, 1985).

In figure 5.2, α_s stands for static angle of repose (with feeder stationary) and α_d stands for dynamic angle of repose (with feeder operating).

The method used to measure the angle of repose in this study was similar to method (d) shown above and it was used recently by Singh and Goswami (1996), Morisawa (1999), Chandrasekar and Viswanathan (1999). This method was chosen because it is simple, recently published and gives accurate and reproducible results that differ by only a fraction of a degree. In this method, a clear plastic box 20x20x20 cm in size that is opened from one end was used. The box was filled with the sample then a sheet of cardboard was used to cover the opened upper face of the box. The box was rotated 90° keeping the cardboard held tight against the open end and was placed on another box to elevate it from the table level. After that, the cardboard was quickly removed, and the wheat grains where allowed to flow out of the box and assume a natural slope. Figure 5.3 shows a photograph of the plastic box with the wheat grains forming the natural slope.



(a) (b)

Fig. 5.3 Method used to measure the angle of repose: (a) side view of the box, (b) rear view of the box.

Finally, the angle of repose was calculated by measuring the free surface height of the sample at the centre and from the width of the box. The free surface was taking a curve shape with maximum heights near the side walls. The height was measured at the centre to minimise the wall effects. The equation used to calculate the angle of repose is:

$$\text{Angle of repose}(\phi) = \tan^{-1}\left(\frac{\text{Measured height from the centre of the box}}{\text{Width of the box}}\right) \qquad (5.4)$$

The method discussed above was used to measure the angle of repose for the samples with different wheat thickness and the samples with different moisture contents.

5.6 GENERAL PROCEDURE FOR MEASURING THE FLOWRATE FROM THE HOPPER

In order to measure the flowrate from the hopper, the following procedure was followed:

1. The hopper was set to the required geometry depending on the factor to be investigated.
2. A small wooden wedge was placed at the hopper outlet to keep the wheat grains inside the hopper while filling.
3. The hopper was filled by raining the wheat particles from the top at the middle of the hopper with no attempts to consolidate the particles accumulated inside the hopper.
4. The flow was initiated by removing the wooden wedge from its place at the orifice and the grains were discharged freely under the influence of gravity.

5. The flowrate was measured by weighing a sample of wheat collected over a measured time interval. A stopwatch was used to measure the time with a timing resolution of ± 0.01 second and that of the weight about ± 0.1 gram.
6. All the experiments were repeated several times to minimise the errors and to make sure that the results were reproducible.

5.6.1 EXAMINING THE EFFECT OF MATERIAL HEAD ON THE FLOWRATE

In this experiment the flowrate was measured when the material head reached six different heights during the batch discharge. These six heights were 76, 63.5, 51, 38.5, 26.5 and 13.5 cm above the discharge plane.

The settings of the hopper and the wheat sample used were:

- Initial total height: 95 cm.
- Width: 32 cm.
- Hopper half angle: 35°.
- Discharge opening: 1 cm.
- Sample of wheat used: 3 (Average thickness = 2.54 mm).

5.6.2 EXAMINING THE EFFECT OF HOPPER WIDTH ON THE FLOWRATE

In this experiment the flowrate was measured for six different widths of the hopper. All of these measurements were made when the material head was 26.5 cm above the discharge point. The six different widths were 38, 30, 24, 18 and 10 cm. For the first three runs the initial height was 95 cm and for the last two they were 86 and 82 cm respectively. Each run corresponding to a hopper width was repeated six times and the

average value from each run was used in the data analysis. The settings of the hopper and the sample of wheat used were:

- Sample of wheat used: 3 (Average thickness = 2.54 mm).
- Hopper half angle: 32°.
- Discharge opening: 1.8 cm.
- Height from which the flow rate was measured = 26.5 cm.

5.6.3 EXAMINING THE EFFECT OF PARTICLE SIZE ON THE FLOWRATE

To examine the effect of particle size on the flowrate, four samples representing four size divisions of wheat were used. The average values of the thickness of the wheat particles were 2.75, 2.65, 2.54 and 2.33 mm. Each run was repeated eight times and the average value was calculated. The settings of the hopper for this experiment were:

- Initial total height: 95 cm.
- Width: 30 cm.
- Hopper half angle: 30°.
- Discharge opening: 1.5 cm.
- Height from which the flow rate was measured = 26.5 cm.

5.6.4 EXAMINING THE EFFECT OF HOPPER HALF ANGLE ON THE FLOWRATE

In this experiment the flowrate was measured for six different hopper half angles. These six angles were 33°, 40°, 47°, 52°, 57°, and 61°. Each run was repeated six times. The settings of the hopper and the sample used for these runs were:

- Initial total height: 95 cm.

- Width: 30 cm.
- Discharge opening: 1.7 cm.
- Sample of wheat used: 3 (Average thickness = 2.54 mm).
- Height from which the flow rate was measured = 26.5 cm.

5.6.5 EXAMINING THE EFFECT OF DISCHARGE SIZE ON THE FLOWRATE

Six different discharge sizes were used to investigate the effect of the discharge opening size on the flow rate. These six discharge openings were 1.5, 2.0, 2.4, 2.8, 3.2, and 3.6 cm. The hydraulic mean diameter was used to represent the discharge size. The corresponding hydraulic mean diameters were 1.88, 2.24, 2.44, 2.64, 2.80 and 2.95 cm. In order to calculate the hydraulic mean diameter the following equation is used

$$D_h = \frac{4(lxb_s)}{2(l+b_s)} \tag{5.5}$$

Where

l is the slot length,

and b_s is is the breadth of the slot.

The settings of the hopper for this investigation and the sample used were:

- Initial total height: 95 cm.
- Sample of wheat used: 3 (Average thickness = 2.54 mm).
- Hopper half angle: 30°.

- Width: 30 cm.
- Height from which the flow rate was measured = 26.5 cm.

5.6.6 EXAMINING THE EFFECT OF MOISTURE CONTENT ON THE FLOWRATE

The effect of moisture content on the flowrate was investigated in this experiment. The values of the moisture contents used were 11.66%, 13.90%, 15.65%, 18.03%, 19.56% and 21.60 %. The settings of the hopper and the sample used are given below:

- Initial total height: 95 cm.
- Sample 6 (Average thickness = 2.58 mm).
- Hopper half angle: 30°.
- Discharge opening: 1.75 cm.

5.7 PHOTOGRAPHIC STUDY OF FLOW IN THE HOPPER

For this study a digital camera was used to take pictures of the flow at different stages of the batch discharge. The photos were taken from behind a black curtain which was used to minimise the reflection of the front wall so that the photos will be clearer with less reflection. A hole was punched in the curtain to allow the pictures to be taken through without reflecting the image of the person taking the pictures on the hopper walls. Different photographs were used to investigate the flow fields, the shapes of the free surface, the alignment of the wheat grains and the blockages occurring in some of the experiments.

In studying the flow fields, layers of dyed wheat were placed horizontally at different heights inside the bin. Two hundred millilitres of black ink was used to dye 3 kgs. of

the wheat. The wheat was mixed with the black ink and some water and was kept over a night so the wheat could absorb the colour. The next day an oven was used to dry the wheat which after that was kept for one week in a dry place. After this period of time, the dyed wheat grains were observed to be dry enough with a normal moisture content that would not affect the flow characteristics.

CHAPTER 6

RESULTS AND DISCUSSION

6.1 SAMPLES OBTAINED FROM THE SATAKE PURIFIER

The result of the separation using the Satake SPU 125 AU Purifier was 4 major samples which were adequate to fill the hopper and another sample (sample 5) which was not enough. All the samples, including the fifth were used in the angle of repose determination. The original mixture, from which these five samples were obtained, called sample 6, was also used to study the effect of moisture content on the angle of repose and on the flowrate from the hopper.

6.2 GRAIN DIMENSIONS

The mean dimensions of the 300 seeds picked from each sample are shown in table 6.1.

Table 6.1 Size analysis for the six wheat samples.

Sample	*Length*		*Width*		*Thickness*	
	Average (mm)	*S. D. (mm)*	*Average (mm)*	*S. D. (mm)*	*Average (mm)*	*S. D. (mm)*
1	6.45	0.52	3.62	0.55	2.75	0.35
2	6.35	0.58	3.56	0.65	2.65	0.29
3	6.25	0.77	3.29	0.54	2.54	0.24
4	5.99	0.65	2.91	0.41	2.33	0.26
5	5.66	0.69	2.61	0.29	2.17	0.24
6	6.36	0.81	3.43	0.68	2.58	0.33

The full results of the size analysis obtained from the Satake rice image analyser are given in Appendix B.

6.3 MOISTURE CONTENTS OBTAINED

The average moisture content obtained for the mixture of wheat at the beginning was 11.30%. Table 6.2 shows the details of the results obtained for the initial moisture content calculation.

Table 6.2 Results obtained for the initial moisture content.

Trial	*Weight of the original sample (g)*	*Weight of the sample after drying (g)*	*Loss in weight (g)*	*Moisture content (%)*	*Average moisture content (%)*
1	2.8334	2.5141	0.3193	11.27	11.30%
2	3.0034	2.6629	0.3405	11.33	
3	2.6891	2.3801	0.3090	11.30	

The equation used to calculate the % moisture content is equation (5.1) given in the Materials and Methods. On the basis of this, equation (5.2) was used to calculate the amount of water to be added to reach the desired moisture contents. Table 6.3 presents the quantities of water added in addition to the final % moisture contents reached after two weeks.

Table 6.3 Quantities of water added and the %moisture contents achieved.

Sample	*Initial moisture content (%)*	*Target moisture content (%)*	*Quantity of water added (ml)*	*Moisture content obtained (%)*
1	11.30	13	118	13.90
2		15	262	15.65
3		17	412	18.03
4		19	571	19.56
5		21	737	21.60

These five moisture contents were found on the day of performing the experiments. In addition, another moisture content test was performed on a sample from the original mixture.

The moisture content was found to be 11.66% instead of 11.30% that was found two weeks earlier when the five samples were conditioned. This slight change may be due to the different weather conditions between the two days of performing the tests. Table C.1 in Appendix C shows the detailed measurements leading to the moisture contents found.

6.4 GENERAL OBSERVATIONS ON THE PERFORMANCE OF THE EXPERIMENTAL HOPPER

The experimental hopper was built in the Chemical Engineering Department workshop. After that, it was transferred to the Satake Centre lab where the experiments were performed. Most of the results obtained from the hopper were acceptable showing an agreement with what is reported in the literature. This shows that the design and the building of the hopper were successful. In setting the hopper to the required geometry, it was very easy to change the width by moving pieces 5 and 6. However, it was very difficult to reset the discharge to the original value once it had been changed. This was because of the difficulty of moving pieces 3 and 4 precisely. So all the experiments investigating the same factor e.g. the hopper width or the hopper half angle had to be carried out in one batch to avoid changes in the hopper geometry.

A further problem was with the retaining bolts on both sides of the front and back walls which were punched through the whole hopper breadth. These retaining bolts limited the downward movement of pieces 5 and 6 to a certain level making it impossible to reach the flat bottomed hopper.

Filling the hopper manually for all the runs was a tedious job and no control of the flow rate could be achieved once the flow had started. Finally, the hopper stand, which was made of steel, was very heavy and was very difficult to move.

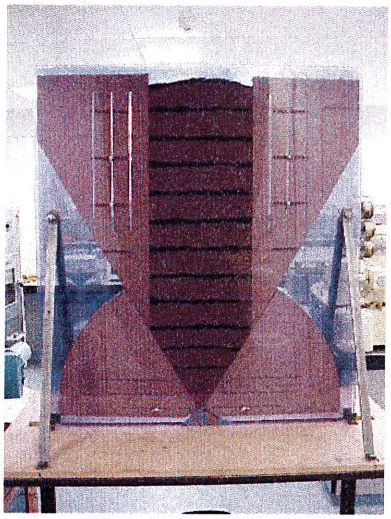
6.5 QUALITATIVE OBSERVATION OF THE FLOW IN THE HOPPER

6.5.1 REPEATABILITY OF THE FLOWS

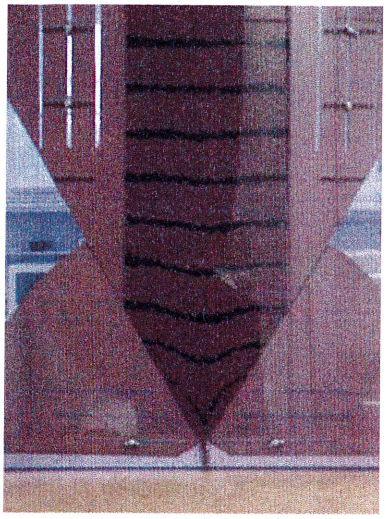
In most of the experiments, it was noticed that the flow was reproducible. The average time to discharge the whole material inside the hopper was almost the same with less than a second difference between different runs. This was noticed when the same quantity of the same material was loaded in the same hopper geometry. For example, when sample 3 with the following hopper geometry: $H = 95$ cm, $\alpha = 32°$, $D_0 = 1.8$ cm and $D = 38$ cm was used, the time needed to empty the hopper in four different runs was 70.46, 69.95, 70.12 and 70.18 seconds. Baxter *et al.* (1989) who worked on batch discharge experiments reported the same observation.

6.5.2 DEFORMATION OF THE LAYERS OF COLOURED PARTICLES

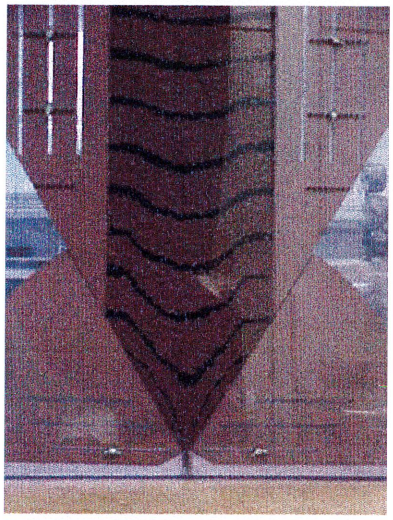
In this investigation, dyed wheat grains were used to make horizontal layers of coloured particles. This was done so that the flow lines would be obvious through the PVC. Twelve pictures were taken to represent the stages of the batch discharge during this experiment. Figure 6.1 shows the first six pictures which are the first set showing the general shape obtained for the flow lines. In the sequence of the pictures it is clear that the flow was developed mainly in the central region, spreading to the sides where the grains were moving at a lower velocity. The grains near and attached to the walls were stationary forming the stagnant zones.



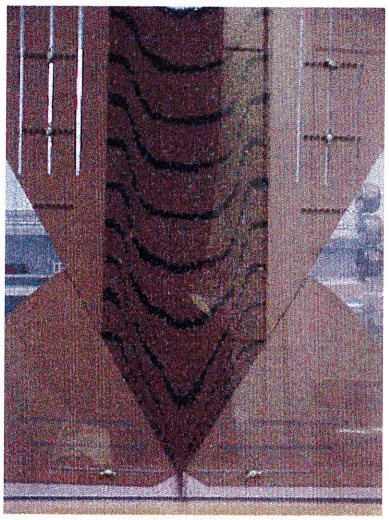
(a) At time = 0 seconds.



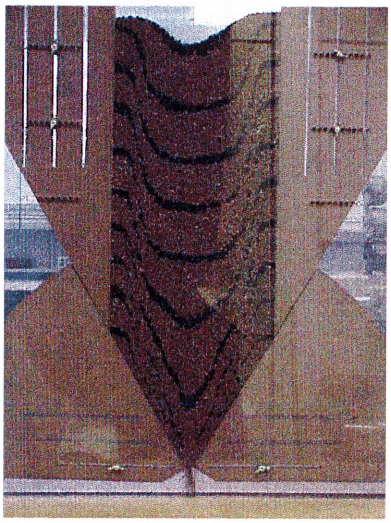
(b) At time = 2 seconds.



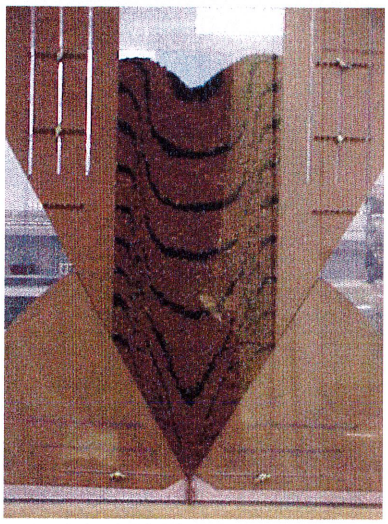
(c) At time = 5 seconds.



(d) At time = 10 seconds.



(e) At time = 20 seconds.



(f) At time = 30 seconds.

Fig. 6.1 Development of the flow lines in the hopper with the following geometry: D = 28 cm, D_o = 1.3 cm, α = 30° and H= 95 cm.

Rhodes (1998) has given a figure sketched from past photographic studies on funnel flow using layers of coloured particles. Figure 6.2 shows the drawings given by Rhodes and the similarity is obvious between these drawings and the photographs obtained from the present experiment.

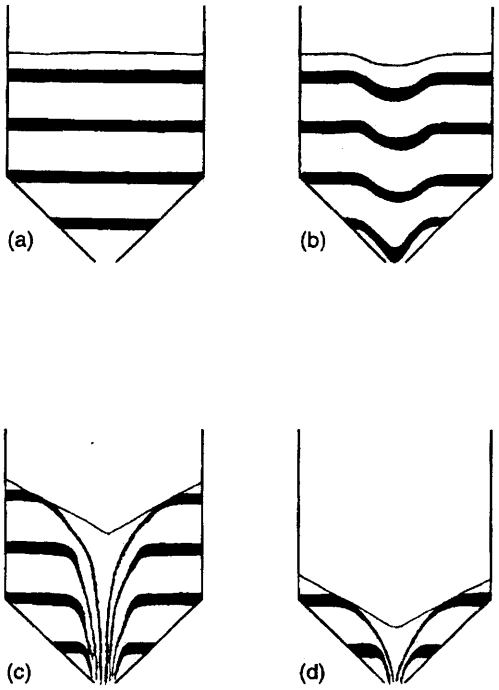


Fig. 6.2 Drawings of flow lines in an experimental hopper (Rhodes, 1998).

Gardner (1966) performed the same kind of experiment using Durite. He described the flow line development as a long ellipsoidal shape located on the axis of symmetry. This ellipsoidal shape was broadening as the flow develops and it penetrates further up the upper section of the bin till it reaches the upper free surface (refer to figure 3.2 (a)). Moreover, he reported that the flow lines near the discharge were almost parallel to each other. The photographs obtained from the present experiment confirmed all of these observations by Gardner (1966).

Nguyen (1979) performed the same experiment using coloured glass beads and coloured sand. The same general observation about the development of the flow was noticed. However, the shape of the flow lines were found to be different for glass beads than for sand. Figure (6.3) shows a comparison of the flow lines obtained for sand and glass beads.

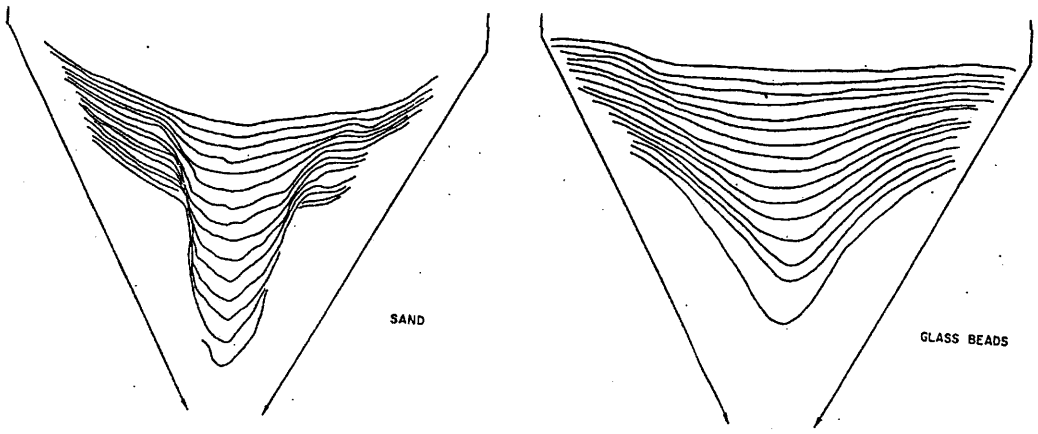


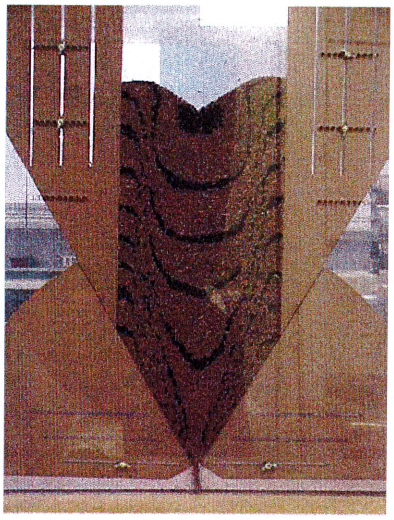
Fig. 6.3 Flow lines for sand and glass beads (Nguyen, 1979).

Nguyen reported, as shown in the figure, that the flow field for glass beads shows a continuous and smooth deformation across the hopper. On the other hand, for sand there was a discontinuity which divides the fast flowing central core from the slower moving material near the hopper walls. The flow lines obtained from the present study agree with the flow lines for the glass beads and show a smoother deformation across the hopper. This may be due to the similar angles of internal friction (angle of repose) for the glass beads used by Nguyen (25°) and for the wheat used in this experiment (25.37°). The angle of internal friction for the sand used by Nguyen was 31°.

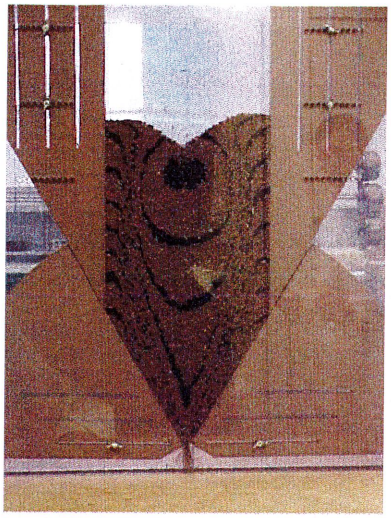
A new observation from the present experiment was a circular structure developed by the dyed material. This circular shape was formed by the top surface which was a layer of the coloured wheat. This circular structure moved towards the outlet as the discharge continued. This means that the coloured wheat grains of the free surface on the sides of the bin were unable to penetrate the stagnant zones near the walls. As a result they started to feed to the central core where they accumulated and continued their way downwards till they discharge. Figure (6.4), which is a continuation of the flow development shown in figure (6.1), shows the initiation and movement of this circular structure.

Contour lines were developed to surround the circular shape. These lines were formed from the upper layers of the dyed wheat when the top free surface descended below the layers of these lines. When the circular shape approached the outlet, it discharged forming a tongue of the coloured material that can be observed clearly in figure 6.4 (f). Gardner (1966) also noticed this tongue as was shown in figure 3.2 (b).

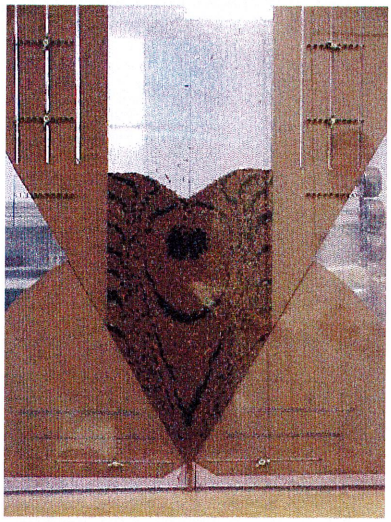
From the above results and discussion, it is manifest that there is an agreement on the general shape of the flow lines. Moreover, all the studies confirmed that the material located above the discharge and along the central core will start to descend faster than the material at the sides of the bin. However, more studies are required to investigate how the characteristics of the material such as the shape and the internal friction and the hopper geometry will affect the general shape of the flow lines developed during the flow.



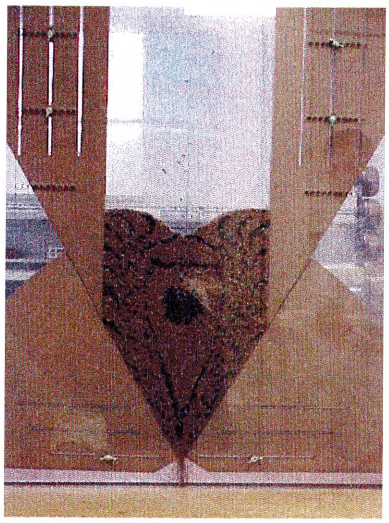
(a) At time = 39 seconds.



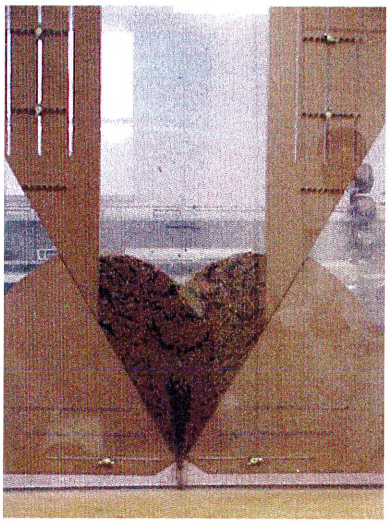
(b) At time = 48 seconds.



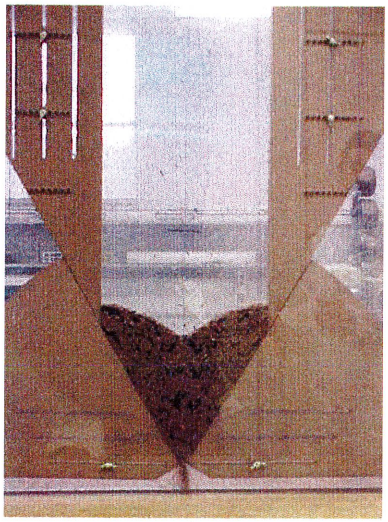
(c) At time = 58 seconds.



(d) At time = 64 seconds.



(e) At time = 76 seconds.



(f) At time = 92 seconds.

Fig. 6.4 Continuation of the flow showing the formation and the movement of the circular structure and the tongue initiated above the orifice.

6.5.3 STAGNANT ZONE

The stagnant zone was observed to develop near the upper part of the inclined walls of the hopper and the vertical walls of the bin. This stagnant zone became larger as the hopper half angle or the width of the hopper increased or as the discharge width decreased. In order to observe this stagnant zone and to observe how it is affected by the hopper geometry, a camera with several seconds exposure time facility is needed. This facility will show the moving grains as a blurry region while the grains in the stagnant zone will be easily observed to be stationary. Since the maximum exposure time for the camera used in these experiments was 1/60 sec, it was not possible to get photographs of the stagnant zone. However, the photographs in figures 6.1 and 6.4 show clearly the existence of the stagnant zone near the walls. The unchanged pattern of the coloured grains near the walls through the discharge operation represent clearly the areas covered by the stagnant zone. The stagnant zones observed in the different experiments were similar to those obtained by Nguyen *et al.* (1980), (figure 3.8), which confirms their observations. However, the limitation in the camera's exposure time makes it impossible to take pictures of the stagnant zones and compare them directly with the published pictures.

Further studies could be done using a camera with a higher exposure time so the stagnant zone will be clear compared to the moving grains. If this facility is available, the effect of the hopper geometry on the stagnant zone shape and development could be studied by analysing the different pictures for the various geometries of the hopper.

6.5.4 ALIGNMENT OF THE WHEAT

When the hopper was filled and before the flow was initiated, the wheat particles aligned themselves parallel to the vertical walls with very few of them vertical to the PVC walls. This alignment of the particles means that the flow is nearly two-dimensional. In addition to the parallel alignment, the grains also made all the possible orientations with their major axis. Baxter and Behringer (1990) also reported these observations. Figure 6.5 represents the above observations.



Fig. 6.5 Initial alignment of the wheat grains inside the hopper, shortly after filling and before starting the discharge.

Once the discharge operation was in progress, the grains within the flowing region tended to align themselves with the direction of the flow. The grains above the orifice were aligned vertically towards the opening and the grains in the nearby area were also directed with their major axis towards the discharge opening. When the final discharge stage is reached, it was obvious that almost all the wheat particles were directed towards the orifice. Figure 6.6 shows how the grains are all directed towards the outlet at the bottom of the hopper. Nguyen (1979) who used rice with an elongated

shape and Baxter and Behringer (1990) who used grass seeds reported the same thing concerning the grain orientation during flow.

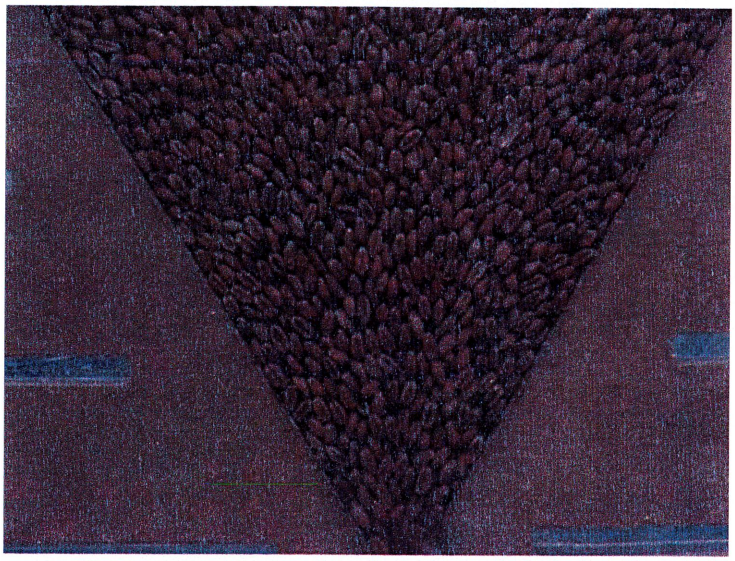
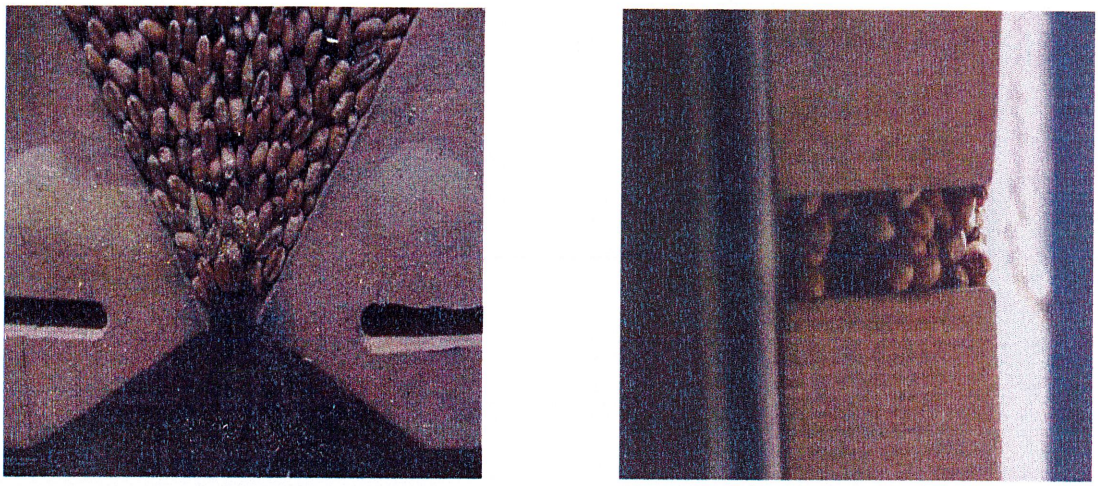


Fig. 6.6 alignment of grains near the outlet of the hopper during discharge .

6.5.5 BLOCKAGES

In some of the experiments, with a small discharge size, the flow stopped for a while (1 or 2 seconds) and then continued. In other experiments, the flow stopped permanently and shaking the hopper was needed to resume the flow. This was the result of arching near the outlet (figure 2.1). This shows the importance of making the orifice large enough in real hoppers to avoid blockage problems. Figure 6.7 (a) is a front view showing the arch shape formed by the grains. Figure 6.7 (b) shows a bottom view of the grains interlocking at the outlet. Spink and Nedderman (1978) reported infrequent arch formation in their experiments in the orifice region. The blockage occurred for beds that had become heavily compacted while staying in the hopper. They reported that the arches could be broken easily by gentle tapping and once the flow restarted, no further blocking occurred.



(a) (b)

Fig. 6.7 Front and bottom views of an arch blockage in the hopper with a small discharge size ($D_o = 7$ mm with $\alpha = 30°$).

6.5.6 SHAPES OF THE FREE SURFACE

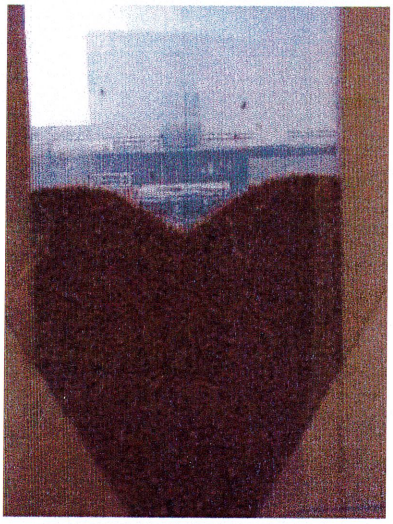
The upper free surface of the grain took different shapes as the discharge operation progressed. At the beginning the surface was dome shaped. This shape was the result of filling the bin at the line of symmetry. For a few seconds, after the start of the batch discharge operation, the upper surface started to descend while maintaining its dome like shape. At a level where the top surface reached the stagnant zones near the vertical bin walls, the middle of the upper surface, which was the highest point, started to fall relative to the other points located on the free surface. The dome shape continued to flatten more and more as the material continued to discharge until it reached an almost straight line (figure 6.8 (b)). The middle point continued to fall at a faster rate than the other points on the free surface till the hopper emptied completely (figure 6.8 (c) and (d)).



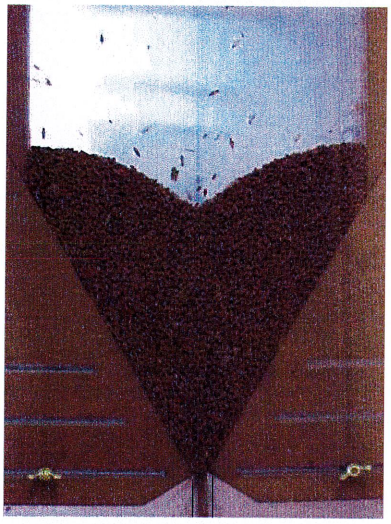
(a) At time = 0 seconds.



(b) At time = 34 seconds.



(c) At time = 60 seconds.



(d) At time = 90 seconds.

Fig. 6.8 Shapes of the free surface during the discharge (a) The original domed shape. (b) An almost straight line shape. (c) and (d) decline of the surface at the middle.

Baxter and Behringer (1990) did not discuss the shape of the free surface. They only mentioned that the free surface passes through complex shapes. Drescher *et al.* (1978) used sand in a mass flow hopper and they reported the same observation for the free surface. This means that the shape of the free surface is independent of the type of the flow whether it is a mass flow or a funnel flow which was observed in this experiment.

Seville *et al.* (1997) reported the same shapes for the free surface. They divided the discharge operation into three main stages (i) initial transient stage, (ii) pseudo steady-state and (iii) final transient stage. Figure 6.9 shows the shapes provided by Seville *et al.* (1997) which show an agreement with the observations of the present experiment.

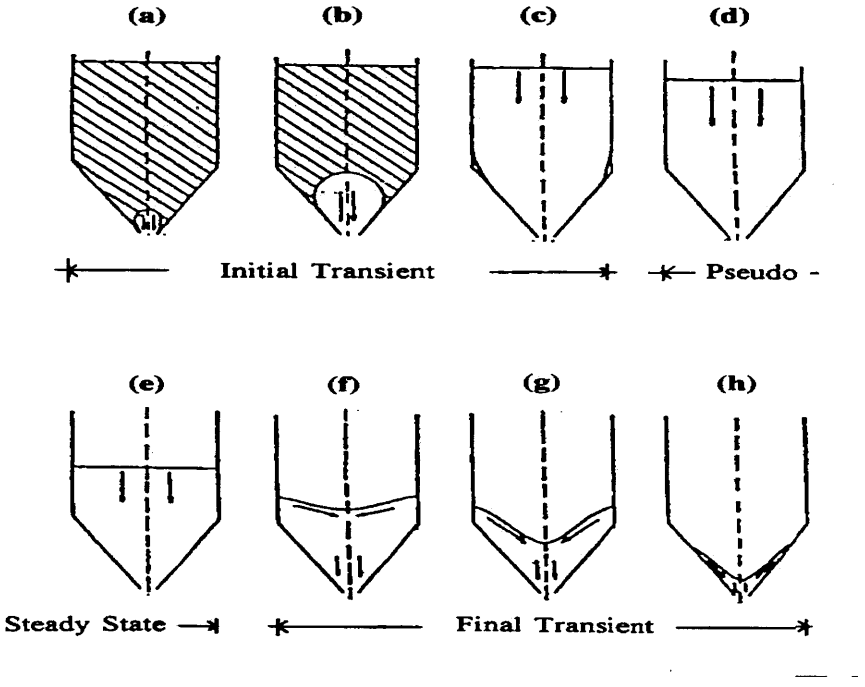


Fig. 6.9 Different stages of the discharge and the free surface shape (Seville *et al.* 1997).

The first stage could not be confirmed by the present experiment since it needs a radiograph method to be able to visualise the propagating wave. The second and third stages were both obtained from the present experiment. The reason behind the centreline decline in the free surface is the fast movement of the grains located on the centreline above the discharge relative to those at the sides near the walls (Seville *et al.*, 1997).

For the narrower hopper configurations e.g. 10 cm., with an aspect ratio of $H / D \approx 8$, it was noticed that more time was required for the free surface to decline and change its shape. This was the result of the fast movement of the whole bulk of the material in the bin with the same speed without any formation of stagnant zones. This observation agrees with that reported by Seville *et al.* (1997), namely for high aspect ratios ($H > 3\text{-}4D$), the upper surface will retain its shape for a longer time. On the other hand, faster transition between the different stages was observed for wider hopper configurations e.g. 38 cm with lower aspect ratios $H / D = 2.5$. This agrees with Seville *et al.* (1997) who reported the same observation for aspect ratios of $H <$ 1-2 D.

Another factor affecting the free surface shape is the ratio between the hopper width (D) to the discharge width (D_0). An increase in this ratio will make the transition between the different stages faster. However, more time will be needed for the surface to transform from one shape to another for smaller D: D_0 ratios.

The shapes obtained from this study are in total agreement with what is reported in the literature. It is suggested to make further studies to find a mathematical expression to represent the shape at different time intervals. Moreover, it is recommended to investigate more how the aspect ratio will affect the free surface shapes and to get more precise values of the aspect ratios representing the transition from one stage to another.

6.6 ANGLE OF REPOSE

6.6.1 EFFECT OF THE PARTICLE SIZE

In this experiment, samples 1-5 were used for the angle of repose measurements. The five samples used represent the five main divisions obtained from the sieve analysis for the original mixture (sample 6). Tables D.1- D.5 in Appendix D give the different values of the angle of repose obtained for the different samples used. Also the tables show how the standard deviations between the results are very small ranging between 0.115 and 0.23 degrees. The average values from the tables were used to draw the angle of repose as a function of particle thickness as shown in figure 6.10.

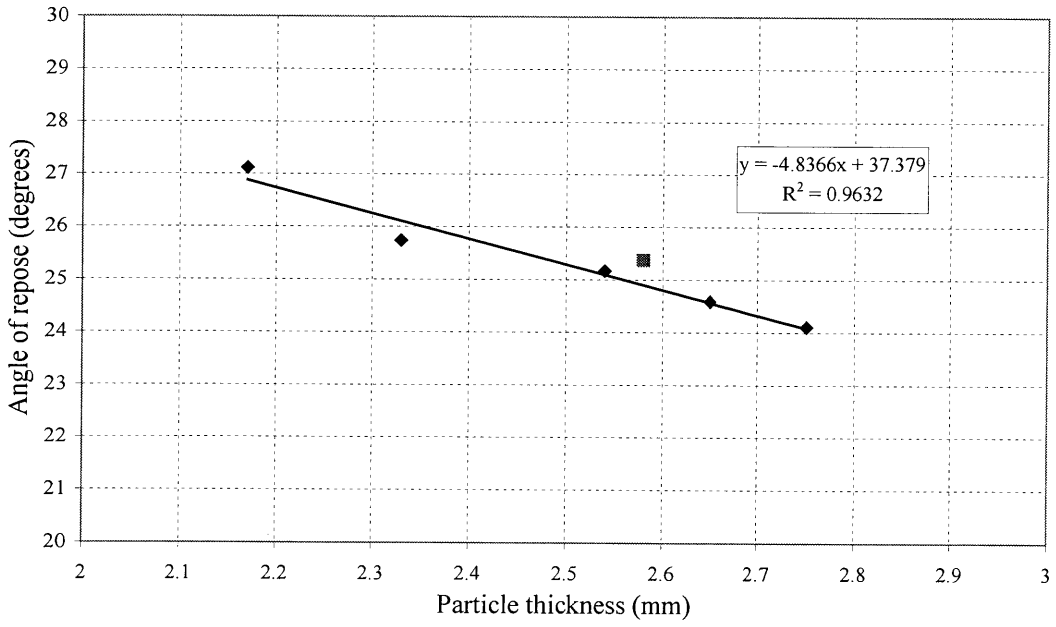


Fig. 6.10 Angle of repose as a function of particle thickness with a point representing the angle of repose for the mixture with a different marker.

A linear relationship was found between the angle of repose and the particle thickness. As the wheat thickness decreased the angle of repose increased. This may be due to the relative shapes of the particles which tends to be more rectangular for small grains, helping them to interlock and form a higher pile. On the other hand, the larger particles are more spherical in their shape which will help them to slide easily

and form a smaller angle of repose. No clear relation between the angle of repose and the particle size of a granular material could be found in the literature. Over the range of wheat grain sizes studied, angle of repose could be reasonably predicted from the following equation:

$$\phi = 37.4 - 4.84\, t_p \qquad (6.1)$$

With t_p stands for thickness of the wheat particles.

Carr (1965) stated that the angle of repose provides an indirect indication of many properties of the materials. One of those mentioned was the particle size. However, Carr did not go further and discuss how the particle size will affect the angle of repose. Jenike (1964) reported that the angle of repose is not a function of the flowability and its popularity is due to the ease with which it is measured.

Brennen and Pearce (1978) found that the angle of internal friction increases as the standard deviation in particle size increases. The greater interlocking in the materials with larger variations in particle size was the reason they proposed in their paper. However, no effect on the size variation of the samples was observed in the current study on the angle of repose. Spink and Nedderman (1978) used four grades of sands with different size ranges from 63-90 μm for the smallest grade to 210-300 μm for the largest size grade. The angles of internal friction for the sizes were around 35° and again no further conclusion could be drawn from their measurements. Tüzün and Nedderman (1982) measured the angle of repose for glass ballotini with mean particle sizes ranging from 0.6 to 2.0 mm. No clear relationship was given in their results.

In this study, the difference in the angle of repose for the different samples was very small (approximately 0.5°). This is expected since the difference in the thickness of the samples was only approximately 0.1 mm. It is recommended to try to measure the angle of repose for a wider range of sizes of wheat. Moreover, studies on other agricultural seeds with different shapes could be done to see if the same relation applies to other grains or if it is only specific to wheat or particles with elongated shapes.

6.6.2 EFFECT OF MOISTURE CONTENT

In this experiment, wheat samples with different moisture contents were used to investigate the effect of moisture content on the angle of repose. The different moisture contents used were 11.66%, 13.90%, 15.65%, 18.03%, 19.56% and 21.60% (see table 6.3) and sample (6), the mixture, was the one used in this investigation. The results obtained of the angle for repose of the six samples are given in Appendix E in tables E.1- E.6. The *S.D.* was always less than 0.27°. The average angle of repose is plotted for each moisture content in figure 6.11.

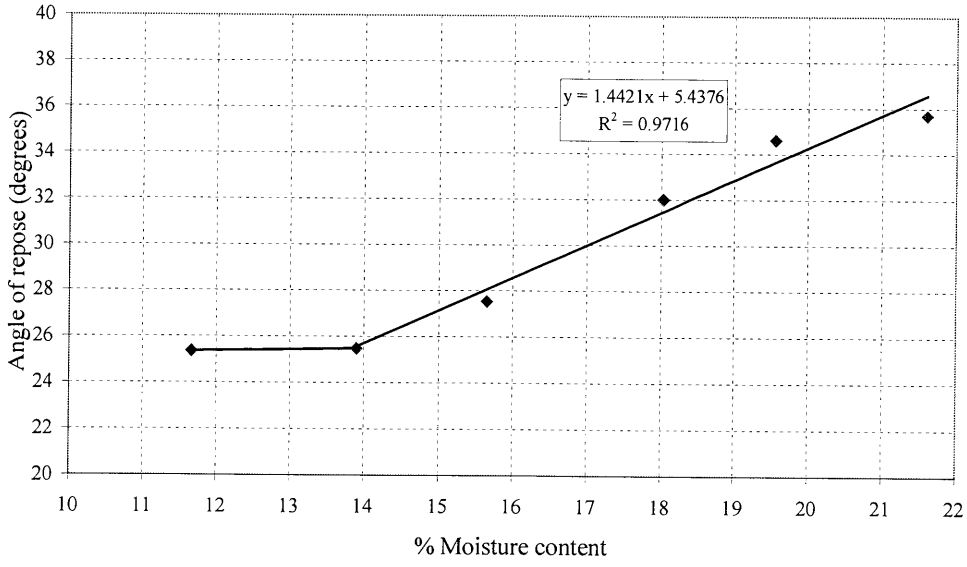


Fig. 6.11 Angle of repose as a function of moisture content for sample 6 (original mixture) with an average thickness of 2.58 mm.

The figure shows a constant value of the angle of repose obtained for the lower two values of moisture content, 11.66% and 13.90%. However, the relation becomes almost a linear increase in the angle of repose from 25.33° to 35.69° when the moisture content increases from 13.90% to 21.60%. For moisture contents within this range, the angle of repose can be estimated from:

$$\phi = 1.44\, MC + 5.44 \tag{6.2}$$

Where MC represents the moisture content of the wheat samples.

The linear relationship obtained here is similar to that obtained by Singh and Goswami (1996) who found a linear increase in the angle of repose as the moisture content increases for Cumin seeds. Other linear relationships were obtained by Suthar and Das in 1996 for Karingda seed and by Visvanathan *et al.* (1996) for Neem nuts. Jha (1999) and Aviara *et al.* (1999) found the same general relation between the moisture content and the angle of repose, however, they did not choose a straight line to represent the data. Aviara *et al.* (1999) used an equation of the power law type to fit the values obtained for Guna seeds. Jha (1999) joined the points by a curve without giving any equation to relate the moisture content with the angle of repose for Makhana.

The increase in the angle of repose for higher moisture contents may be due to the increase in the surface roughness (Singh, 1996) or due to some cohesion between the agricultural grains. There is an agreement between all the articles that the angle of repose increases with increasing moisture content for seeds.

The only difference between the results obtained from the experiment for wheat and the other results found in the literature is that from this experiment, there is a point were the moisture content starts to affect the angle of repose. Below this critical moisture content, about 13.90% for wheat, no effect was noticed. In all the articles mentioned above, a continuous increase in the angle of repose was obtained as the moisture content increased.

In figure 6.11 it can be seen that the last two values of moisture content, which differ by 2.04% gave a difference of 1.09° which is relatively small when compared to the other differences. This makes one wonder about the nature of the relationship after the 21.60% moisture content if it is going to follow the same linear trend or the angle of repose will move towards a constant value no matter how much the moisture content increases. More investigation is needed for moisture contents greater than 21.60% and less than 13.90% in order to improve confidence in the relationship.

6.7 DISCHARGE RATE FROM THE HOPPER

It was mentioned in section 2.1 that bins, silos, bunkers and hoppers are all used to store granular material and every category is different from the others. However, the term "hopper" is used below to represent the experimental rig which consists of a tall bin or silo and a converging hopper part.

6.7.1 EFFECT OF MATERIAL HEAD

The mass flowrate was measured at six different material heads that cover the whole hopper height from the top till the hopper is nearly empty. The result of these measurements was that the flow rate was constant for almost the whole height of the hopper. Tables F.1- F.4 in Appendix F represent the data obtained from this experiment. Figure 6.12 below shows the average values from the tables against different material heads.

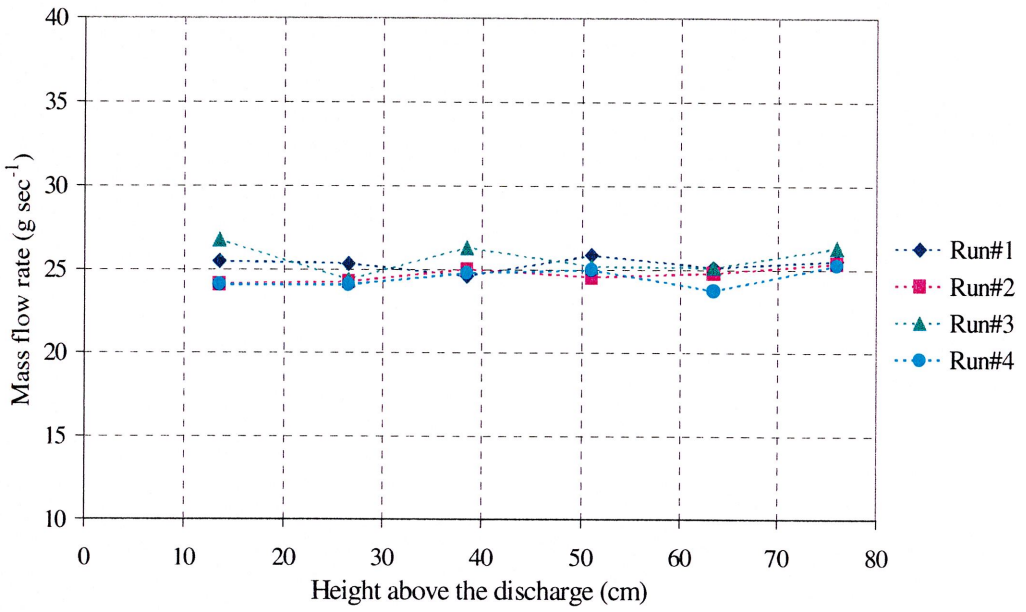


Fig. 6.12 Effect of material head in the hopper on the flowrate (Hopper settings were: initial H = 95 cm, D = 32 cm, D_o = 1 cm, α = *35* ° and sample used: 3).

In all the runs the mass flowrate fluctuated between 24.10 and 26.74 g sec^{-1} and this is clear in figure 6.12. The independence of the flowrate from the height of material in the hopper is complete contrast to the behaviour of liquids and gives a clear reason why modelling the flow of solids as fluid flow is not realistic.

The findings from this experiment confirm what is reported in the literature (Bosley *et al.*, 1969; Nedderman *et al.*, 1982; Gao, 1997) that W is independent of the material

head in the hopper till it is nearly empty. This means that no effect on the flowrate is caused by pressure changes resulting from the different heads of material inside the hopper. While the hopper is discharging, the pressure created by the particles is dissipated by the interactions between the discrete granular particles. The result will be that the walls will take the pressure from above and the discharge rate will not be affected by the amount of granular particles inside the hopper (Gao, 1997).

In this study, no indication was found of the material head below which a change in the flowrate will occur. Nedderman *et al.* (1982) reported the following attempts to predict this critical height of the material: Demming and Mehring (1929) suggested the critical height to be 2.5 D, Brown and Richards (1959) indicated that the change will be noticed after D becomes greater than H and Myers and Sellers (1978) reported the critical height to be equal to D_o. It is manifest that there is no agreement on when the critical height will be reached in the hopper (Nedderman *et al.,* 1982).

The conclusion from this experiment is that the flowrate is independent of the material head. For the critical height determination, more work is required concentrating on small material heads above the discharge when the hopper is almost empty.

6.7.2 EFFECT OF HOPPER WIDTH

In this study, the flowrate was measured at five different values of width, which were 10, 18, 24, 30 and 38 cm. These five widths cover a wide range over which to observe any effect on the flowrate. Despite this, it was found that the flowrate was independent of the hopper width and no effect was discovered. The flow rate values

obtained were very close with average values ranging between 86.68 and 88.53 g sec^{-1}. All the tables showing the details for this experiment are given in Appendix G. The average values of flowrates for the different runs were drawn against the different widths in figure 6.13.

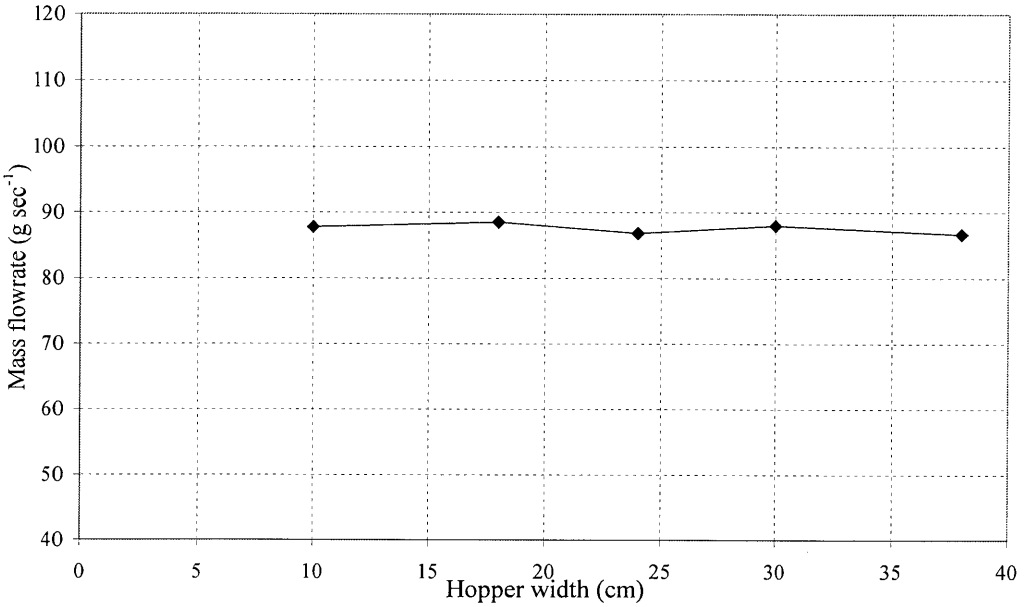


Fig. 6.13 Effect of hopper width on the flowrate (Hopper settings were: initial $H = 95$ cm, height from which flow rate was measured = 26.5 cm , $D_0 = 1.8$ cm, $\alpha = 32$ ° and sample used: 3).

This result confirms what is reported in the literature that the flow rate remains constant at different hopper widths, or diameters in the cylindrical configuration. It was mentioned before that the minimum width that could be achieved by the experimental hopper was 10 cm. This limit makes it impossible to go further for smaller widths to obtain a critical value of the hopper width after which a change in the flowrate may occur.

Nedderman *et al.* (1982) reviewed the previous work done to find the critical value of the hopper width. Ketchum in 1929 and Browns and Richards (1960) declared that W is constant provided $D > 2.5D_o$. Moreover, Franklin and Johanson in 1955 mentioned

that no effect on the flow rate could be noticed if D-$D_o > 30d$ where d is the particle diameter (Nedderman *et al.*, 1982). For the last run of this experiment, D_h of the hopper was equal to 4 cm and D_h of the outlet was 2.09 cm. The ratio of the two values is 1.92 which is lower than the values mentioned by Ketchum and Browns and Richards for cylindrical hoppers. Even with this smaller ratio of the hydraulic diameters no effect on the flowrate was noticed. No further attempts in this experiment were done to study the critical ratio between the diameters of the discharge and the hopper because of the limitation of the hopper width.

It is clear that no effect on changing the width of the hopper can be observed on the flowrate. However, further studies are required to investigate how very small hopper widths may affect the flowrate and to find the ratio between the hopper and discharge widths below which the flowrate will be affected.

6.7.3 EFFECT OF PARTICLE SIZE

This investigation was done using wheat samples with different sizes based on their thickness. The sample average thicknesses are shown in table 6.1. Only four divisions (samples 1-4) were used to study the effect of particle size on the flowrate since the quantity obtained of sample 5 from the separation was not enough to fill the hopper. The different flowrates obtained for the four different samples are given in tables H.1-H.4 in Appendix H. The mean values from these tables were used to plot the flowrate vs. the particle thickness as shown in figure 6.14.

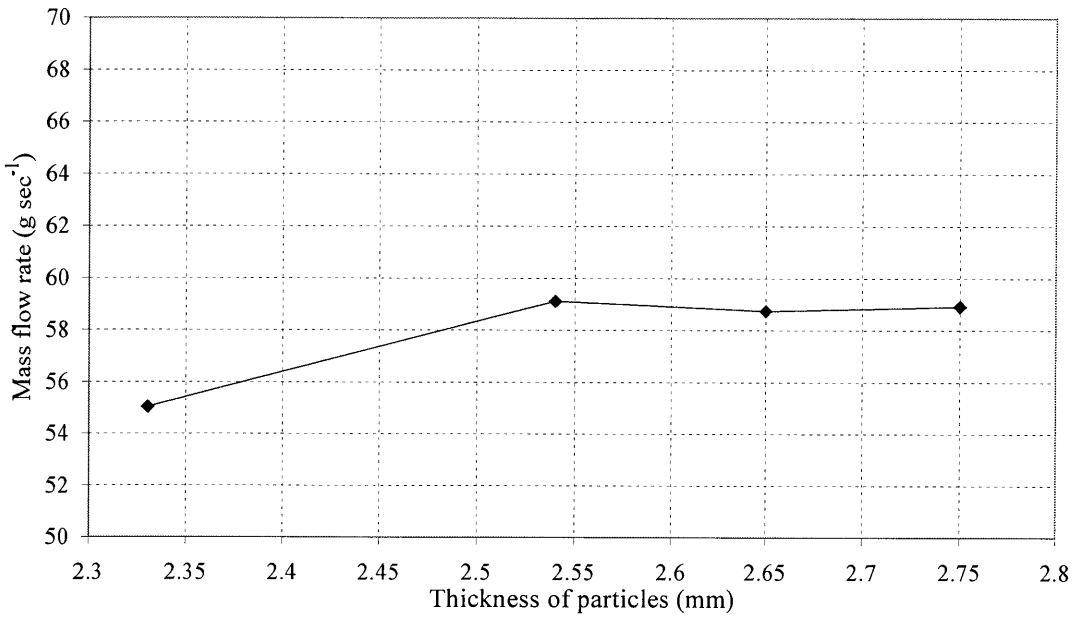


Fig. 6.14 Effect of particle size on the flowrate (Hopper settings were: initial $H = 95$ cm, height from which flow rate was measured = 26.5 cm , $D = 30$ cm, $D_o = 1.8$ cm, $\alpha = 30$ °)

As shown in the tables and in figure 6.14 the differences in the average thickness of the samples is very small which makes it very difficult to estimate the effect of the size on the flow rate. The average thickness differs only by approximately 0.1 mm for the first three samples, that is from 2.75 to 2.54 mm. For the fourth sample the average thickness was 2.33 mm which is 0.21 mm less than the third sample.

Figure 6.14 shows that the flow rate is almost the same for samples 1, 2 and 3 varying between 58.63 and 59.12 g sec^{-1}. However, for the last sample, which represents the smallest thickness, a slight drop in the flow rate to 55.14 g sec^{-1} was obtained. This result does not agree with the Beverloo correlation, equation (2.2), or equation (2.4) by Fowler and Glastonburry. These two equations indicate that the flow rate of non-cohesive particles increases slowly as particle size decreases. Moreover, it does not agree with the experimental results obtained by Bosely *et al.* (1969) who found that

the flowrates for larger diameter granules are significantly lower than those for smaller granules.

It was shown that the angle of repose increases as the wheat grain thickness decreases. Carr (1965) reported that the angle of repose is a measure of flowability and lower angles mean better flow. The results obtained from this experiment agree in part with Carr since the smallest size sample, with the largest angle of repose, gave the lower flowrate. This conclusion can not be extended to the other samples since the flowrate was almost constant with the very slight changes in the angle of repose.

No clear relation could be obtained between the flowrate and the size of the particles from this study. This may be due to the small range of wheat thickness used in the experiment. For further investigation, samples with larger deviation in their sizes should be used so that the effect of particle size on the flowrate will be more evident.

6.7.4 EFFECT OF HOPPER HALF ANGLE

In this part, the flowrates for six different hopper half angles were measured with constant discharge opening. The angles used were 33°, 40°, 47°, 52°, 57° and 61°. The flowrates obtained are given in Appendix I. Figure 6.15 represents the average flowrates as a function of the hopper half angle. From figure 6.15 it is obvious that the largest flow rate, 93.89 g sec^{-1}, was obtained for the smallest hopper half angle, 33°. It is clear that W decreases as the hopper half angle increases. This increase continues till the hopper half angle reaches a critical value above which no further change in the flow rate occurs.

In this experiment, no change in the flowrate was observed for $\alpha > 52°$, where the flowrate remains almost constant between 64.14 and 65.94 g sec^{-1}. The 52° hopper half angle or an angle close to it (but larger than 47°) could be called a critical angle

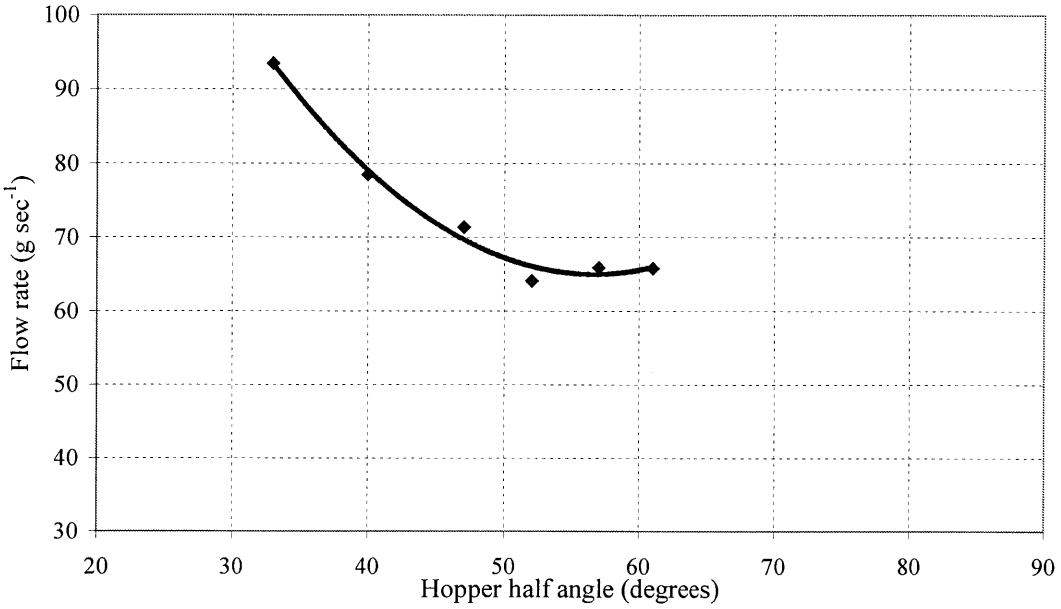


Fig. 6.15 Effect of hopper half angle on the flowrate (Hopper settings were: initial $H = 95$ cm, height from which flow rate was measured = 26.5 cm , $D_o = 1.7$ cm, $D = 30$ cm and sample used: 3).

after which the flow rate will not be further affected by any change in the hopper half angle. The reason for getting constant flowrates for large values of the hopper half angle is that stagnant zones will occur and the walls will be totally covered with the stagnant material. This will give little or no effect if the angle is increased further (Nedderman *et al.*, 1982).

The finding of this experiment does not agree with O'Callaghan (1960) who reported, for a conical hopper, increases in flow when the hopper half angle is less than ($\pi/2$ - ϕ) where ϕ is the angle of repose. The angle of repose for the sample used was 25.17° and according to O'Callaghan the critical angle is approximately 65°. However, the

experiment shows this angle to be around 50° (a 23% difference from O'Callaghan's value). Tüzün and Nedderman (1982) used ϕ_d instead of ϕ where ϕ_d is the angle which the flow boundary makes with the centre line of the discharge orifice. Verghese and Nedderman (1993) recommended ϕ_d to be 45° in the absence of any other information. If this value is substituted instead of ϕ, the result will be 45° which is closer to 50°, obtained from the experiment than that predicted by O'Callaghan.

The shape of figure 6.15 obtained agrees qualitatively with what is reported in the literature (Williams, 1977; Brennen and Pearce, 1978; Nguyen *et al.*, 1980; Ducker *et al.*, 1985). For future work, it is suggested to find ϕ_d and investigate the validity of the criterion for the critical half angle proposed by Tüzün and Nedderman (1992). Also, it is recommended to try different wall materials and to study the effect of wall roughness on the flowrate.

6.7.5 EFFECT OF DISCHARGE SIZE

The effect of the discharge opening size on the flowrate was the greatest among all the factors studied in the project. Very slight changes in the outlet size lead to great effect on the flowrate. The discharge sizes used were 1.5, 2.0, 2.4, 2.8, 3.2 and 3.6 cm. The mass flowrates obtained for each discharge size (D_0) are shown in tables J.1-J.6 in Appendix J. The average values from the tables are used to get figure 6.16 which represents the relation between the mass flow rate (W) vs. D_0. The result of plotting W vs. D_0 was a straight line with the following equation (see figure 6.16):

$$W = 148.63\, D_O - 172.99 \qquad (6.3)$$

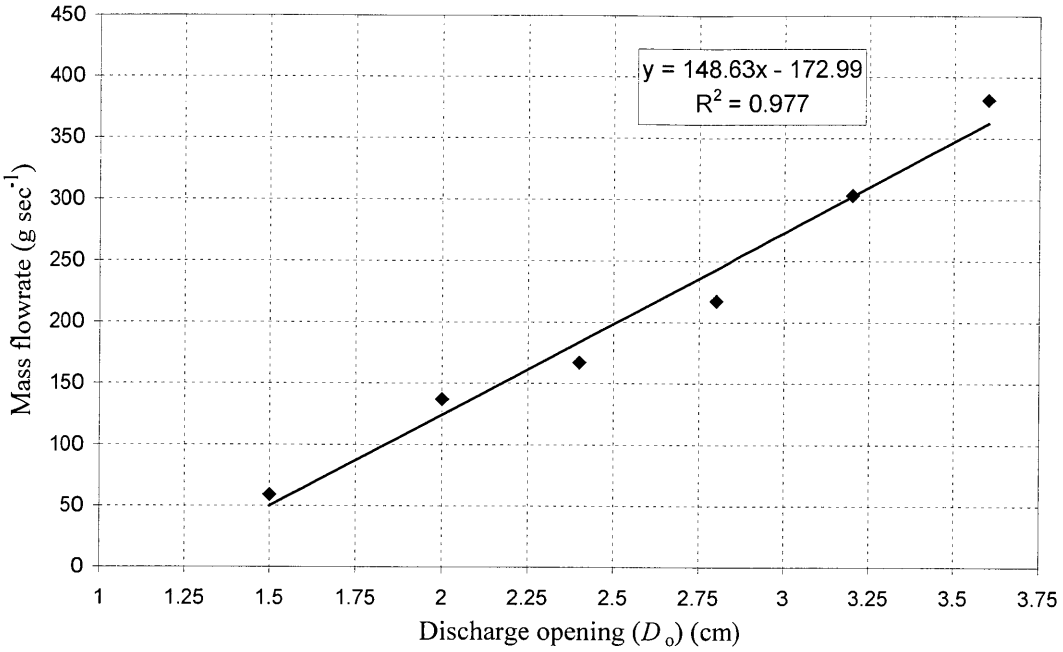


Fig. 6.16 Effect of discharge size on the flowrate (Hopper settings were: initial $H = 95$ cm, height from which flow rate was measured = 26.5 cm , $D = 30$ cm, , $\alpha = 30°$ and sample used: 3).

Spink and Nedderman (1978) reported equation 2.2 in another form:

$$W = C\rho\sqrt{g}\left(D_h - kd\right)^{5/2} \tag{6.4}$$

With D_h representing the mean hydraulic diameter of the orifice replacing D_o for the diameter of a conical shaped hopper. It was shown before that the effect of the particle size is very small on the flowrate, so equation (6.4) could be written as

$$W = C\rho\sqrt{g}\left(D_h - \text{constant}\right)^{5/2} \tag{6.5}$$

i.e.

$$W^{2/5} = \left(C\rho\sqrt{g}\right)^{2/5} D_h - \left(C\rho\sqrt{g}\right)^{2/5} k\, d \tag{6.6}$$

As equation (6.6) suggests a straight line should be obtained if $W^{2/5}$ is plotted against D_h. The measurements of the flowrates for different discharge openings are given in Appendix J. The average values from the tables are used to get figure 6.17 which represents the relation obtained between $W^{2/5}$ vs. D_h.

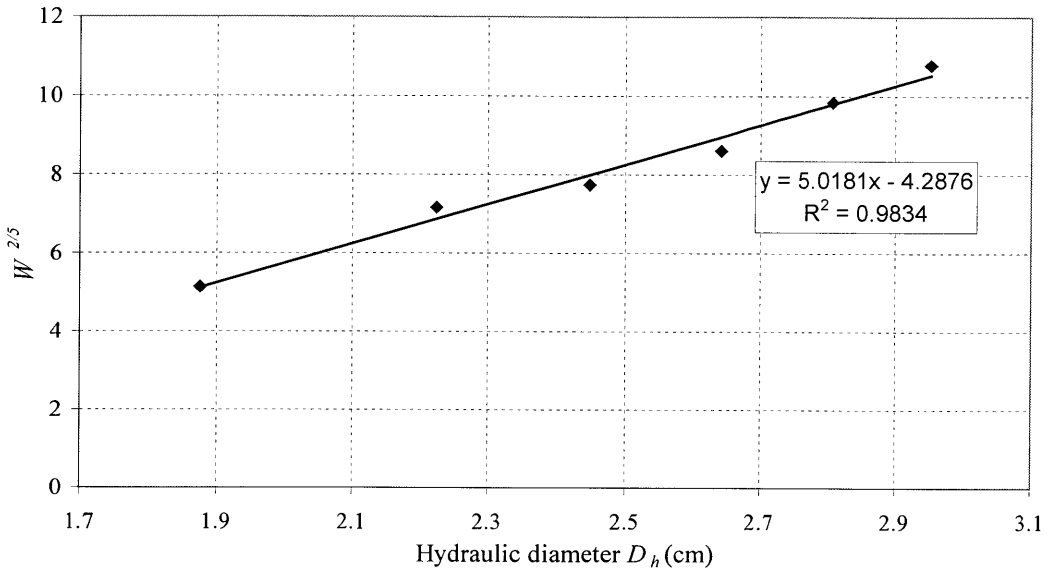


Fig. 6.17 The linear relation obtained between $W^{2/5}$ and D_h.

As equation 6.6 suggested, a linear relationship was obtained between $W^{2/5}$ and D_h with a slope equal to 5.02. Using this slope, the value of C in equation (6.4) can be calculated knowing the bulk density of wheat, 0.781 g cm^{-3}, and g = 980.66 cm sec^{-2}. Here C was found to be 0.21 which is a lower value compared with the range of values given by Beverloo (0.55 to 0.65). And even by using the multiplicative factor $F(\alpha, \chi)$ given by Rose and Tanaka (1959) in equation (2.7) and using χ to be 45° as Verghese and Nedderman (1993) recommended, $F(\alpha, \chi)$ will be equal to 1.21. If, the value of C obtained from Beverloo correlation, is divided by the correction factor, 1.21, the corrected C will be equal to 0.17 which represents a very low value compared with other values obtained for agricultural seeds.

Ducker *et al.*(1985) found C to be 0.58 for kale seed, 0.57 for mustard seed and 0.66 for Diakon. Verghese and Nedderman (1993) reported that C is almost independent of the nature of the material and is commonly quoted as 0.58. The value obtained of C for wheat is very low when compared to the other values reported in the literature. This may be due to the elongated shape of the wheat particles. Another reason could be the bulk density achieved after filling the hopper which may differ from that used in calculating C. The difficulty in setting precise discharge size may be one of the reasons behind obtaining such a low value for the constant C.

Although a straight line was obtained between $W^{2/5}$ and D_h which confirms the Beverloo correlation, the value of C was very small and does not agree with values reported in the literature. If the same apparatus is to be used for further investigations regarding the effect of the discharge size, it is recommended to try seeds with spherical shapes. This trial will justify the reason behind obtaining a low value of C if it is due to the particle shape or due to the difficulty in setting the discharge size.

6.7.6 EFFECT OF MOISTURE CONTENT

The effect of six different moisture contents of wheat on the flowrate was investigated in this experiment. These moisture contents were 11.66%, 13.90%, 15.65%, 18.03%, 19.56% and 21.60%. The flowrate measurements for different moisture contents are given in tables K.1- K.6 in Appendix K. As was expected, the increase in the moisture content affects the flowrate negatively. Figure 6.18 shows the flowrate against % moisture content.

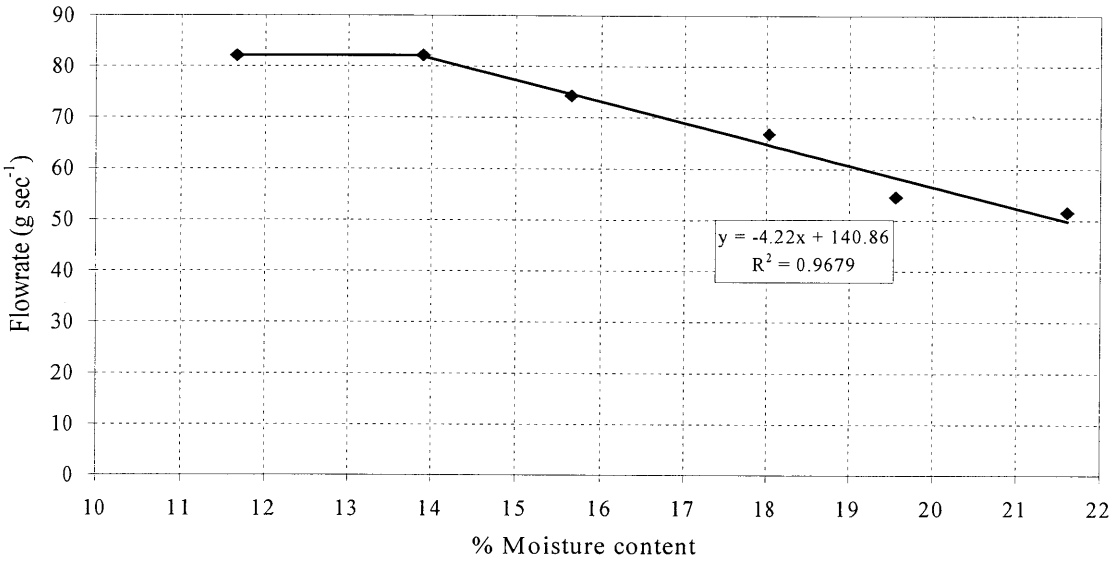


Fig. 6.18 Effect of moisture content on the flowrate (Hopper settings were: initial $H = 95$ cm, height from which flow rate was measured = 26.5 cm, $D = 30$ cm, $D_0 = 1.75$ cm, $\alpha = 30°$ and sample used: 6).

As shown in Figure 6.18, no effect on the flowrate was noticed for the lowest values of moisture contents, 11.66% and 13.90%. At these two values, the flowrate was almost the same, 82.14 and 82.66 g sec^{-1} respectively. The difference was clear when the moisture content reached 15.65%, a clear decline in the average flowrate of 7.54 g sec^{-1} was found. This decrease in the flowrate continued for all the other moisture content values giving a relation that can be presented by a straight line with a negative slope, as shown in figure 6.18. Above a moisture content of 13.90% the flowrate can be confidently predicted by:

$$W = 140.86 - 172.99\,MC \qquad (6.7)$$

It is interesting to note that for the last two values of the moisture content which differ by 2.04%, the decrease in the flowrate was small (3.03 g sec^{-1}) compared to the other drops in the flowrate for successive values of the moisture content. This leads one to wonder about the shape of the graph for moisture contents greater than 21.60 if it is going to follow the same trend or reach a constant value.

The result from this experiment supports what was mentioned earlier in section 6.5.1 about the relation between the angle of repose and the flowability of the material. It was shown previously in section 6.6.2 that as the moisture content increases, the angle of repose also increases. Here, the idea of connecting the angle of repose with the flowability could be used again after it was used for the different size samples, section 6.7.2. Figure 6.19 shows the flowrate for the different angles of repose obtained for different moisture contents. This figure shows clearly that the angle of repose and the flowability of the material are inversely related. A straight line with a negative slope was found to represent the relation between the flowrate and the angle of repose obtained for different moisture contents of wheat samples. Over the range studied, flowrate can therefore be predicted from:

$$W = 155.42 - 2.88\,\phi \qquad (6.8)$$

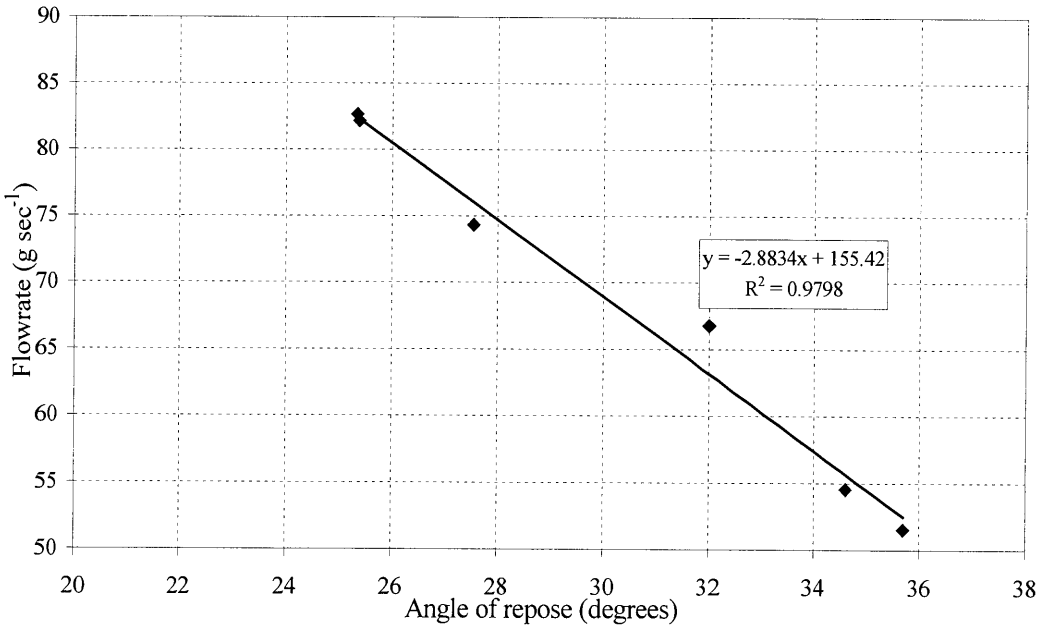


Fig. 6.19 Effect of the angle of repose obtained for different moisture contents on the flowrate.

This experiment stressed the effect of the moisture content and the angle of repose on the flowability of the material. However, greater values of moisture contents should be tried for future work to investigate if the linear relationship will continue or whether a critical moisture content is reached after which no effect will appear on the flowrate or the angle of repose.

CHAPTER 7

CONCLUSIONS AND SUGGESTIONS FOR FURTHER WORK

7.1 CONCLUSIONS

In general, the results obtained from the experimental hopper were consistent showing an agreement with the past work reported in the literature. This means that the performance of the experimental hopper was very good showing a successful design and building of the apparatus. However, adjusting the pieces to their original position once it is changed was not an easy thing. Moreover, filling the hopper by hand was a very tedious job and no control on the discharge rate was possible once it was started. The hopper stand was too heavy which made it very difficult to move it between different places. In addition, the retaining bolts limited the movement of pieces 5 and 6 to a certain level making it impossible to reach a flat bottomed configuration. Finally, light reflecting in the front and back walls required the use of black curtain to get better pictures with less reflection.

The photographic study helped to visualise many observations during the experiments. It was concluded that the wheat particles located on the centreline of the hopper above the discharge opening are moving faster than the particles on the sides or near the walls. A stagnant region was found to exist for wide hopper configurations or those with large hopper half angles. One of the effects of the different velocities of the grains was a dip at the centre of the free surface relative to the other points located on the surface. The second effect was that the deformation of the flow lines at the centre was more than that at the sides. Another interesting observation was the alignment of the particles with their major axis towards the discharge and the arches formed for small discharge sizes.

In studying the effect of the particle size and the moisture content on the angle of repose two linear relations were obtained. The first showed that as the wheat size increases the angle of repose decreases linearly. The second revealed that below a certain value of the moisture content no effect on the angle of repose is noticed. Above this value, a linear increase in the angle of repose with increasing the moisture content was observed.

The effect of the hopper geometry, wheat size and moisture content on the flowrate was a major part of this study. The rate of discharge was found to be independent of the head of material in the hopper. Moreover, no effect on the flowrate was noticed for a large range of hopper widths investigated. The effect of the particle size on the flowrate was negligible with the lower rate obtained for the smallest particles. A linear relationship was obtained between $W^{2/5}$ vs. D_h and it was clear that a small increase in the discharge area results in a large increase in the discharge rate. The effect of increasing the hopper half angle was to decrease the flowrate till a critical angle is reached. As the half angle increased further, no further effect could be noticed on the discharge rate and it remained constant. For the moisture content, it was clear that the increase in the moisture content resulted in a decrease in the flowrate. This decrease was observed after a critical moisture content. A straight line with a negative slope was found to fit the data points obtained. A very clear relationship was observed between the angle of repose and the discharge rate. From the present work, it can be confidently said that the angle of repose gives an indication of the flowability of the material and an increase in the angle of repose resulted in a clear decrease in the discharge rate.

7.2 SUGGESTIONS FOR FURTHER WORK

The first thing recommended here is to make some adjustments in the experimental hopper. Adding threaded adjusters for pieces 3 and 4 to make their adjustments easier in the required positions is very important. In addition, changing the positions of the retaining bolts is essential to get the flat bottomed configuration. Moreover, fixing wheels at the stand legs will make movement of the hopper much easier. Finding other ways to fill the hopper, instead of the manual filling, and to control the discharge is recommended to make the filling and discharging operations more effective.

Further work in the qualitative part, photographic study, requires the use of a camera with several seconds exposure time to visualise the stagnant zones without the need to dye the particles. Moreover, it is important to find a way to recover the dyed particles from the mixture for subsequent use in stead of using them only once. In studying the free surface shapes, finding a mathematical formula to represent the shape at different time intervals is recommended. In addition, more investigation could be done to see how the aspect ratio would affect the transition between the different free surface shapes. Finally, the effect of different agricultural seeds with different shapes and angle of repose on the flow line shapes and development is suggested.

In the quantitative study, more work could be done to investigate the effect of different particle shapes and sizes on the angle of repose and the discharge rate. More over, higher moisture contents than those used in this study could be tried to see if the linear relation obtained here will continue. The effect of the aspect ratio on the flowrate is still unclear and more studies could be directed towards finding the critical

aspect ratio after which an effect on the flowrate will be noticed. Using different materials to construct the hopper walls and see how the characteristics of different materials will affect the flowrate is also recommended. Finally, investigating the effect of the hopper discharge on the flowrate will require more work to find the reason behind getting a low value of C. Whether this low value was the result of the elongated shape of the wheat grains or due to uncertainty in setting and measuring the discharge size will be clear by repeating the experiment with particles having different shapes.

REFERENCES

American Association of Cereal Chemists (1995). Approved Methods of the American Association of Cereal Chemists. American Association of Cereal Chemists Inc., USA.

Aviara, N. A., Gwandzang, M. I. and Haque, M. A. (1999).Physical properties of Guna seeds. *J. Agric. Engng. Res.* **73**, 105-111.

Babic, M. (1995). A connection between continuum and discrete models of particulate materials. *Procs. of Engg. Mechanics*. **2**, 790-793.

Baival, B. (1998). Quality testing of cereal grains in relation to processing performance. MSc Dissertation. UMIST.

Bates, L. (1996). Better bulk. *The Chemical Engineer*. **622**, 27-34.

Baxter, G. W., Behringer, R. P. (1990). Cellular automata models of granular flow. *Phys. Rev. A*. **42**, 1017-1020.

Baxter, G. W., Behringer, R. P., Fagert, T. and Johnson, A. (1989). Pattern formation in flowing sand. *Phys. Rev. Lett*. **62**, 2825-2828.

Behringer, R. P. (1995). Mixed predictions. *Nature*. **374**,15.

Berkovitch, I. (1983). Bulk handling of particles. *Manuf. Chemist*. **54**, 40-41.

Bosley, J., Schofield, C. and Shook, C. A. (1969). An experimental study of granule discharge from model hoppers. *Trans. Instn Chem. Engrs*. **47**, T147-T153.

Brennen, C. and Pearce, J. C. (1978). Granular material flow in two-dimensional hoppers. *ASME Journal of Applied Mechanics*. **45**, 43-50.

Bridgwater, J. (1995). Particle technology. *Chem. Eng. Sci*. **50**, 4081-4089.

Carr, R. C., Jr. (1965). Evaluating flow properties of solids. *Chemical Engineering*. Jan 18th, 1965, 163-168.

Chase, G. G. (1999). "Hopper design", The University of Akron, see WWW site *http: //www. ecgf.uakron.edu/~chem /fclty/chase/solids.html*.

Chandrasekar, V. and Viswanathan, R. (1999). Physical and thermal properties of coffee. *J. Agric. Engng. Res*. **73**, 227-234.

Clift, R. (1996). Powder technology and particle science. *Powder Technol*. **88**, 335-339.

CMIS.(1999)."Modelling of industrial granular flows", CSIRO Mathematical and Information Science, see WWW site *http:// www. cmis.csiro.au /cfd/dem/index.htm*.

Cundall, P. A. and Strack, O. D. L. (1979). A discrete numerical model for granular assemblies. *Geotechnique*. **29**, 47-65.

Das, S., Behera, S. and Murty, J. S. (1997). Practical design consideration for hoppers and silos. *Chemical Engineering World.* **32**,91-95.

Deen, W. M. (1998). Analysis of transport phenomena. New York: Oxford University Press. 597 pp.

De Josselin De Jong, G. (1971). The double sliding, free rotating model for granular assemblies. *Geotechnique*. **21**, 155-163.

Drescher, A., Cousens, T. W. and Bransby, P. L. (1978). Kinematics of the mass flow of granular material through a plane hopper. *Geotechnique*. **28**, 27-42.

Ducker, J. R., Ducker, M. E. and Nedderman, R. M. (1985). The discharge of granular materials from unventilated hoppers. *Powder Technol.* **42**, 3-14.

Flekkøy, E. G. and Måløy, K. J. (1998). Continuum description of granular flows: Simulation and experiment. *Phys. Rev. E.* **57**, 6962-6972.

Gao, S. (1997). "Intro-of-research", Clemson University, see WWW site *http://www.eng.clemson.edu/~sgao/index.html*.

Gardner, G. C. (1966). The region of flow when discharging granular materials from bin-hopper systems. *Chem. Eng. Sci.* **21**, 261-273.

Gu, Z. H., Arnold, P. C. and Mclean, A. G. (1992). Prediction of the flow rate of bulk solids from mass flow bins with conical hoppers. *Powder Technol.* **72**, 157-166.

Haff, P. K. (1997). Why prediction of grain behaviour is difficult in geological granular systems. Powders & Grains, 97, Proc. 3rd . Int. Conf. on Powders and Grains. Edited by R. P. Behringer and J. T. Jenkins, 61-64.

Haff, P. K. (1983). Grain flow as a fluid-mechanical phenomenon. *J. Fluid Mech.* **134**, 401-430.

Hogue, C. and Newland, D. (1994). Efficient computer simulation of moving granular particles. *Powder Technol.* **78**, 51-66.

Hsiau, S. S. (1997). "Granular Flow", North Central University, see WWW site *http://www.ncu.edu.tw/~sshsiau/egranu.html*.

Hunt, M. L. (1998). "The Caltech Granular Flows homepage", California Institute of Technology, see WWW site *http://www.cco.caltech.edu/~granflow/homepage.html*.

Hustrulid, A. I. (1999). "The discrete element method", Colorado School of Mines, see WWW site *http: // www .mines .edu / academic / eng / research /dem.*

Jaeger, H. M., Nagel, S. R. and Behringer, R. P. (1996). "An Introduction to Granular Physics: What are granular materials and why are they interesting?", The University of Chicago, see WWW site *http: //mrsec .uchicago.edu /~jaeger/granular2.*

Jaeger, H. M. and Nagel, S. R. (1992). Physics of the granular state. *Science*. **255**, 1523-1531.

Jenike, A. W. (1964). Storage and flow of solids. *Bul. 123* . Utah Engineering Experimental Station, University of Utah.

Jenike & Johanson, Inc.(1999). "Case histories", see WWW site *http://www.jenike.com/cases.html*.

Jha, S. N. (1999). Physical and hygroscopic properties of Makhana. *J. Agric. Engng. Res*. **72**, 145-150.

Johanson, J. R. (1985). Design of bins and hoppers. In Materials handling handbook, pp. 901-1010. Edited by R. A. Kulwiec. New York: John Wiley & Sons.

Knowlton, T.M., Carson, J. W., Klinzing, G. E. and Yang, W. C. (1994). The importance of storage, transfer, and collection. *Chem. Eng. Prog*. **90**, 44-54.

Kooi, V. D. (1999). "Silo design, well begun is half done: Avoiding flow problems through adequate design", Bulk Solid Engineering, see WWW site *http://www.bse-enschede.demon.nl*.

Lee, J., Cowin, S. C. and Templeton III, J. S. (1974). An experimental study of the kinematics of flow through hoppers. *Trans. Soc. Rheology*. **18**, 247-269.

Lu, Z., Negi, S. C. and Jofriet, J. C. (1997). A numerical model for flow of granular materials in silos, part 1: Model development. *J. Agric. Engng. Res*. **68**, 223-229.

Marinelli, J. and Carson, J. W. (1992). Solve solids flow problems in bins, hoppers, and feeders. *Chem. Eng. Prog*. **88**, 22-28.

Mehrabadi, M. M. and Cowin, S. C. (1978). Initial planar deformation of dilatant granular materials. *Journal of the Mechanics and Physics of Solids*. **26**, 269-284.

Morisawa, M. (1999). "Stable angles of slopes", see WWW site *http://www.beioit.edu/~SEPM/Earth_Works/stable_angles_of_slopes.html*.

Nedderman, R. M., Tüzün, U., Savage, S. B. and Houlsby, G. T. (1982). The flow of granular materials-I: Discharge rates from hoppers. *Chem. Eng. Sci*. **37**, 1597-1609.

Negi, S. C., Lu, Z. and Jofriet, J. C. (1997). A numerical model for flow of granular materials in silos, part 2: Model validation. *J. Agric. Engng. Res*. **68**, 231-236.

Nguyen, T. V. (1979). Studies in the flow of granular materials. PhD Thesis. California Institute of Technology.

Nguyen, T. V., Brennen, C. E. and Sabersky, R. H. (1980). Funnel flow in hoppers. *ASME Journal of Applied Mechanics*. **47**, 729-735.

Nguyen, T. V., Brennen, C. E. and Sabersky, R. H. (1979). Gravity flow of granular materials in conical hoppers. *ASME Journal of Applied Mechanics*. **46**, 529-535.

O'Callaghan, J. R., (1960). Internal flow in moving beds of granular material. *J. Agric. Engng. Res*. **5**, 200-217.

Odhuba, E. K. D. (1999). Optimisation of wheat breakage in flour milling. PhD Thesis. UMIST.

Rhodes, M. J. (1998). Introduction to particle Technology. Chichester: John Wiley & Sons Ltd. 320pp.

Roberts, A. W. and Scott, O. J. (1991). Silo- quaking- a pulsating load problem during discharge in bins and silos. In Bulk 2000: Bulk materials handling- towards the year 2000, pp. 7-12. Suffolk: Mechanical Engineering Publications Limited.

Rombach, G. and Eibl, J. (1995). Granular flow of materials in silos: Numerical results. *Bulk Solids Handling*. **15**, 65-70.

Singh, K. K. and Goswami, T. K. (1996). Physical properties of Cumin seed. *J. Agric. Engng. Res*. **64**, 93-98.

Seville, J. P. K., Tüzün, U. and Clift, R. (1997). Processing of particulate solids.pp.298-367. Edited by B. Scarlett and G. Jimbo. London: Blackie Academic & Professional.

Spencer, A. J. M. (1964). A theory of the kinematics of ideal soils under plane strain conditions. *Journal of the Mechanics and Physics of Solids*. **12**, 337-351.

Spink, C. D. and Nedderman, R. M. (1978). Gravity discharge rate of fine particles from hoppers. *Powder Technol*. **21**, 245-261.

StanleyWood, N. (1996). Bulk handling. *The Chemical Engineer*. **609**,15-18.

Suthar, S. H. and Das, S. K. (1996). Some physical properties of Karingda[Citrullus lantus(Thumb) Mansf] seeds. *J. Agric. Engng. Res*. **65**, 15-22.

Thomson, F. M. (1985). Storage of particulate solids. In Handbook of powder science and technology, pp. 365-463. Edited by M. E. Fayed and L. Otten. New York: Van Nostrand Reinhold Company.

Tüzün, U. and Nedderman, R. M. (1982). An investigation of the flow boundary during steady-state discharge from a funnel-flow bunker. *Powder Technol*. **31**, 27-43.

Verghese, T. M. and Nedderman, R. M. (1993). A theoretical prediction of the discharge rate from conical hoppers in both the mass flow and core flow regimes. *Chem. Eng. Res. Des*. **71**, 637-642.

Visvanathan, R., Palanisamy, P. T., Gothandapani, L. and Sreenarayanan, V. V. (1996). Physical properties of Neem Nut. *J. Agric. Engng. Res*. **63**, 19-26.

Wassgren, C. (1998). "Carl Wassgren's research activities", Purdue University, see WWW site *http :// widget. ecn.purdue .edu/ ~wassgren /research/ #index.*

Wieghardt, K. (1975). Experiments in Granular flow. *Annu. Rev. fluid mech.* **7**, 89-114.

Williams, J. C. (1977). The rate of discharge of coarse granular materials from conical mass flow hoppers. *Chem. Eng. Sci.* **32**, 247-255.

APPENDICES

APPENDIX A

MOISTURE – AIR OVEN METHODS

Definition

These methods determine moisture content as loss in weight of a sample when heated under specified conditions.

Scope

Applicable to flour, farina, semolina, bread, grain, soybeans, rice, beans, peas, lentils, cornmeal, corn grits, rolled oats, bulgur, rolled wheat, and breakfast cereals (except those that are sugar-coated). This method gives results closely approximating those obtained by Method **44-40** (vacuum-oven). This method is not recommended for feeds and feedstuffs when fat determination is to be made on dried samples.

Apparatus

1. Wiley laboratory mill, intermediate model, equipped with 18- or 20-mesh screen and 4-ounce receiving bottle; or any other mill that will grind to same degree of fineness without undue exposure to atmosphere and without appreciable heating.

2. Oven (either gravity-convection or mechanical-convection), capable of being maintained at 130° (±1°) uniformly throughout oven and provided with good ventilation. Thermometer shall be so situated in oven that tip of bulb is level with top of moisture dishes but not directly over any dish.

3. Oven for drying corn and soybeans, meeting requirements of oven in item 2 except that it is maintained at 103° (±1°). Testing at 130° is not recommended for corn and soybeans.

4. Moisture dishes having diameter of about 55 mm and height of about 15 mm. They should be of heavy-gauge aluminum with slightly tapered sides and provided with tightly fitting slip-in covers that are designed to fit snugly under dishes when they are placed in oven. Both dish and cover should be identified by same number. Before using, dry for 1 hour (hr) at 130°, cool in desiccator, and obtain tare weight. (See Note 1.)

5. Airtight desiccator containing activated alumina, molecular sieves (type 4A or 4A X W), or other equally suitable desiccant. (See Note 2.)

6. Balance, accurate to at least 1 mg.

Procedure

One-stage

For samples containing less than 13% moisture, except soybeans, for which level of 10% is applicable; also for flour, cornmeal, farina, and semolina except for grinding.

1. Grind 30- to 40-g sample in mill. Mix rapidly with spoon or spatula and

transfer immediately a 2- to 3-g portion to each of two or more tared moisture dishes. Cover and weigh dishes at once. Subtract tare weights and record weight of sample. Clean mill between samples.

2. Uncover dishes and place them on shelf of oven and place covers under dishes. Insert shelf in oven at level of thermometer bulb. Heat for exactly 60 minutes (min) after oven recovers its temperature (See Note 3.)

3. Remove shelf and dishes from oven, cover rapidly (using rubber finger insulators), and transfer to desiccator as quickly as possible. Weigh dishes after they reach room temperature (45–60 min usually). Determine loss in weight as moisture (see equation 1). Replicate determinations must check within 0.2% moisture; otherwise repeat determination.

Two-stage

For samples containing 13% or more moisture (10% for soybeans), loss of moisture incident to grinding is likely to be excessive; hence, following two-stage procedure should be used.

1. Fill two or more tared moisture dishes nearly full with representative portions of unground sample. Cover and weigh dishes. Subtract tare weights and record weight of sample.

2. Uncover dishes and place covers under dishes. Place tins in well-ventilated place (preferably on top of heated oven protected from dust) so that sample will dry reasonably fast and reach approximate air-dry condition. This will usually be accomplished in 14–16 hr when top of heated oven is used, or approximately 60 hr when room temperature is used for this preliminary drying. In all cases, moisture content should be reduced to less than 10%, ideally to 7–8% in air-drying stage.

3. Cover dishes containing air-dried samples and weigh them soon after they cool to room temperature. Determine loss in weight and record it as moisture loss due to air-drying, using equation 1.

4. Using air-dried sample, follow one-stage procedure described above, starting with grinding step. Calculate total moisture content by using equation 3.

Air-oven, for corn and soybeans, at 103°

Place approximately 15 g of representative portion of unground sample in each of two or more tared moisture dishes. Weigh covered dishes and contents. Subtract weight of each dish from total weight and record result as weight of sample. Put covers under dishes and heat for 72 hr in oven regulated at 103 ± 1°. Dishes should be placed on single shelf with bulb of oven thermometer as close as possible to them. At end of heating period, remove shelf containing dishes, cover dishes immediately, and place in desiccator. Weigh dishes when they reach room temperature. Determine loss in weight as moisture by using

equation 1.

Replicate determinations should check within 0.2% moisture.

Air-oven, for flax, at 103°

Proceed as above for corn and soybeans, except use 5- to 7-g sample and 4-hr oven time.

Bread, two-stage

Air-dry and grind sample as directed in Method **62-05**. Using 2- to 3-g portion of ground air-dried sample, follow one-stage procedure described above. Calculate total moisture loss by using equation 2. To obtain percent of total solids in fresh loaf, subtract percent total moisture from 100.

Calculation

Equation 1 (one-stage and 103° air oven):

$$\% \text{ Moisture} = \frac{A}{B} \times 100$$

in which A = moisture loss in grams, B = original weight of sample.

Equation 2 (two-stage):

$$\% \text{ Total solids} = \frac{Y \times Z}{X}$$

where X = weight of original sample used for air-drying, Y = weight of sample after air-drying, Z = percent total *solids* in prepared ground sample (total solids = 100% – percent moisture at assay).

Equation 3:

$$\% \text{ Total moisture} = A + \frac{(100 - A)B}{100}$$

where A = percent moisture loss on air-drying, B = percent moisture loss as determined by oven-drying.

Notes

1. Tare weight will usually remain constant within a few tenths of milligrams for approximately 1 year if dishes are dumped and then carefully wiped clean with a soft cloth.
2. Silica gel and anhydrous $CaCl_2$ are not suitable desiccants.
3. Oven should regain temperature within 15–20 min after insertion of a full load (24 moisture dishes). If oven requires a longer time to recover, it should not be used.

APPENDIX B

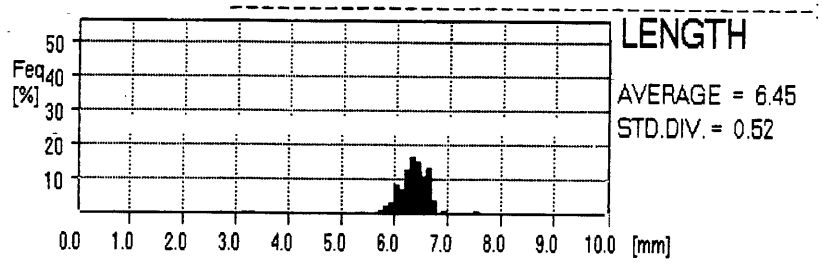
RESULTS OF THE SIZE ANALYSIS FROM THE GRAIN IMAGE ANALYSER

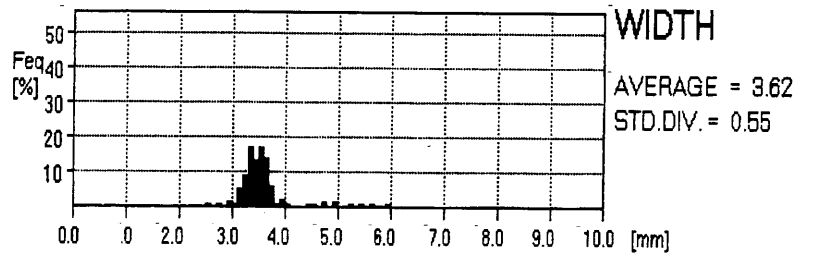
B.1: Results of sample 1.

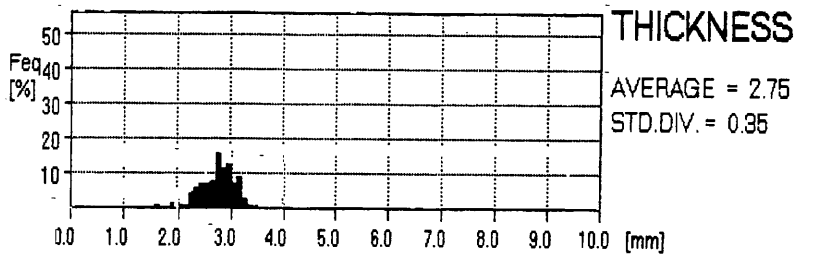
RICE IMAGE ANALYZER

MEASURING DATE : 07/21/99
COMMENT :
SORTING : NO SORTING
NUMBER OF GRAIN: 300

ITEM	AVERAGE	STD.DIV.
LENGTH	6.45	0.52
WIDTH	3.62	0.55
THICKNESS	2.75	0.35
AREA	17.56	1.55
CIRC.	19.54	6.05
THRU.AREA	15.84	1.45





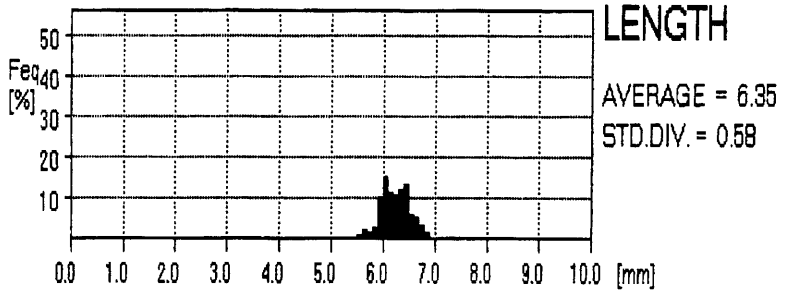


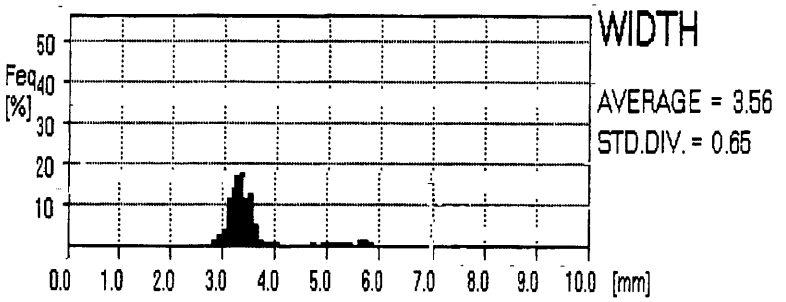
B.2: Results of sample 2.

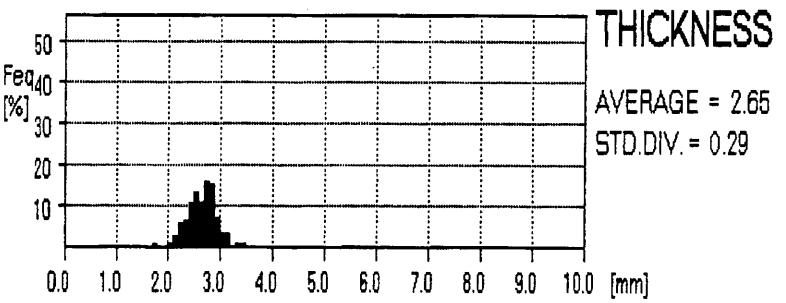
RICE IMAGE ANALYZER

MEASURING DATE : 07/21/99
COMMENT :
SORTING : NO SORTING
NUMBER OF GRAIN: 300

ITEM	AVERAGE	STD.DIV.
LENGTH	6.35	0.58
WIDTH	3.56	0.65
THICKNESS	2.65	0.29
AREA	16.59	1.57
CIRC.	19.75	15.23
THRU.AREA	14.92	1.45





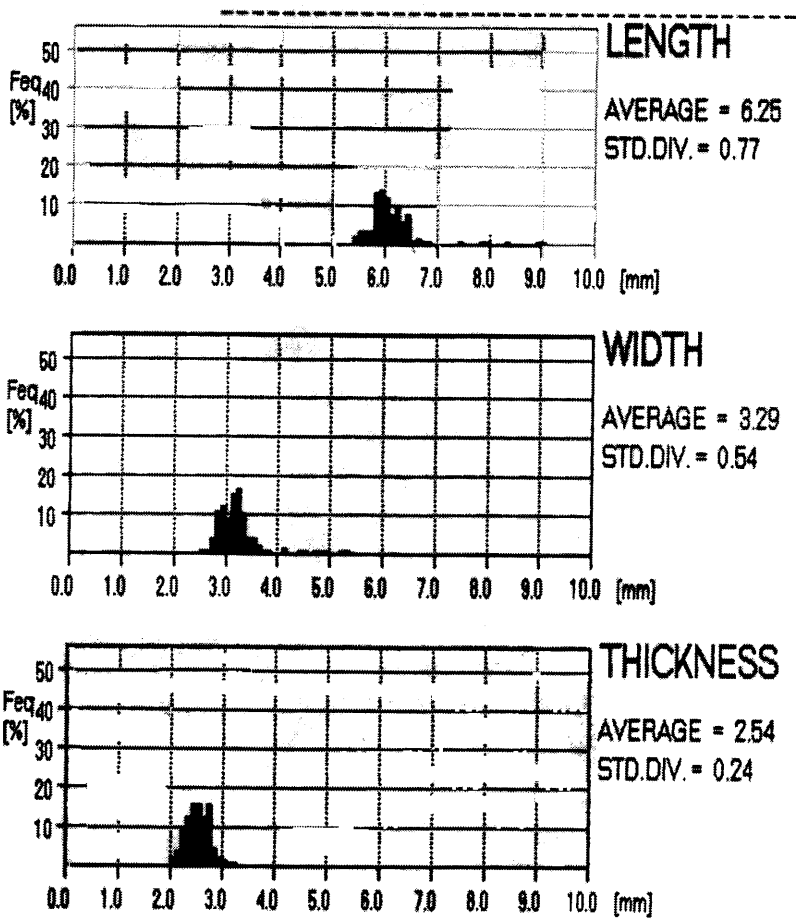


B.3: Results of sample 3.

RICE IMAGE ANALYZER

MEASURING DATE : 07/21/99
COMMENT :
SORTING : NO SORTING
NUMBER OF GRAIN: 300

ITEM	AVERAGE	STD.DIV.
LENGTH	6.25	0.77
WIDTH	3.29	0.54
THICKNESS	2.54	0.24
AREA	14.91	1.68
CIRC.	18.07	5.18
THRU.AREA	13.38	1.58

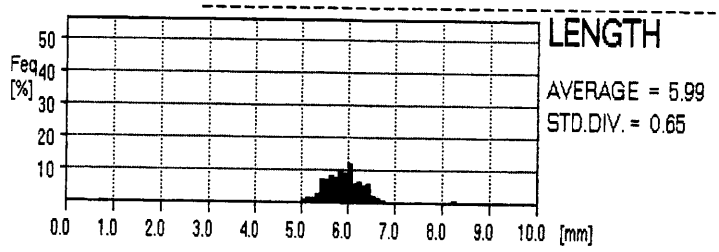


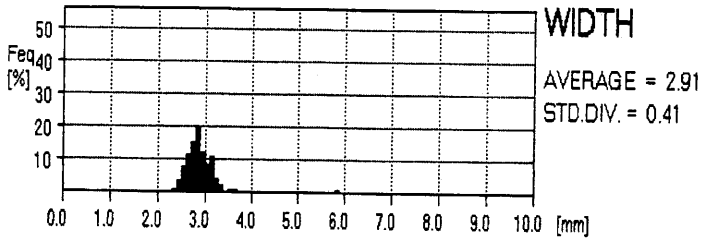
B.4: Results of sample 4.

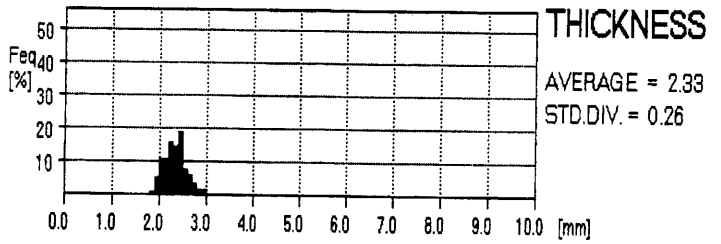
RICE IMAGE ANALYZER

MEASURING DATE : 07/20/99
COMMENT :
SORTING : NO SORTING
NUMBER OF GRAIN: 300

ITEM	AVERAGE	STD.DIV.
LENGTH	5.99	0.65
WIDTH	2.91	0.41
THICKNESS	2.33	0.26
AREA	13.45	1.91
CIRC.	17.32	3.11
THRU.AREA	11.99	1.86





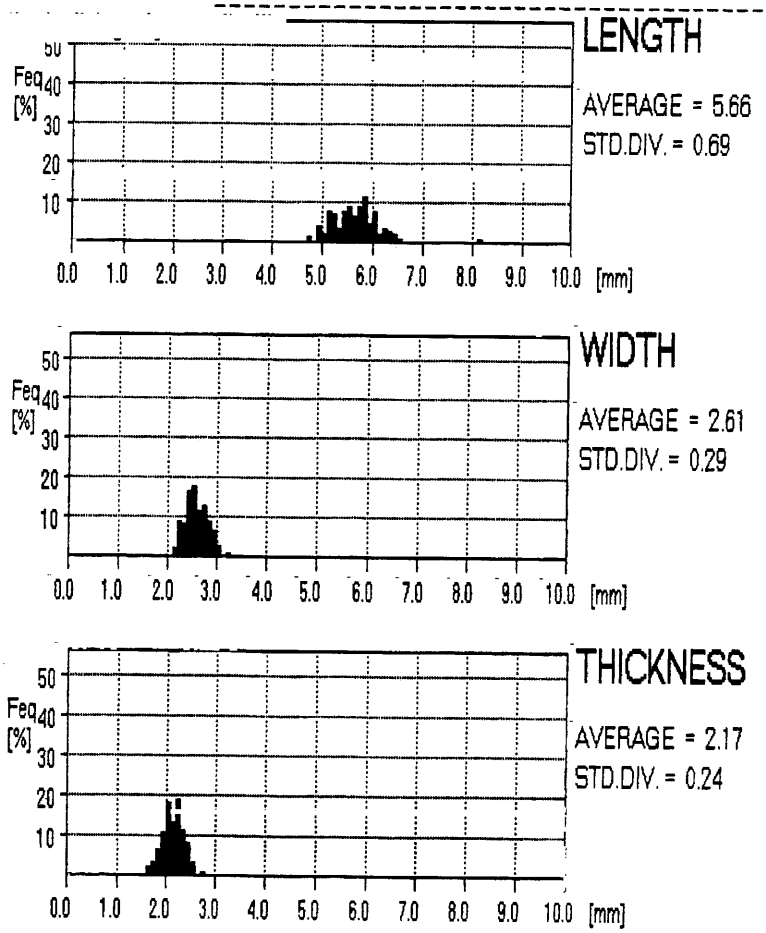


B.5: Results of sample 5.

RICE IMAGE ANALYZER

MEASURING DATE : 07/21/99
COMMENT :
SORTING : NO SORTING
NUMBER OF GRAIN: 300

ITEM	AVERAGE	STD.DIV.
LENGTH	5.66	0.69
WIDTH	2.61	0.29
THICKNESS	2.17	0.24
AREA	11.63	1.97
CIRC.	16.88	4.40
THRU.AREA	10.23	1.82

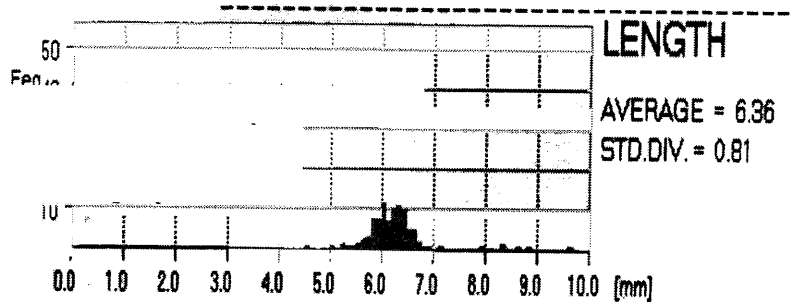


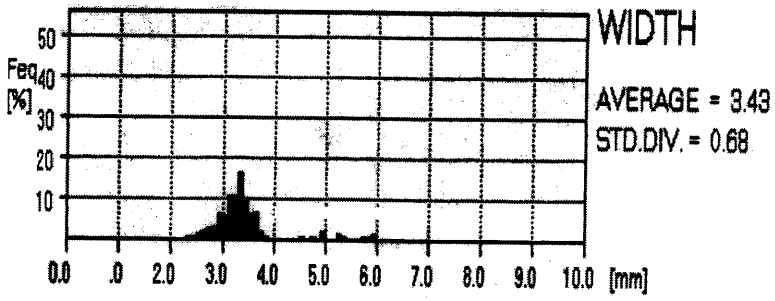
B.6: Results of sample 6 (original mixture).

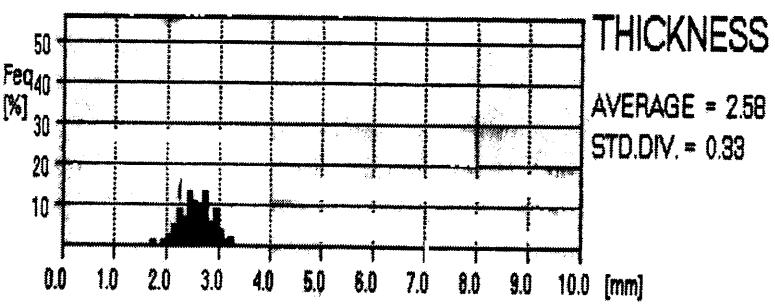
RICE IMAGE ANALYZER

MEASURING DATE : 07/21/99
COMMENT :
SORTING : NO SORTING
NUMBER OF GRAIN: 300

ITEM	AVERAGE	STD.DIV.
LENGTH	6.36	0.81
WIDTH	3.43	0.68
THICKNESS	2.58	0.33
AREA	15.82	2.33
CIRC.	19.48	12.81
THRU.AREA	14.22	2.23







APPENDIX C

MOISTURE CONTENT CALCULATIONS

Table C.1: Calculation of the moisture content for the six samples on the day of the experiments.

Sample	*Weight of the sample before air drying (g)*	*Weight of the sample after air drying (g)*	*Loss (g)*	*Loss by air drying %*	*Weight of the sample before air oven drying (g)*	*Weight of the sample after air oven drying (g)*	*Loss (g)*	*Loss by air oven drying %*	*Moisture content %*
1	71.1853	67.5232	3.6621	5.14	2.0362	1.8483	0.1879	9.23	13.90
2	74.6166	70.2562	4.3604	5.84	2.1634	1.9380	0.2254	10.42	15.65
3	81.1051	73.6209	7.4842	9.23	2.0586	1.8590	0.1996	9.70	18.03
4	67.3675	60.4630	6.9045	10.25	2.0538	1.8408	0.2130	10.37	19.56
5	66.9487	58.7122	8.2365	12.30	2.0629	1.8442	0.2187	10.60	21.60
6	-----	------	-----	------	2.0316	1.7947	0.2369	-----	11.66

- Equation (5.3) was used to calculate % moisture content given in this table except for sample 6 where equation (5.1) was used.

APPENDIX D

EXAMINING THE EFFECT OF PARTICLE SIZE ON THE ANGLE OF REPOSE

Table D.1: Calculation of the angle of repose for sample 1 (Avg. Thickness = 2.75mm).

Trial	*Height(H) (cm)*	*Width(W) (cm)*	*H/W*	*Angle degrees*	*Avg. degrees*	*Standard deviation*
1	8.9	20	0.445	23.99	24.11	0.12
2	9.0	20	0.45	24.23		
3	9.0	20	0.45	24.23		
4	8.9	20	0.445	23.99		0.50 %
5	8.9	20	0.445	23.99		
6	9.0	20	0.45	24.23		

Table D.2: Calculation of the angle of repose for sample 2 (Avg. thickness = 2.65mm).

Trial	*Height(H) (cm)*	*Width(W) (cm)*	*H/W*	*Angle degrees*	*Avg. degrees*	*Standard deviation*
1	9.1	20	0.455	24.47	24.58	0.115
2	9.1	20	0.455	24.47		
3	9.2	20	0.46	24.70		
4	9.1	20	0.455	24.47		0.47 %
5	9.2	20	0.46	24.70		
6	9.2	20	0.46	24.70		

Table D.3: Calculation of the angle of repose for sample 3 (Avg. thickness = 2.54mm).

Trial	*Height(H) (cm)*	*Width(W) (cm)*	*H/W*	*Angle degrees*	*Avg. degrees*	*Standard deviation*
1	9.4	20	0.47	25.17	25.17	0.19
2	9.5	20	0.475	25.41		
3	9.5	20	0.475	25.41		
4	9.3	20	0.465	24.94		0.75 %
5	9.4	20	0.47	25.17		
6	9.3	20	0.465	24.94		

Table D.4: Calculation of the angle of repose for sample 4 (Avg. thickness = 2.33mm).

Trial	*Height(H) (cm)*	*Width(W) (cm)*	*H/W*	*Angle degrees*	*Avg. degrees*	*Standard deviation*
1	9.6	20	0.48	25.64	25.74	0.12
2	9.65	20	0.483	25.76		
3	9.55	20	0.478	25.52		
4	9.7	20	0.485	25.87		0.47 %
5	9.7	20	0.485	25.87		
6	9.65	20	0.483	25.76		

Table D.5: Calculation of the angle of repose for sample 5 (Avg. thickness = 2.17mm).

Trial	*Height(H) (cm)*	*Width(W) (cm)*	*H/W*	*Angle degrees*	*Avg. degrees*	*Standard deviation*
1	10.1	20	0.50	26.79	27.12	0.23
2	10.15	20	0.508	26.91		
3	10.3	20	0.515	27.25		
4	10.4	20	0.52	27.47		0.85 %
5	10.2	20	0.51	27.02		
6	10.3	20	0.515	27.25		

APPENDIX E

EXAMINING THE EFFECT OF MOISTURE CONTENT ON THE ANGLE OF REPOSE

Table E.1: Calculation of the angle of repose for 11.66% moisture content.

Trial	*Height(H) (cm)*	*Width(W) (cm)*	*H/W*	*Angle degrees*	*Avg. degrees*	*Standard deviation*
1	9.5	20	0.475	25.41	25.37	0.16
2	9.6	20	0.48	25.64		
3	9.5	20	0.475	25.41		
4	9.4	20	0.47	25.17		0.63 %
5	9.5	20	0.475	25.41		
6	9.4	20	0.47	25.17		

Table E.2: Calculation of the angle of repose for 13.90% moisture content.

Trial	*Height(H) (cm)*	*Width(W) (cm)*	*H/W*	*Angle degrees*	*Avg. degrees*	*Standard deviation*
1	9.4	20	0.47	25.17	25.33	0.11
2	9.5	20	0.475	25.41		
3	9.5	20	0.475	25.41		
4	9.4	20	0.47	25.17		0.43 %
5	9.5	20	0.475	25.41		
6	9.5	20	0.475	25.41		

Table E.3: Calculation of the angle of repose for 15.65% moisture content.

Trial	*Height(H) (cm)*	*Width(W) (cm)*	*H/W*	*Angle degrees*	*Avg. degrees*	*Standard deviation*
1	10.5	20	0.525	27.70	27.54	0.17
2	10.4	20	0.52	27.47		
3	10.3	20	0.515	27.25		
4	10.5	20	0.525	27.70		0.62 %
5	10.4	20	0.52	27.47		
6	10.5	20	0.525	27.70		

Table E.4: Calculation of the angle of repose for 18.03% moisture content.

Trial	*Height(H) (cm)*	*Width(W) (cm)*	*H/W*	*Angle degrees*	*Avg. degrees*	*Standard deviation*
1	12.5	20	0.625	32.00	32.00	0.27
2	12.4	20	0.62	31.80		
3	12.5	20	0.625	32.00		
4	12.7	20	0.635	32.42		0.84 %
5	12.3	20	0.615	31.59		
6	12.6	20	0.63	32.21		

Table E.5: Calculation of the angle of repose for 19.56% moisture content.

Trial	*Height(H) (cm)*	*Width(W) (cm)*	*H/W*	*Angle degrees*	*Avg. degrees*	*Standard deviation*
1	13.8	20	0.69	34.60	34.60	0.25
2	13.7	20	0.685	34.41		
3	13.9	20	0.695	34.80		
4	13.8	20	0.69	34.60		0.72 %
5	14.0	20	0.70	34.99		
6	13.6	20	0.68	34.22		

Table E.6: Calculation of the angle of repose for 21.60% moisture content.

Trial	*Height(H) (cm)*	*Width(W) (cm)*	*H/W*	*Angle degrees*	*Avg. degrees*	*Standard deviation*
1	14.5	20	0.725	35.94	35.69	0.21
2	14.5	20	0.725	35.94		
3	14.4	20	0.72	35.75		
4	14.3	20	0.715	35.56		0.59 %
5	14.3	20	0.715	35.56		
6	14.2	20	0.71	35.37		

APPENDIX F

EXAMINING THE EFFECT OF MATERIAL HEAD IN THE HOPPER ON THE FLOWRATE

Table F.1: First run to calculate the flowrate at different material heights.

Height from the bottom (cm)	*Mass collected (g)*	*Time (sec)*	*Mass flow rate ($g\ sec^{-1}$)*	*Avg. Mass flow rate ($g\ sec^{-1}$)*	*Standard deviation*
76	126.79	4.97	25.51	25.3	0.39
63.5	117.65	4.69	25.09		
51	140.56	5.44	25.84		
38.5	130.79	5.32	24.58		1.5 %
26.5	141.52	5.59	25.32		
13.5	142.60	5.60	25.46		

Table F.2: Second run to calculate the flowrate at different material heights.

Height from the bottom (cm)	*Mass collected (g)*	*Time (sec)*	*Mass flow rate ($g\ sec^{-1}$)*	*Avg. Mass flow rate ($g\ sec^{-1}$)*	*Standard deviation*
76	127.53	5.03	25.35	24.66	0.43
63.5	139.14	5.62	24.76		
51	136.57	5.57	24.52		
38.5	136.18	5.46	24.99		1.7 %
26.5	141.74	5.85	24.23		
13.5	137.86	5.72	24.10		

Table F.3: Third run to calculate the flowrate at different material heights.

Height from the bottom (cm)	*Mass collected (g)*	*Time (sec)*	*Mass flow rate ($g\ sec^{-1}$)*	*Avg. Mass flow rate ($g\ sec^{-1}$)*	*Standard deviation*
76	132.96	5.06	26.28	25.66	0.84
63.5	138.13	5.50	25.11		
51	139.19	5.53	25.17		
38.5	138.85	5.28	26.30		3.3%
26.5	131.08	5.38	24.36		
13.5	136.09	5.09	26.74		

Table F.4: Fourth run to calculate the flowrate at different material heights.

Height from the bottom (cm)	*Mass collected (g)*	*Time (sec)*	*Mass flow rate ($g\ sec^{-1}$)*	*Avg. Mass flow rate ($g\ sec^{-1}$)*	*Standard deviation*
76	135.89	5.38	25.26	24.48	0.55
63.5	136.53	5.75	23.74		
51	142.08	5.69	24.97		
38.5	142.45	5.75	24.77		2.2%
26.5	140.63	5.84	24.08		
13.5	147.62	6.13	24.08		

APPENDIX G

EXAMINING THE EFFECT OF HOPPER WIDTH ON THE FLOWRATE

Table G.1: Calculation of the flowrate with a hopper width of 38 cm.

Trial	*Mass collected (g)*	*Time (sec)*	*Mass flow rate ($g\ sec^{-1}$)*	*Avg. Mass flow rate ($g\ sec^{-1}$)*	*Standard deviation*
1	443.7	5.13	86.49	86.68	0.95
2	456.3	5.15	88.60		
3	442.6	5.16	85.78		
4	445.7	5.13	86.88		1.10 %
5	452.0	5.22	86.59		
6	440.8	5.14	85.76		

Table G.2: Calculation of the flowrate with a hopper width of 30 cm.

Trial	*Mass collected (g)*	*Time (sec)*	*Mass flow rate ($g\ sec^{-1}$)*	*Avg. Mass flow rate ($g\ sec^{-1}$)*	*Standard deviation*
1	454.5	5.25	86.57	87.99	0.97
2	448.2	5.13	87.37		
3	457.8	5.22	87.70		
4	465.8	5.19	89.75		1.10 %
5	494.7	5.60	88.34		
6	476.3	5.40	88.20		

Table G.3: Calculation of the flowrate with a hopper width of 24 cm.

Trial	*Mass collected (g)*	*Time (sec)*	*Mass flow rate ($g\ sec^{-1}$)*	*Avg. Mass flow rate ($g\ sec^{-1}$)*	*Standard deviation*
1	443.7	5.13	86.49	86.88	0.86
2	456.3	5.15	88.60		
3	442.6	5.16	85.78		
4	445.7	5.13	86.88		0.99 %
5	452.0	5.22	86.59		
6	460.8	5.30	86.94		

Table G.4: Calculation of the flowrate with a hopper width of 18 cm.

Trial	*Mass collected (g)*	*Time (sec)*	*Mass flow rate ($g\ sec^{-1}$)*	*Avg. Mass flow rate ($g\ sec^{-1}$)*	*Standard deviation*
1	471.7	5.31	88.83	88.53	1.00
2	440.6	5.07	86.90		
3	456.8	5.19	88.02		
4	453.5	5.15	88.06		1.13 %
5	470.8	5.26	89.51		
6	462.9	5.15	89.88		

Table G.5: Calculation of the flowrate with a hopper width of 10 cm.

Trial	*Mass collected (g)*	*Time (sec)*	*Mass flow rate ($g\ sec^{-1}$)*	*Avg. Mass flow rate ($g\ sec^{-1}$)*	*Standard deviation*
1	470.7	5.25	89.66	87.80	1.39
2	441.4	5.16	85.54		
3	451.5	5.19	86.99		
4	460.0	5.15	89.32		1.58 %
5	465.7	5.31	87.70		
6	457.2	5.22	87.59		

APPENDIX H

EXAMINING THE EFFECT OF PARTICLE SIZE ON THE FLOWRATE

Table H.1: Calculation of the flowrate with a wheat thickness of 2.75 mm.

Trial	*Mass collected (g)*	*Time (sec)*	*Mass flow rate ($g\ sec^{-1}$)*	*Avg. Mass flow rate ($g\ sec^{-1}$)*	*Standard deviation*
1	401.1	7.03	57.06	58.91	1.20
2	417.8	7.29	57.31		
3	418.7	7.12	58.81		
4	426.4	7.22	59.06		
5	423.9	6.94	61.08		2.04 %
6	423.5	7.19	58.90		
7	429.3	7.22	59.46		
8	424.3	7.12	59.59		

Table H.2: Calculation of the flowrate with a wheat thickness of 2.65 mm.

Trial	*Mass collected (g)*	*Time (sec)*	*Mass flow rate ($g\ sec^{-1}$)*	*Avg. Mass flow rate ($g\ sec^{-1}$)*	*Standard deviation*
1	415.9	7.12	58.41	58.63	0.37
2	424.6	7.22	58.81		
3	422.1	7.22	58.46		
4	417.5	7.19	58.07		
5	420.3	7.12	59.03		0.63 %
6	421.1	7.18	58.65		
7	432.6	7.42	58.30		
8	429.8	7.25	59.28		

Table H.3: Calculation of the flowrate with a wheat thickness of 2.54 mm.

Trial	*Mass collected (g)*	*Time (sec)*	*Mass flow rate ($g\ sec^{-1}$)*	*Avg. Mass flow rate ($g\ sec^{-1}$)*	*Standard deviation*
1	423.3	7.16	59.12	59.12	0.69
2	434.7	7.25	59.96		
3	428.7	7.16	59.87		
4	436.1	7.40	58.93		
5	416.5	7.19	57.93		1.17 %
6	436.7	7.45	58.62		
7	440.2	7.35	59.89		
8	439.6	7.50	58.61		

Table H.4: Calculation of the flowrate with a wheat thickness of 2.33 mm.

Trial	*Mass collected (g)*	*Time (sec)*	*Mass flow rate ($g\ sec^{-1}$)*	*Avg. Mass flow rate ($g\ sec^{-1}$)*	*Standard deviation*
1	389.3	7.00	55.61	55.14	0.65
2	395.7	7.25	54.58		
3	395.5	7.25	54.55		
4	390.7	7.22	54.11		
5	408.8	7.28	56.15		1.18 %
6	403.7	7.32	55.15		
7	395.0	7.16	55.16		
8	406.2	7.28	55.80		

APPENDIX I

EXAMINING THE EFFECT OF HOPPER HALF ANGLE ON THE FLOWRATE

Table I.1: Calculation of the flowrate with a 33° Hopper half angle.

Trial	*Mass collected (g)*	*Time (sec)*	*Mass flow rate ($g\ sec^{-1}$)*	*Avg. Mass flow rate ($g\ sec^{-1}$)*	*Standard deviation*
1	503.1	5.41	92.99	93.89	1.47
2	488.2	5.22	93.52		
3	496.8	5.18	95.51		
4	475.9	5.19	91.70		1.57 %
5	497.7	5.32	93.55		
6	492.6	5.15	95.65		

Table I.2: Calculation of the flowrate with a 40° Hopper half angle.

Trial	*Mass collected (g)*	*Time (sec)*	*Mass flow rate ($g\ sec^{-1}$)*	*Avg. Mass flow rate ($g\ sec^{-1}$)*	*Standard deviation*
1	508.1	6.38	79.64	78.43	0.88
2	484.7	6.22	77.93		
3	482.1	6.25	77.14		
4	481.1	6.06	79.39		1.12%
5	490.7	6.30	77.89		
6	483.2	6.15	78.57		

Table I.3: Calculation of the flowrate with a 47° Hopper half angle.

Trial	*Mass collected (g)*	*Time (sec)*	*Mass flow rate ($g\ sec^{-1}$)*	*Avg. Mass flow rate ($g\ sec^{-1}$)*	*Standard deviation*
1	436.7	6.19	70.50	71.38	0.76
2	451.5	6.35	71.10		
3	437.4	6.12	71.47		
4	441.9	6.09	72.56		1.06 %
5	449.8	6.24	72.08		
6	432.8	6.14	70.49		

Table I.4: Calculation of the flowrate with a 52° Hopper half angle.

Trial	*Mass collected (g)*	*Time (sec)*	*Mass flow rate ($g\ sec^{-1}$)*	*Avg. Mass flow rate ($g\ sec^{-1}$)*	*Standard deviation*
1	398.6	6.22	64.08	64.14	0.51
2	376.4	5.94	63.37		
3	398.0	6.13	64.93		
4	387.4	6.05	64.03		0.80 %
5	407.3	6.38	63.84		
6	401.8	6.22	64.60		

Table I.5: Calculation of the flowrate with a 57° Hopper half angle.

Trial	*Mass collected (g)*	*Time (sec)*	*Mass flow rate ($g\ sec^{-1}$)*	*Avg. Mass flow rate ($g\ sec^{-1}$)*	*Standard deviation*
1	410.1	6.29	65.20	65.94	0.96
2	407.1	6.32	64.41		
3	413.8	6.18	66.96		
4	420.6	6.36	66.13		1.46 %
5	405.8	6.04	67.19		
6	422.2	6.42	65.76		

Table I.6: Calculation of the flowrate with a 61° Hopper half angle.

Trial	*Mass collected (g)*	*Time (sec)*	*Mass flow rate ($g\ sec^{-1}$)*	*Avg. Mass flow rate ($g\ sec^{-1}$)*	*Standard deviation*
1	406.4	6.09	66.73	65.85	0.73
2	403.5	6.22	64.87		
3	405.3	6.22	65.16		
4	414.8	6.32	65.63		1.11 %
5	407.3	6.18	65.91		
6	410.8	6.15	66.80		

APPENDIX J

EXAMINING THE EFFECT OF DISCHARGE SIZE ON THE FLOWRATE

Table J.1: Calculation of the flowrate with a discharge opening of 1.5 cm x 2.5 cm (D_h = 1.88 cm).

Trial	*Mass collected (g)*	*Time (sec)*	*Mass flow rate ($g\ sec^{-1}$)*	*Avg. Mass flow rate ($g\ sec^{-1}$)*	*Standard deviation*
1	423.3	7.16	59.12	59.12	0.69
2	434.7	7.25	59.96		
3	428.7	7.16	59.87		
4	436.1	7.40	58.93		
5	416.5	7.19	57.93		1.17 %
6	436.7	7.45	58.62		
7	440.2	7.35	59.89		
8	439.6	7.50	58.61		

Table J.2: Calculation of the flowrate with a discharge opening of 2.0 cm x 2.5 cm (D_h = 2.24 cm).

Trial	*Mass collected (g)*	*Time (sec)*	*Mass flow rate ($g\ sec^{-1}$)*	*Avg. Mass flow rate ($g\ sec^{-1}$)*	*Standard deviation*
1	730.9	5.12	142.75	137.33	2.81
2	705.5	5.22	135.15		
3	711.0	5.16	137.79		
4	720.8	5.13	140.51		
5	719.7	5.28	136.31		2.05 %
6	690.8	5.18	133.36		
7	714.5	5.25	136.10		
8	713.4	5.22	136.67		

Table J.3: Calculation of the flowrate with a discharge opening of 2.4 cm x 2.5 cm (D_h = 2.44 cm).

Trial	*Mass collected (g)*	*Time (sec)*	*Mass flow rate ($g\ sec^{-1}$)*	*Avg. Mass flow rate ($g\ sec^{-1}$)*	*Standard deviation*
1	898.4	5.31	169.19	167.15	1.75
2	874.3	5.22	167.49		
3	872.7	5.22	167.18		
4	868.0	5.25	165.33		
5	866.7	5.29	163.84		1.05 %
6	873.2	5.16	169.22		
7	864.7	5.19	166.61		
8	867.1	5.15	168.37		

Table J.4: Calculation of the flowrate with a discharge opening of 2.8 cm x 2.5 cm (D_h = 2.64 cm).

Trial	*Mass collected (g)*	*Time (sec)*	*Mass flow rate ($g\ sec^{-1}$)*	*Avg. Mass flow rate ($g\ sec^{-1}$)*	*Standard deviation*
1	947.2	4.28	221.31	217.39	6.78
2	897.1	4.06	220.96		
3	868.0	4.06	213.79		
4	898.4	4.13	217.53		
5	903.2	4.19	215.56		3.12 %
6	863.1	4.15	207.98		
7	952.6	4.12	231.21		
8	864.3	4.10	210.80		

Table J.5: Calculation of the flowrate with a discharge opening of 3.2 cm x 2.5 cm (D_h =2.80 cm).

Trial	*Mass collected (g)*	*Time (sec)*	*Mass flow rate ($g\ sec^{-1}$)*	*Avg. Mass flow rate ($g\ sec^{-1}$)*	*Standard deviation*
1	991.3	3.28	302.23	303.50	2.45
2	978.9	3.19	306.87		
3	941.5	3.10	303.71		
4	995.0	3.28	303.35		
5	977.2	3.25	300.68		0.81 %
6	975.4	3.22	302.92		
7	958.7	3.19	300.53		
8	1018.6	3.31	307.73		

Table J.6: Calculation of the flowrate with a discharge opening of 3.6 cm x 2.5 cm (D_h = 2.95 cm).

Trial	*Mass collected (g)*	*Time (sec)*	*Mass flow rate ($g\ sec^{-1}$)*	*Avg. Mass flow rate ($g\ sec^{-1}$)*	*Standard deviation*
1	829.4	2.13	389.39	381.31	6.62
2	845.9	2.16	391.62		
3	889.1	2.35	378.34		
4	853.1	2.25	379.16		
5	889.5	2.35	378.50		1.74 %
6	819.8	2.12	386.70		
7	930.2	2.50	372.08		
8	903.0	2.41	374.69		

APPENDIX K

EXAMINING THE EFFECT OF MOISTURE CONTENT ON THE FLOWRATE

Table K.1: Calculation of the flowrate for 11.66% moisture content.

Trial	*Mass collected (g)*	*Time (sec)*	*Mass flow rate ($g\ sec^{-1}$)*	*Avg. Mass flow rate ($g\ sec^{-1}$)*	*Standard deviation*
1	596.8	7.22	82.66	82.14	0.65
2	581.1	7.18	80.93		
3	597.0	7.22	82.69		
4	585.1	7.15	81.83		0.79 %
5	604.2	7.30	82.77		
6	590.3	7.20	81.98		

Table K.2: Calculation of the flowrate for 13.90% moisture content.

Trial	*Mass collected (g)*	*Time (sec)*	*Mass flow rate ($g\ sec^{-1}$)*	*Avg. Mass flow rate ($g\ sec^{-1}$)*	*Standard deviation*
1	602.8	7.28	82.80	82.66	0.51
2	597.2	7.22	82.71		
3	583.8	7.12	81.99		
4	580.2	7.05	82.29		0.62 %
5	592.3	7.15	82.83		
6	604.3	7.22	83.70		

Table K.3: Calculation of the flowrate for 15.65% moisture content.

Trial	*Mass collected (g)*	*Time (sec)*	*Mass flow rate ($g\ sec^{-1}$)*	*Avg. Mass flow rate ($g\ sec^{-1}$)*	*Standard deviation*
1	536.1	7.25	73.94	74.32	1.76
2	535.6	7.15	74.91		
3	536.1	7.06	75.93		
4	507.5	7.18	70.68		2.37 %
5	539.4	7.12	75.76		
6	527.5	7.06	74.72		

Table K.4: Calculation of the flowrate for 18.03% moisture content.

Trial	*Mass collected (g)*	*Time (sec)*	*Mass flow rate ($g\ sec^{-1}$)*	*Avg. Mass flow rate ($g\ sec^{-1}$)*	*Standard deviation*
1	462.6	7.19	64.34	66.78	1.13
2	472.5	7.16	65.99		
3	481.1	7.12	67.57		
4	482.2	7.22	66.79		
5	489.4	7.19	68.07		1.69 %
6	485.8	7.15	67.94		
7	476.8	7.12	66.97		
8	468.1	7.03	66.59		

Table K.5: Calculation of the flowrate for 19.56% moisture content.

Trial	*Mass collected (g)*	*Time (sec)*	*Mass flow rate ($g\ sec^{-1}$)*	*Avg. Mass flow rate ($g\ sec^{-1}$)*	*Standard deviation*
1	396.0	7.25	54.62	54.55	0.76
2	384.3	7.19	53.45		
3	400.0	7.28	55.05		
4	392.2	7.28	53.87		
5	398.4	7.25	54.95		1.39 %
6	386.5	7.19	53.76		
7	432.9	7.90	54.80		
8	401.9	7.19	55.90		

Table K.6: Calculation of the flowrate for 21.60% moisture content.

Trial	*Mass collected (g)*	*Time (sec)*	*Mass flow rate ($g\ sec^{-1}$)*	*Avg. Mass flow rate ($g\ sec^{-1}$)*	*Standard deviation*
1	351.3	7.18	48.93	51.52	1.61
2	362.2	7.22	50.17		
3	375.7	7.22	52.04		
4	388.6	7.37	52.73		
5	388.8	7.25	53.63		3.13 %
6	358.6	7.19	49.87		
7	373.1	7.25	51.46		
8	384.4	7.21	53.31		